Functionally Coated Titanium Plate and its Performance as Bipolar Plate Material for Hydrogen Fuel Cells

A thesis submitted to Auckland University of Technology in fulfilment of the requirements for the degree of

Doctor of Philosophy (PhD)

Author: **Dhelipan Mahenthiran**

Supervisors: Dr. Maximiano Ramos, Prof. Ahmed Al-Jumaily

Institute of Biomedical Technologies

School of Engineering

Faculty of Design & Creative Technology

Auckland University of Technology

Auckland, New Zealand

AUT INSTITUTE OF BIOMEDICAL TECHNOLOGIES

Abstract

A fuel cell is an electrochemical device which converts a hydrogen containing chemical into electricity with less environmental impact. But cost is a major hurdle to commercialisation of fuel cells. Bipolar plate accounts for 80% of weight and 45% of the cost of the Proton Exchange Membrane Fuel cell (PEMFC) stack. Bipolar plate is the multifunctional component responsible for electrical conduction from anode to cathode, distributing reactant gas to electrode, removing heat from the active region and preventing coolant – reactant gas cross-over. Graphite has long been used as Bipolar Plate because it performs most of the required functions but weight, cost, brittleness and poor machinability makes it a poor choice for portable applications.

Metal plates are a better alternative to graphite as these can satisfy most of the qualities of bipolar plate (High electrical and thermal conductivity, easily stamped to get desired shape and good mechanical strength) but are prone to corrosion in the fuel cell environment and need protective coating. While major automakers use noble metal as the coating material, the need for non-noble coating is immense. Even though various researches have been done on non-noble metal coatings, very few reports are available on carbon based coatings and their long term significance for fuel cell performance. The performance of Titanium Nitride (TiN) and amorphous carbon (a-C) coatings are compared along with a novel tungsten carbide carbon (WCC) coating as bipolar coating materials.

The corrosion current density and Interfacial Contact Resistance (ICR) of WCC coating are less than 1 $\mu A/cm^2$ and 10 $m\Omega.cm^2$ respectively. This makes WCC the only coating material that satisfies the US DOE (Department of Energy) target 2025 for bipolar plate. The other coating materials satisfy or are on a par with DOE target either for corrosion resistance or ICR but not both.

A die and punch was designed to fabricate plates using ANSYS software. The fabricated stamped plate showed no cracks and the thickness distributions at the critical spots were comparable with the simulation. The novel coating was extensively tested in the simulated fuel cell environment and coated on the stamped plate to study their long term performance in fuel cell single stack.

The fuel cell performance of the coated plate was analysed and the peak power density of WCC was 0.321 W/cm^2 at 0.8 A/cm^2, while bare Ti shows peak power of 0.21 W/cm^2 at 0.63 A/cm^2. The long term performance of the bipolar plate in fuel cell environment was determined by maintaining fuel cell at constant current mode 0.50A/cm^2 for 500 hours. The need for non-noble protective coating is immense for bipolar plate application. In this research it is successfully coated and tested in fuel cell environment, achieving all the objectives.

ACKNOWLEDGEMENTS

First I would like to take this opportunity to express my heartfelt gratitude to my supervisors Dr. Maximiano Ramos and Prof. Ahmed Al-Jumaily from the Institute of Biomedical Technologies of Auckland University of Technology (AUT) for showing immense patience and faith in me to pursue the goal. Their timely support and guidance have helped me a lot throughout this program.

I would like to thank New Zealand Ministry of Foreign Affairs and Trade (MFAT) for providing me with "Commonwealth Scholarship" to undertake this research program at AUT and also would like to thank AUT- scholarship office for their impeccable assistant throughout this journey.

I would like to thank Dr. Mani Narayanasawmy, Director, Aatral Innovations, India for mentoring and providing with all necessary equipments to analyse the fuel cell performance. His expertise on electrochemistry and surface characterization has been immensely useful in this research. Thanks to Mr. Sathya Shankaran Aatral Innovations, India for assisting in assembling and testing long term fuel cell performance.

I would like to acknowledge Dr. Santhosh Bhatt and Dr. Kalpana from CECRI, Madras Complex, India for providing facility to conduct corrosion studies.

I would like to thank my wife for continuous support and encouragement throughout this journey. Without her understanding completion of this thesis might have been more difficult. I would like to express my gratitude to my cousin Anna and Viswa for their moral support.

There are no words to express my love and gratitude towards my parents whose inspiration and support have helped me to overcome major hurdles in my life.

ATTESTATION OF AUTHORSHIP

I hereby declare that this submission is my own work and that, to the best of my knowledge and belief, it contains no material previously published or written by another person, nor material which to substantial extent has been accepted for the award of any other degree or diploma of a university or other institution of higher learning, except where due acknowledgement within this document.

Dhelipan Mahenthiran

Signature: 

Date: 30/09/2022

TABLE OF CONTENTS

LIST OF FIGURES

LIST OF TABLES

ABBREVIATIONS

Pt/C	Platinum on Carbon
BP/BPP	Bipolar plate
DLC	Diamond like carbon
PEMFC	Polymer Electrolyte Membrane Fuel Cell
AFC	Alkaline Fuel Cell
MCFC	Molten Carbonate Fuel Cell
PAFC	Phosphoric Acid Fuel Cell
SOFC	Solid Oxide Fuel Cell
DMFC	Direct Methanol fuel cell
PVD	Physical vapor deposition
CVD	Chemical vapor deposition
DOE	United States Department of Energy
EDM	Electrical discharge mechanism
RHE	Reversible hydrogen electrode
EDX	Energy Dispersive X-Ray Analysis
GDL	Gas diffusion layer
ICR	Interfacial Contact Resistance
SCE	Saturated calomel electrode
SEM	Scanning electron microscopy
XRD	X-ray diffraction
XPS	X-ray photoelectron spectroscopy
EIS	Electrochemical Impedance Spectroscopy

AEGD	Arc Enhanced Glow Discharge
DC	Direct Current
EBPVD	Electron Beam Physical Vapour Deposition
ICP	Inductively coupled plasma

CHAPTER 1 INTRODUCTION

In this chapter, the present energy infrastructure and the necessity to transfer from fossil fuel to renewable energy usage are discussed, along with the possibility of the hydrogen economy and the suitability of PEMFC (Polymer Electrolyte Membrane Fuel Cell), for the automobile and aviation sectors. The main components of PEMFC problems associated with metal bipolar plates and the possible solutions are discussed.

1.1 The energy transition from fossil fuel to the renewable energy source

Climate change has been the most persistent environmental issue over the last several decades. The global economy has experienced drastic growth because of increasing urbanisation and industrialisation. According to the World Bank, global GDP has doubled since 2000, rising from $33.6 trillion US dollars to $84.7 trillion US dollars in 2020 [1]. At the same time world energy usage has increased from 1637.204 kg of oil equivalent per capita to 1922.13 kg of oil equivalent per capita [1]; this illustrates the direct

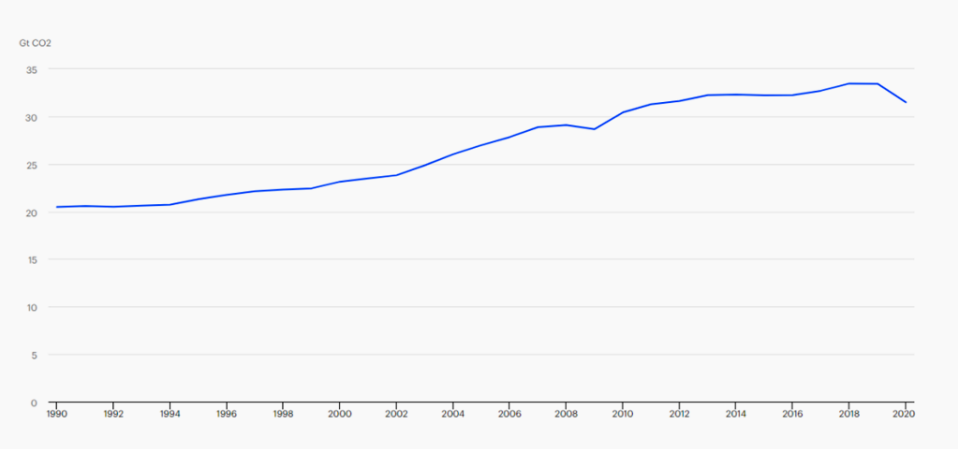

Figure 1: Global energy-related CO2 emissions, 1990-2020 [2]

relation between GDP and energy usage. During the twenty-first century energy usage has skyrocketed, while most of it comes from non-renewable sources. The extraction of fossil fuels, including oil, gas, and coal, accounts for about 80% of global energy use [3]. The peak oil camp claims that the world will run out of natural resources like oil in 2052, coal in 2088, and gas in 2060, but those subsequent discoveries such as shale gas will

keep the supply expanding. The COVID-19 pandemic temporarily reduced industrial energy demand and it has resulted in a 5.8% annual decline of global energy-related carbon dioxide emissions, the most significant yearly percentage decline since WWII. After hitting a low in April 2020, global emissions increased strongly surpassing 2019 levels in December. Global CO_2 emissions increased by 2%, in December 2020 compared to the December 2019 [4].

High energy density, an established ecosystem, and job prospects are all advantages of hydrocarbon fuels which come with the price of air pollution, health issues, and rising global temperature. Non-conventional energy use must be ramped up at least six times faster for the nations to begin meeting the Paris Agreement targets of keeping average global temperature rise in the twenty-first century "well below 2°C" relative to pre-industrial levels.

The prejudice that is hard to leave behind is that sustainable energy solution comes with a cost, but it’s not true. A complete shift in the paradigm can create new professional roles; new investment in renewable energy projects and sustainable growth can be achieved.

1.2 Hydrogen Economy

Most of the renewable energy sources like solar, wind, and hydropower are firmly climate dependent. In comparison, hydrogen energy is considered one of the least dependent renewable energy sources on climate conditions. Even though vast amounts of hydrogen are available in the world, it is found bonded to other elements as molecules rather than being a free element. Due to its immense availability and superior energy efficiency from production to utilisation in fuel cell, hydrogen has long been advocated for future energy generation. Hydrogen can be produced through different methods like electrolysis [5], steam reforming [6], and photocatalytic processes [7]. Hydrogen production technology is well-established, with the majority of hydrogen produced coming from fossil fuels: 50% from natural gas, 20% from coal, and 30% from oil [8], while hydrogen produced through the electrolysis of water accounts for just 4%. The most popular and least expensive method for producing hydrogen is by steam methane reforming (SMR), but it releases carbon monoxide and dioxide into the environment. Producing hydrogen from water through a solar-driven photocatalyst is the most cost-effective and environmentally friendly method of producing hydrogen fuel, but the requirement of larger surface area and slow reaction time makes it unsuitable for larger scale applications.

Another challenge associated with hydrogen infrastructure is its storage. The lightest gas, hydrogen is 3.2 and 2700 times less energy-dense than natural gas and petrol, but its energy density per kg is 3.4 times that of petrol. The most conventional method to store hydrogen is using gas cylinders. The latest compressed pressure vessel design is a type 4 cylinder with a polymer liner wrapped with carbon fibre resin composite and having a maximum pressure rating of 700bar [9]. Type 4 cylinders are predominantly used in hydrogen fuel cell vehicles. Another application in which type 4 hydrogen cylinder has a vital role is a hydrogen fuel cell-powered UAV (Unmanned Aerial Vehicle) where the weight to power ratio needs to be kept as low as possible.

For high-volume transportation in the absence of pipes, hydrogen is typically carried and delivered as a liquid. A liquefaction technique must cool the hydrogen to cryogenic temperatures to liquefy it. Australia aims to expand its hydrogen industry by investing 1.2 billion into creating hydrogen production infrastructure and making Australia a key player in supplying hydrogen gas to Europe, Japan, and Korea [10]. It is believed that the hydrogen economy can be realised by overcoming existing technical barriers using bio-methanol. Methanol from natural resources can be reformed to produce hydrogen, which can then be supplied to fuel cells to power vehicles. Transporting methanol to hydrogen filling stations is easier and more economical than transporting liquid hydrogen [11].

1.3 Fuel cell

The fuel cell is an electrochemical device that converts chemical energy into electrical energy through a redox reaction. A fuel cell is different from batteries because it is an energy conversion device whereas a battery is an energy storage device. Unlike internal combustion engines, where most of the energy is lost due to the heat generated and the mechanical work needed in the process, fuel cells produce electricity directly from hydrogen-containing fuel and oxygen. The efficiency of the fuel cell is greater than the conventional combustion engine because it is not limited by Carnot efficiency and it has no moving parts. The hydrogen-containing fuel cell oxidises at the anode and that oxygen is reduced at the cathode to produce electricity with water as by-product.

Figure 2 illustrates the fuel cell working principle; here the hydrogen (H_2) gas enters at the anode side and diffuse through GDL (Gas Diffusion Layer), which is coated with catalyst (Pt/C). The catalyst strips of an electron from H_2 molecule (Eq. 1.1), and the ionised atom (H^+) enters the humidified polymer electrolyte membrane, which can

conduct only H^+ ions from anode to cathode. The electron released from anode enters the external circuit producing DC [direct current] and reaches cathode to combine with oxygen. At the cathode side, (1.2) a reduction reaction occurs where oxygen, the hydrogen ion, and the electron are combined by the catalyst to form water.

Reaction at Anode side (oxidation)

$$H_2 \rightarrow 2H^+ + 2e^- \quad \text{..... (1.1)}$$

Reaction at Cathode side (reduction)

$$\tfrac{1}{2} O_2 + 2H^+ + 2e^- \rightarrow H_2O \quad \text{..... (1.2)}$$

Net reaction (the redox reaction)

$$2H_2 + O_2 \rightarrow 2H_2O \quad \text{..... (1.3)}$$

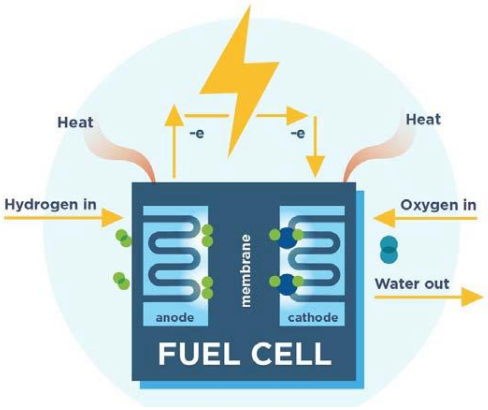

Figure 2: Schematic representation of single fuel cell [12]

1.3.1 Type of fuel cell

The fuel cell is classified into different types based on the fuel supplied, electrolyte, and operating tempreature.

Table 1: Types of Fuel cell

Fuel cell type	Operating temperature(°C)	Efficiency(%)	Electrolyte Conduction and direction	Suitable application
Alkaline Fuel cell(AFC)	50-90	50-70	OH- (Cathode to anode)	Domestic/Small scale power/Transport
Proton Exchange membrane fuel cell(PEMFC)	50-120	40-50	H+ (Anode to cathode)	Domestic/Small scale power/Transport
Phosphoric acid fuel cell(PAFC)	175-220	40-50	H+ (Anode to cathode)	Small Scale power
Molten carbonate fuel cells (MCFC)	600-650	50-60	CO32- (Cathode to anode)	Small Scale Power/Large scale cogenration
Solid oxide fuel cells (SOFC)	800-1000	50-60	OH-	Domestic Power/small scale power/Large scale cogeneration

PEMFC is the most preferred fuel cell for transportation applications due to its simple operating condition and high efficiency. Here, the hydrogen gas is supplied at the anode and the oxygen is

supplied at cathode. The hydrogen gas is oxidised at anode to release electrons from the outer shell, passing through the electrolyte. Hydrogen ions (H^+) pass through the proton exchange membrane to the cathode, combining with oxygen to form water. The platinum on carbon (Pt/C) catalyst loading on the anode and cathode has been drastically reduced to 0.1mg/cm^2 over the past few years. The electrolyte material is a perfluoro sulfonic acid membrane. The DMFC (Direct Methanol Fuel Cell) is a type of fuel cell that uses methanol as a fuel source at the anode, and these can be classified into PEMFC as their working principle is similar.

AFC is the first kind of fuel cell that has been used in the space shuttle and the Apollo missions. This type of fuel cell uses an alkaline medium as an ion conductor. KOH (Potassium Hydroxide) is the electrolyte. AFC can operate at both low and high temperatures and the advantage of the alkaline fuel cell is that it will allow the use of non-noble metals as catalyst. The world's first fuel cell boat (Hydra) uses the AFC 5KW system as its power source [13]. The main disadvantage of AFC is its intolerance to carbon dioxide; here the KOH will be converted to K_2CO_3, which will eventually poison the fuel cell. So the system requires purified oxygen to feed the cathode; this is not needed for the other types of fuel cell.

PAFC is the first fuel cell to be commercialised, and the electrolyte of PAFC is liquid phosphoric acid, which is saturated in a Teflon-based silicon carbide (SiC) matrix and porous carbon paper electrodes with a platinum catalyst. Unlike other types of fuel cells, PAFC has more tolerance towards carbon monoxide and dioxide. But they are less efficient (37%–42%) in terms of electricity generation and also the weight to power ratio is higher than other fuel cells which makes them suit only for stationary applications.

MCFC uses an electrolyte made up of a mix of alkali metal carbonates (Sodium and Potassium carbonate) held in a ceramic ($LiAlO_2$) matrix to retain the liquid in between the electrodes. MCFC is operated at high temperatures (600°C–700°C) to enhance the ionic conductivity. Less costly non-precious metals can be employed as catalysts at the anode and cathode since the working temperature is high. MCFC is an efficient fuel cell which can be operated at 85% when the waste heat is supplied to maintain the working temperature. The main disadvantage of MCFC is its lack of durability. The corrosive nature of the electrolyte decreases the life of the components.

SOFC is a high-temperature fuel cell that uses ceramic electrolytes. The advantage of the solid oxide fuel cell is the fuel flexibility and high efficiency. Here, the negative ion is conducted from cathode to anode through the ceramic electrolyte. The operating temperature of SOFC is 500–1000°C, and a noble metal catalyst is not required. The disadvantage of SOFC is sulphur poisoning of the catalyst, a common occurrence, so the sulfur must be eliminated from the cell

before it enters by using adsorbent beds. This type of fuel cell can be used where there are requirments for both heat (space heating) and power.

The selection of a fuel cell for a specific application should be considered after analysing the load profile, weight to power ratio, and fuel availability. This research focuses on the development of PVD coating for metal bipolar plates and its suitability for PEMFC.

1.3.2 Components of PEMFC fuel cell

Fuel cells consist of two major components MEA [Membrane Electrode Assembly] and bipolar plates which together account for 90% of the stack volume and cost.

a. MEA (Membrane Electrode Assembly)

Figure 3 shows the exploded view of the MEA. It consists of a solid electrolyte membrane sandwiched between catalyst coated GDL (Gas diffusion layer) using a hot pressing process at temperature 120–150°C and pressure 20–50 Bar (depending upon membrane thickness). GDL is a porous layer between the bipolar plates and is the catalyst layer that doesn't take part in the chemical reaction but acts as a gas diffuser and collects current from the catalyst layer to the bipolar plate. The electron released from the three-phase interface (electrically connected catalyst, membrane and reactant gas) is transferred to the external circuit through the current collector. The most commonly used catalyst for oxidation and reduction reaction in hydrogen-based PEMFC is Platinum on carbon (Pt/C). The technological development have helped to reduce the catalyst usage in electrodes from milligrams per square centimeter to a few micrograms per square centimeter.

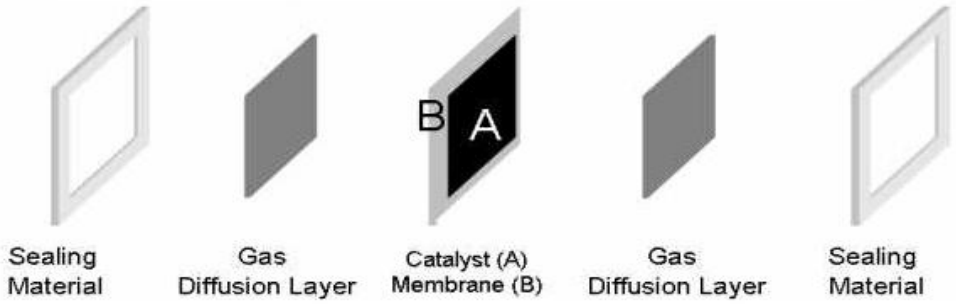

Figure 3: Exploded view of Membrane Electrode assembly (MEA) [14]

[Sealing Material-Silicon Gasket, GDL-Carbon fiber paper, Catalyst-Pt/C, Membrane- Polytetrafluoroethylene (PTFE)]

The membrane is one of the vital components of PEMFC. It exhibits high proton conductivity with zero electron conductivity, high mechanical strength, and chemical stability. The membrane acts as a barrier to stop fuel cell cross over, and it must be hydrated well to conduct protons effectively. One of the widely used membrane for PEMFC is called Nafion^{TM} manufactured by Dupont. Incorporating perfluorovinyl ether with sulfonate groups onto a Polytetrafluoroethylene (PTFE) backbone gives Nafion unique ionic characteristics.

.

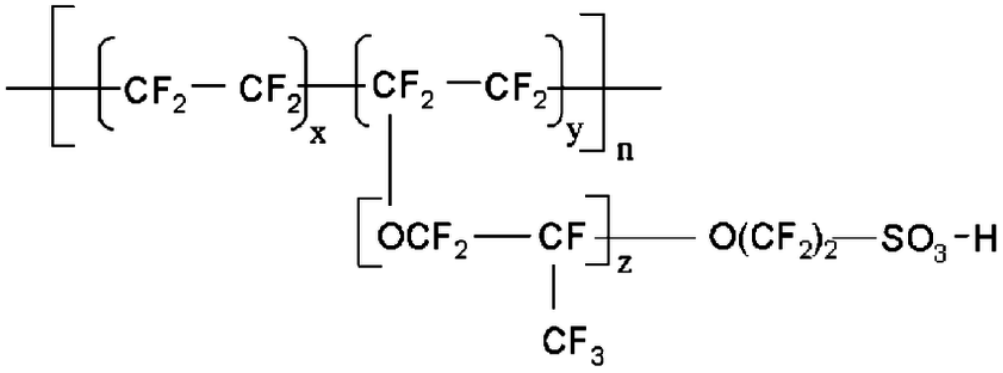

Figure 4: Chemical structure of Nafion [15]

The commercial Nafion membrane is categorised by its thickness and equivalent weight (grams of dry Nafion/mol of sulfonic acid). The equivalent weight is divided by 100 and represented by the first two-digit ("11"), and the third digit (7) refers to thickness in mils. For example, Nafion 117 represents a membrane with an equivalent weight of 1100g/mol and 7 mils thick. Generally, membrane with an equivalent weight ranging from 800–1500 is preferred for PEMFC since it provides the optimum proton conductivity [16]. Maintaining adequate humidity for the membrane is still challenging, dehydration or flooding of water on the cathode side both impact the fuel cell performance.

The electrodes are made of carbon paper or carbon cloth which acts as a gas diffusion layer. A thin layer of platinum on carbon (Pt/C) catalyst is coated onto the carbon paper or on the membrane surface to fasten the hydrogen oxidation reaction. When using reformed fuel, hydrogen may contain carbon monoxide (CO), which can block the catalyst reaction site (catalyst poisoning). Catalyst poisoning can be avoided by alloying platinum with rare earth or other non-noble metal catalysts like Pt-Co, Pt-Fe, Pt-Ru and Pt-Mo [17, 18]. The oxygen reduction reaction is 10^6 times slower than the oxidation reaction [19] so the quantity of Pt/C needed at the cathode is higher than at the anode.

b. Bipolar plate.

As shown in Figure 5, the essential functions of the bipolar plate are collecting the electrons from one MEA and transferring to another in the stack, supplying reactant gas to the electrode and providing coolant to manage heat inside the cell. There is grooving on both sides of the BPP's to facilitate reactant gas access to the electrode on one side and to supply coolant on the other side. The ideal material for BPP should have good thermal conductivity, electrical conductivity, be lightweight, with low Interfacial Contact Resistance (ICR) and high electrochemical corrosion resistance.

The electron released through the oxidation reaction at the anode at the three-phase interface (where porosity (transporting gases), catalytically connected electrode (electrical conductivity), and ionic conductive membrane are all in contact with each other), is transferred to the bipolar plate. The bipolar plate is in contact with the gold coated current collector plate which transfers the electron to the load. The energy reduced electron is then transferred to cathode side for the reduction reaction. If more plates are connected as a stack, the electron released from each anode of the bipolar plate will reach the cathode side to reduce the oxygen and form water/water vapour.

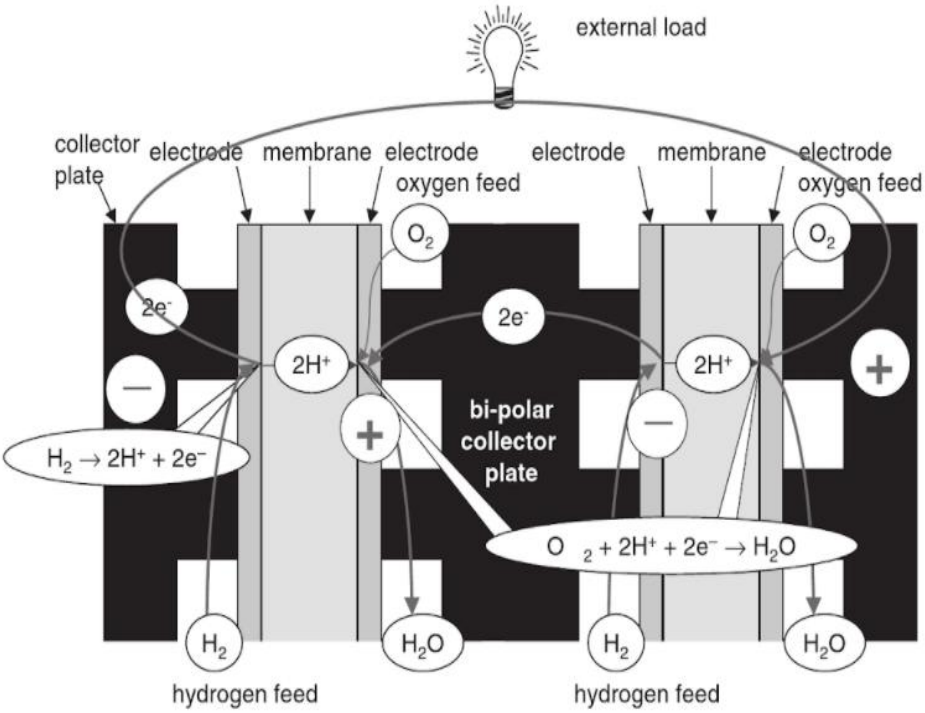

Figure 5: Schematic representation of bipolar plate in the stack [20]

1.4 Polarisation behaviour and losses associated with fuel cells

Figure 6 represents the polarisation curve of the PEMFC, and the voltage losses associated with the fuel cell (FC) performance. The theoretical open circuit voltage of the FC is 1.23V and it will diminish when the current is allowed to flow into the load due to the losses associated with fuel cell. The voltage is varied to find the corresponding current density and it is plotted to find the power density. Fuel cell characterisation techniques allow comparison of almost every characteristic of every part of the fuel cell stack. The information on the performance (Good or poor) of fuel cell can be explained by using best characterisation technique or by utilizing combination of techniques.

Figure 6 shows the voltage losses in a fuel cell and the resulting polarisation curve. When the cell circuit is open, the cell potential is expected to be same or close to theoretical potential for any given condition (concentration of reactant, pressure and temperature).

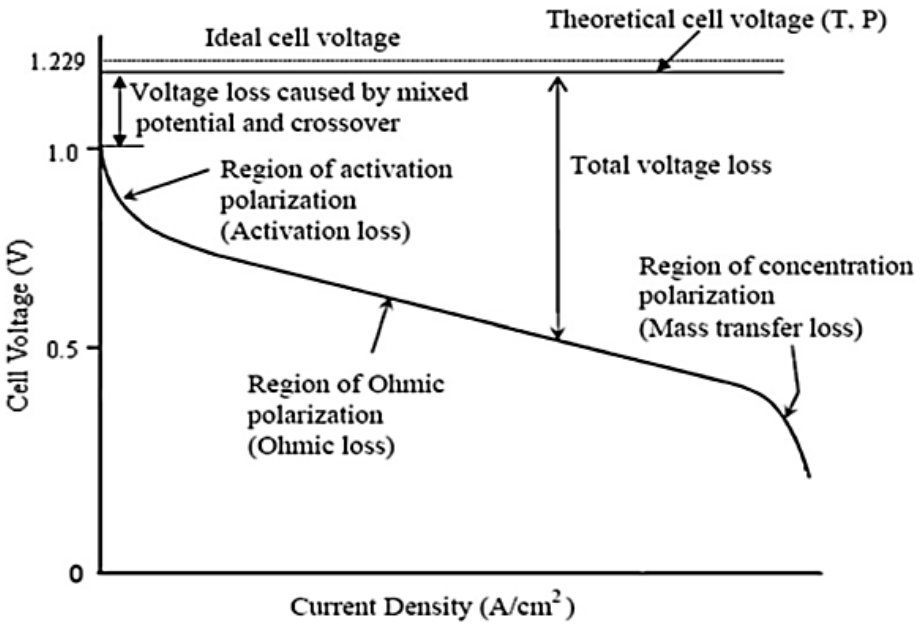

Figure 6: Voltage losses and resulting polarisation [21]

The maximum amount of electrical energy generated in a fuel cell corresponds to the Gibbs free energy, ΔG[22]

$$\Delta G=-nFE \quad \ldots\ldots\ldots\ldots\ldots\ldots\ldots\ldots\ldots\ldots\ldots\ldots (1.4)$$

$$E= -\Delta G/nF \quad \ldots\ldots\ldots\ldots\ldots\ldots\ldots\ldots\ldots\ldots\ldots\ldots (1.5)$$

F→ Faraday constant (96,485 C/ mol)

-ΔG→ Gibbs free energy (237.34kJ/mol)

n → No of electrons (2)

Substituting values into equation (1.5)

$$E=237340/ (2*96485)$$

$$E= 1.23 V$$

At 25°C, the theoretical hydrogen/oxygen fuel cell potential is 1.23 V.

The actual open circuit of the fuel cell is around 0.95–1.05V which is 20% less than theoretical voltage, this decrease in voltage is due to the inherent losses associated with fuel cells.

1.4.1 Reaction rate loss

Even though platinum is used as a catalyst, it requires a certain amount of energy to initiate the chemical reaction which is called the activation energy. Oxygen reduction reaction requires a higher over-potential, that is, it is a slower reaction than hydrogen oxidation. This loss is predominant only in the low current density region (1–100mA/cm^2). The activation overvoltage is represented by the following equation

$$\eta_{act}= \frac{RT}{\alpha nF}\ln(\frac{i}{io}) \text{ ……..(1.6)}$$

Where α represents the electron transfer coefficient of the reaction, n refers to the number of electrons transferred, i_0 is the exchange current density, and F is the Faraday constant.

1.4.2 Resistive loss

Resistive losses arise due to the ionic conduction in the membrane and the electrical conductive in the electrode. This loss predominates in the intermediate current density (100–500 mA/cm^2).

$$\Delta V_{ohm}=iR_i \text{ ……..(1.7)}$$

Where,

i= Current density, A cm^{-2}, and

Ri= Total cell internal resistance which include ionic, electronic, and contact resistance, Ωcm^2

$$R_i= R_{i,i} + R_{i,e}+R_{i,c} \text{ ……..(1.8)}$$

Electronic resistance is almost negligible if graphite/polymer graphite composite is used as current collectors. Ionic and contact resistance are approximately of the same magnitude and predominate in the intermediate current density [23].

1.4.3 Concentration losses and Reactant Cross-over losses

Concentration losses arise due to the rapid consumption of reactant at the electrode site due to the electrochemical reaction. The effects of these losses are most pronounced at high current densities (>500 mA/cm^2).

Cross over is one of the inevitable losses of the most PEMFC is cross-over loss. Here, the anode fuel migrates to the cathode via electrolyte membrane and reacts with oxygen to produce heat which eventually decreases the fuel cell performance [24].

1.5 Research Questions

1. Which part of the conventional fuel cell needs replacement to make it suitable for portable application?
2. Can metal bipolar plate replace conventional graphite plate as bipolar plates?
3. Which flow field design will provide optimal fuel cell performance?
4. What protocol or target can be used to compare the performance of bipolar plate?
5. What technique can produce uniform coating with less environmental impact?
6. Can a non-noble metal coating perform well in the fuel cell environment?

1.6 Closure

The fuel cell basic working principle and their types are explained in detail. From this introductory chapter, it is understood that PEMFC has more advantages such as high power density, low tempreature operation and less startup time compared with other types of fuel cell. Due to these factors, PEMFC has been chosen for this research as the outcome of this research work is intended to apply to the aviation sector.The losses associated with fuel cells are unavoidable but these can be minimised by careful material choice for different components (catalyst, bipolar plate, electrode). The following flowchart illustrate the discussion made in each of the following chapters.

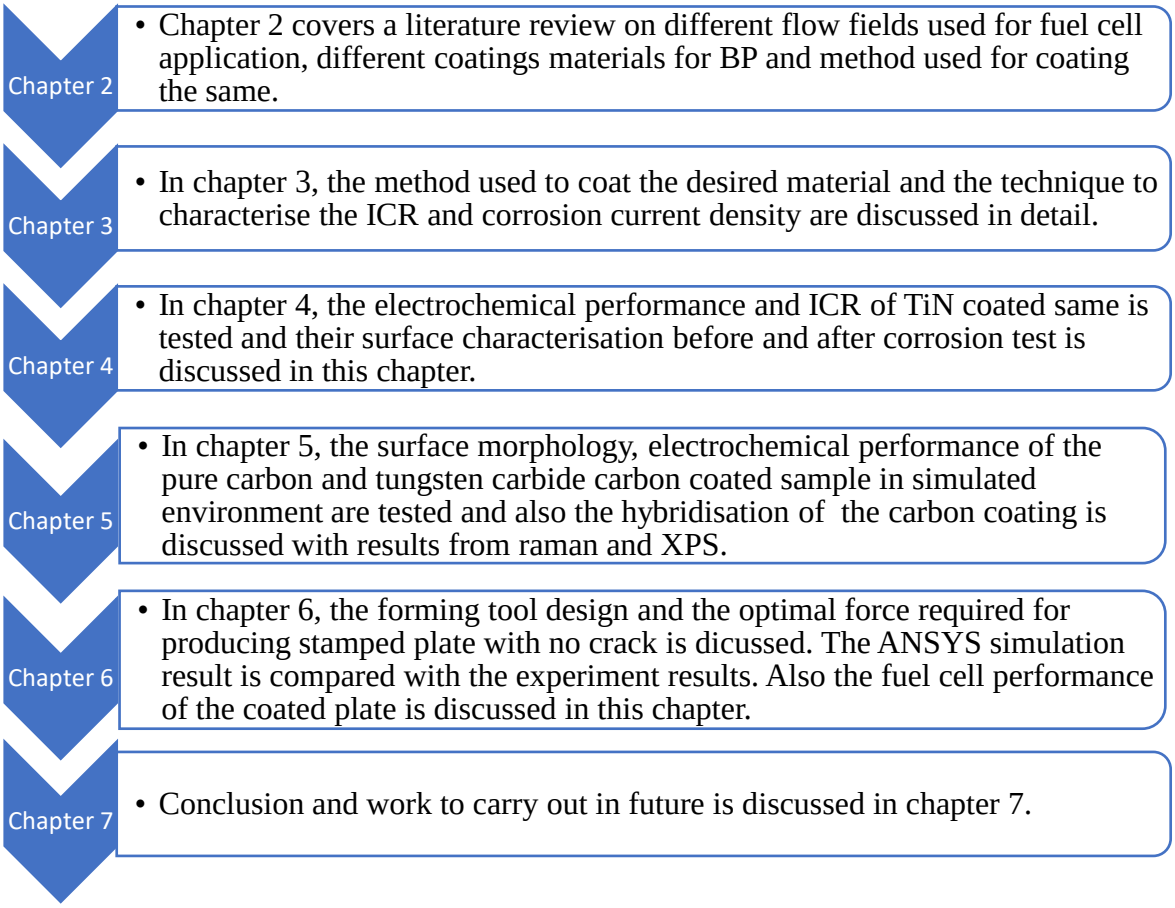
Chapter 2
• Chapter 2 covers a literature review on different flow fields used for fuel cell application, different coatings materials for BP and method used for coating the same.
Chapter 3
• In chapter 3, the method used to coat the desired material and the technique to characterise the ICR and corrosion current density are discussed in detail.
Chapter 4
• In chapter 4, the electrochemical performance and ICR of TiN coated same is tested and their surface characterisation before and after corrosion test is discussed in this chapter.
Chapter 5
• In chapter 5, the surface morphology, electrochemical performance of the pure carbon and tungsten carbide carbon coated sample in simulated environment are tested and also the hybridisation of the carbon coating is discussed with results from raman and XPS.
Chapter 6
• In chapter 6, the forming tool design and the optimal force required for producing stamped plate with no crack is dicussed. The ANSYS simulation result is compared with the experiment results. Also the fuel cell performance of the coated plate is discussed in this chapter.
Chapter 7
• Conclusion and work to carry out in future is discussed in chapter 7.

CHAPTER 2: LITERATURE REVIEW

2.1 Introduction

In this chapter, the complete review of literature on flow channel designs and materials that already have been tested for bipolar plates are presented with an in-depth analysis. The corrosion behaviour of the protective coatings and the methods for coating the same are discussed. At end of this chapter, the research gaps are identified and the main foucs of this research will be addressed.

2.2 Introduction to the bipolar plate

Bipolar plates (BPP) contribute around 80% of the total volume of the fuel cell stack and 45% of the total cost [24]. BPPs form the whole framework of the stack and provide mechanical strength to the MEA. A material with high specific strength is preferred for bipolar plate which can provide support to the MEA but adds less weight to the system, so the power density can be increased. BPPs need to have high electrical conductivity to collect and conduct electrons from anode to cathode.

The role of the BPP is to supply gas to the electrode, supply coolant and collect electrons. The ideal material for a BPP should have high thermal conductivity to dissipate the heat generated due to the electrochemical reaction from the stack. Due to its large contribution to weight of the fuel cell, any suitable material with low density could increase the power to weight ratio of the stack. The performance of the fuel cell deteriorates if any contamination reaches the electrode or ion exchange membrane. BPPs made of metal need to have a high resistance to corrosion to avoid any metal leaching into the MEA. The ICR between the electrode (GDL) and BPP surface is the major contributor in the metal based BPP and this can be reduced by a high conductivity surface coating. There are two types of stack in PEMFC, where in one the water/liquid is used as coolant – the water cooled stack and in the other air is used as coolant – the air cooled stack. The stacks used in the transportation/aviation applications use air as the coolant and air is also a reactant gas at the cathode.

Graphite has long been used in BPP due to its excellent chemical stability, and electrical conductivity. However, due to its poor mechanical strength, fragility and brittleness, it is difficult to handle and process graphite BPP. Increasing the thickness of the graphite BPP can eliminate these drawbacks, but it will increase the overall

weight, electrical resistance, and cost of the stack. In addition, a graphite plate requires machining to form the flow channel, which requires more time and it's not a cost-effective process. Apart from that, graphite plates are prone to reactant gas crossover due to shrinkage of resin graphitisation volume with high temperature graphitisation treatments [25]. These characteristics are considered when finding new materials for BPPs.

2.3 Flow field Design

The flow field for BPPs can be desiged in many configurations to supply gas to the electrode and remove water from the system. The most commonly used flow fields are: parallel flow field, pin type flow field, serpentine flow field and interdigitated flow field. The ideal flow field should have a small gas pressure drop and effective water removal. If anyone of these functions are impaired, the fuel cell performance will deteriorate. The flow field design consist of four parameters; channel distribution pattern, cross sectional area, rib dimension and channel depth.

2.3.1 Single Serpentine flow field

Figure 7a illustrates a single serpentine flow field for a BPP. This is one of the commonly used designs for PEMFC; it can distribute gas evenly to the active area and solve flooding issues at the cathode side. The main drawback of this channel is the requirement of a high pressure compressor to push the reacting gas through the cell because of the substantial pressure drop and concentration gradient from inlet to outlet [26]. Wang et al. [27] suggested that flooding can occur at the channel exit and dehydration at entry due to the supply of high pressure gas which pushes the water downstream.

2.3.2 Parallel Flow field

Figure 7b illustrates the parallel flow field. Here, the reactant gas is distributed easily to the electrode as there are many paths from inlet to outlet, which require less pressure to push reactant through the cell [26]. A fuel cell with this type of flow field is prone to unstable cell voltage due to non-uniform reactant gas supply and poor water dispersion.

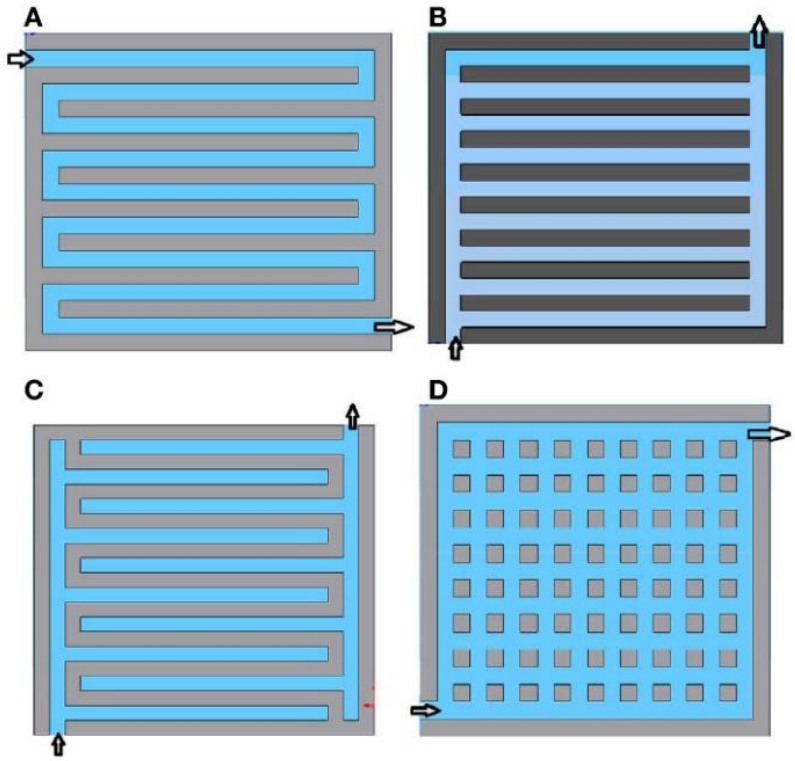

Figure 7: Different flow channels (A) Single serpentine (B) Parallel (C) Interdigitated flow (D) Pin [28]

2.3.3 Interdigitated Flow field

Figure 7c represents the interdigitated flow field where the inlet and outlet channels are not directly connected. Here the gas diffuses through the GDL over the rib to pass to the other channel. The main advantage of this flow field is that it can effectively remove the stagnant water at the channel but the pressure required to push the reactant gas is higher than any other type of flow field which is the major limitation for the interdigitated design. Also the pressure drop in the system is completely dependent on the properties of the GDL (thickness and porosity), which are subjected to aging. The interdigitated flow field outperforms the serpentine flow field only when the inlet gas is over humidified, this is due to its design capacity to remove water effectively [29].

2.3.4 Pin type Flow field

Figure 7d illustrates the pin type flow field. This flow field design consists of array of cubical pins in a regular pattern. The advantage of pin type flow field is the pressure drop is low. The pressure drop in this design is similar to parallel flow field where the reactant gas takes the path of least resistance but this leads to inhomogeneous gas distrubution and poor water removal [26].

2.4 Material for Bipolar plate

The ideal material for BPPs should have certain physical and chemical properties to perform the functions discussed in Chapter 1. Table 2 below shows the target set by the US Department of Energy (DOE) for materials to use in BPPs [30]. The cost of the fuel cell is one of the main hindrances for fuel cell commercialisation. The cost and volume of the fuel cell stack is largely dependent on the BPP, so it is essential to reduce the volume, weight and hence the cost of the BPP. The other properties that are important for a BPP are material density and thermal expansion and hydrophobicity. The materials that are widely used as BPPs are non-porous graphite, polymer composites and metal plates.

Table 2: DOE targets for Bipolar plate

Functions	Characteristic	Units	2025 DOE Target	2020 DOE Target
Connect cells electrically one by one; conduct electrical current	Electrical conductivity Areal specific resistance	Scm^{-1} Ωcm^2	>100 <0.01	100 0.01
Separate the reaction gases	H_2 permeability	$cm^3sec^{-1}cm^{-2}$	2×10^{-6}	1.3×10^{-14}
Facilitate heat management	Thermal conductivity	$Wm^{-1}K^{-1}$	/	10
Durability	Corrosion, anode Corrosion, cathode Lifespan	μAcm^{-2} μAcm^{-2} hours	<1 and no active peak <1 8000	1 and no active peak 1 5000
Light weight	Plate weight	kg/kW	0.18	0.4
Economy	Cost	$\$kW^{-1}$	2	3
Good mechanical properties	Flexural strength	MPa	>40	25

2.4.1 Non-Porous Graphite Bipolar Plates

Graphite satisfies most of the properties of an excellent BPP and it has been used for the past few decades. It has excellent electrical conductivity, low density, low ICR and high corrosion resistance [31]. However, as mentioned above, it has major disadvantages such as porosity, brittleness, and the costly CNC machining process to make the flow field, which also requires more time. Due to the cost of raw material and the further machining process involved, the use of graphite plates has been limited to flow field prototyping [32]. Stacks made of graphite plates are heavy, voluminous, and fragile, which make them unsuitable for transportation applications. Due to these factors, researchers have focused on developing high strength, high conductive and corrosion resistance material for BPPs.

2.4.2 Composite Bipolar plate

Composite materials are a better alternative to graphite plates because of their superior chemical (corrosion resistance) and physical (ease in machining) properties. Such composite materials are manufactured by moulding graphite powder and polymer. The electrical conductivity and strength of the plate is dependent on the graphite. The polymer matrix makes the bipolar plate more flexible and protects it against corrosion. The polymers used for composite BPPs are polypropylene, polyamide, polyether sulfone, polypyrolene and polystyrene [33]. Electrophen is a trade mark composite material produced by Bac2 Ltd, Southampton, UK and is one of the first commercial BPPs to be manufactured on a large scale [34]. Dhakate et al. [35] and Thongrunag et al. [36] identified that the electrical conductivity of composite plates could be increased by adding graphite; however the flexural strength of the bipolar plates (BP) decreases with increasing graphite due to the voids formed when the polymer proportion is not sufficient. Scholta et al. [37] noted that a low cost composite BPP, which shows stable performance during the 120h test, has been developed by SGL Technik Gmbh. No corrosion or leaching of composite material was reported during the testing period. One of the main disadvantages of composite BPPs is the low electrical conductivity, because of the addition of polymers. Ben Hu et al. [38] fabricated a composite BP with 5wt% multi-walled carbon nanotubes, 35% graphite and 60% polyvinylidene fluoride which exhibited electrical conductivity of 161.57 S/cm and area specific resistance of 7.5mΩ cm^2. However, due to the cost of carbon nanotube or graphene, their use as a BPP is restricted because of the need for a low-cost mass producible material.

2.4.3 Metal Bipolar plate

In recent years several researchers have been developing metal BPPs to reduce the cost and time required to manufacturing the fuel cell stack. The weight and power of the stack helps us to identify its field of application (Transportation/portable/stationary). The excellent electrical and thermal conductivity of metal plates makes it a better choice for BPP and also the flow channels can be formed easily on the metal plates. Even though metal plates have properties that are

similar to graphite, it prone to corrosion in the harsh fuel cell working condition where the pH is around 2–3 [39]. Titanium (Ti) and Stainless steel (SS) are the preferred materials by automobile manufacturers for making BPP due to their better corrosion resistance and formability. But the BPP needs to be coated with a protective coating to resist corrosion in long-term operation, as the formation of an oxide layer on the surface of the plates predominate in acidic environment. Corrosion increases the ICR with the GDL and decreases the output power of the fuel cell. Apart from that, corrosion in the metal plates leads to release of metal ions (chromium, nickel, iron) into the MEA, these metal ions affects the reaction at the three phase interface thereby reducing the fuel cell performance by poisoning its catalyst [40]. A coating of noble metal like gold or platinum or their alloys on the stamped metal substrate works excellently but these are expensive [41]. Figure 8 below shows the Treadstone technologies Inc. coating which comprises non-conductive corrosion resistance material TiO_x followed by conductive nano gold dots. Several non-noble metal or carbon-based coating are studied for long term operation of a fuel cell without sacrificing the performance.

Figure 8: Treadstone technologies coating on Ford bipolar plate

Unlike potential-free corrosion, BPPs are exposed to a constant potential closer to -0.1 V vs RHE and 0.8 V vs RHE in the anode and cathode respectively in an acidic environment [42] along with the temperature of 80°C which makes the metal plates prone to corrosion. This problem can be solved by coating with a protective layer which can help to resist corrosion and improve the electrical conductivity.

2.5 Corrosion Behaviour in bipolar plates and types of corrosion

Metal plates are prone to corrosion under fuel cell working conditions due to the low pH value and temperature. The BPPs are simultaneously exposed to both anodic and cathodic reactions. Stainless steel and titanium are commonly used as base material for fuel cell bipolar plate application. The reaction behaviour of Fe (iron) and Ti (titanium) is shown below)

$M \rightarrow M^{n+} + ne^-$ (anodic reaction)

$O_2 + 2H_2O + 4e^- \rightarrow 4OH^-$ (Cathodic reaction)

The catalytic activity is increased by maintaining the fuel cell at around 60-80°C. Increase in temperature leads to increase in corrosion rate due to electrochemical reaction. But also, increasing temperature may evaporate the electrolyte (water) which may decrease the corrosion [43]. However, decreasing the relative humidity will dry the membrane and this will eventually affects the fuel cell performance.

Pourbaix diagram helps to understand the relation between the potential for any metal and pH, where the horizontal line represents the reaction involving only potential, the angled line represents reaction involving both pH and potential, and the vertical line represents by-reaction influenced by pH. It also illustrates the range of pH and potential where a passive layer forms over the metal surface protecting it from corroding further.

Figure 9 illustrates the relation between pH and potential for iron, and it can be seen that iron can become corroded at both the anode and the cathode due to the formation of Fe^{2+} and Fe^{3+} respectively in the pH range 0-3.5 [44].

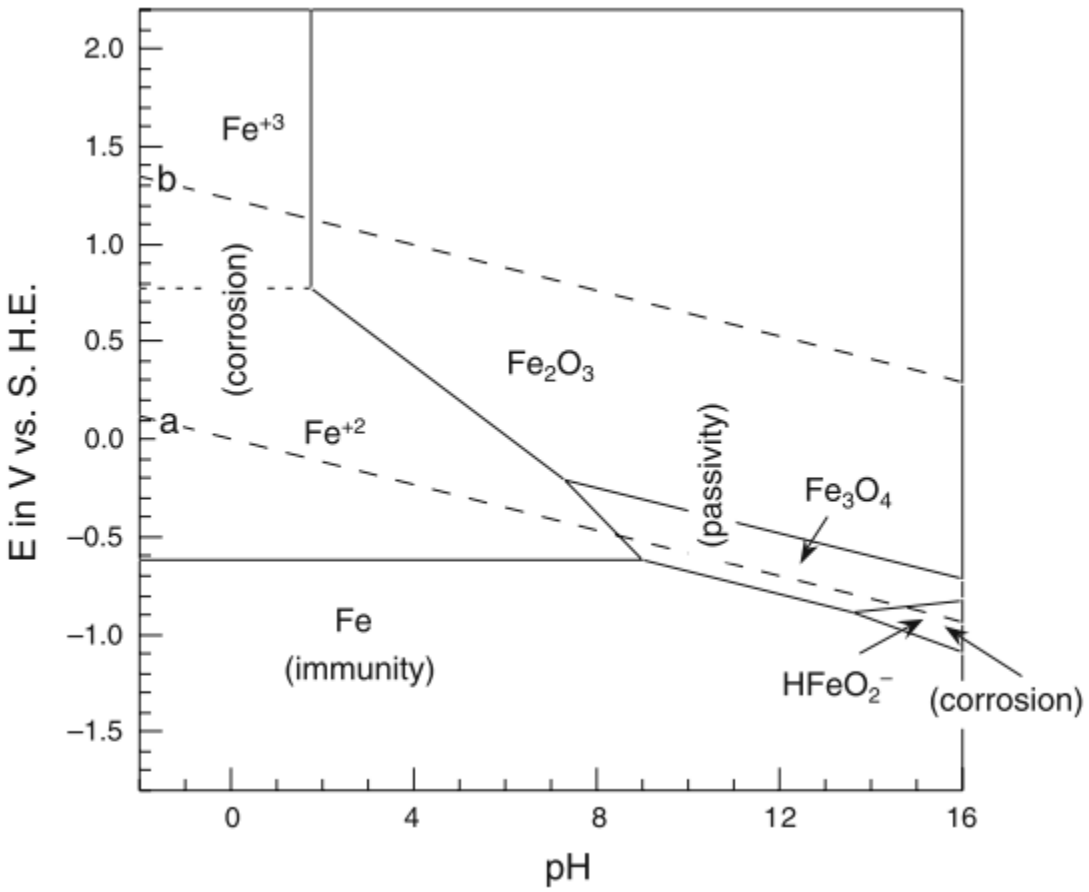

Figure 9: Pourbaix diagram for Fe-water system [44]

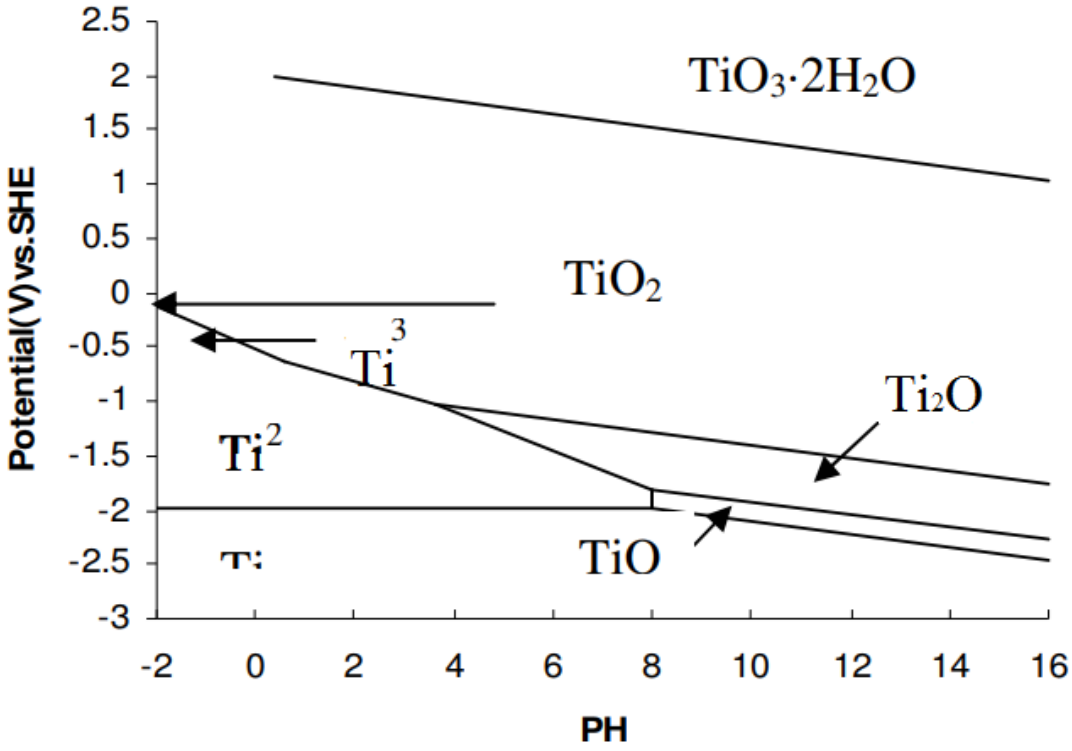

Figure 10: Pourbaix diagram for Titanium [44]

It is understood from the Figure 10 that the Ti metal forms TiO_2 in both at anode and cathode potential which prevents the base metal from corrosion but this passive layer decreases the surface conductivity of the BP.

2.5.1 Types of Corrosion in BPP

The most common forms of corrosion that take place in BPPs are pitting and crevice corrosion. The pitting is a localised corrosion due to the breakdown of protective coating or oxide layer formed. This breakdown of protective layer may be due to improper coating technique, morphology, or adhesion of the metal coating to the surface. Oxygen depletion occurs at the initiated pit, and it acts as a localised anode due to the change in potential. Anode current density will be high and rapid corrosion occurs due to the difference in the size between anode and cathode. The pit grow deeper inside the metal and creates permanent damage to the base metal [45].

Crevice corrosion is like pitting but it takes place due to the stagnation of water produced in the fuel cell. The water formed in the fuel cell can be contaminated with metal ions and corrosive ions (fluorine ions) released from the membrane. Crevice corrosion occurs when the contaminated water stays in-between the GDL and the BPP which increases the metal ion concentration near the plate. The pH is reduced in this area due to the hydrolysis of the metal ions which further increases the corrosion [46]. Galvanic corrosion occurs when two conductive surfaces (BP and GDL) are connected together and one is nobler than the other. Carbon GDL is nobler than any metal plate which tends to corrode in the acidic fuel cell electrolytic environment [47].

2.6 Coating for metallic bipolar plate

Metal plates have excellent mechanical strength, thermal and electrical conductivity. The metal BP can be easily formed to desired shape through a stamping process which is cheaper than other BP fabrication techniques. However, bare metal plates get corroded easily in PEMFC environments and the metal ions can leach into the membrane thereby affecting the FC performance. Furthermore, the resulting oxidation layer formed will increase the contact resistance between the BP and GDL. Therefore, several metals including titanium, stainless steel, aluminium, and nickel have been

investigated as base materials for BP uncoated and with protective coating as coating as discussed below.

2.6.1 Bare metal plate

Due to the excellent electrical conductivity, superior corrosion resistance and easy formability, titanium and stainless steel are preferred as base metal for a BPP. Presence of chromium and nickel in austenitic Stainless Steel (SS316L, SS304) makes them a better base metal for BPP [48]. The fuel cell performance of a uncoated SS316L plate is studied by Miyazawa et al. [49] in a 300 hrs test and showed that the oxide layer formation (Fe+) decreases the conductivity between GDL and BP, and consequently degrades the fuel cell performance. Davies et al. [50] studied the corrosion behaviour of the SS316L, SS310, and SS904L. It has been found that, the corrosion resistance depends on the alloy content. Grade SS904L, which contains more chromium and nickel content compared to other stainless steels, showed less contact resistance. Silva et al. [51] investigated the influence of oxide film composition on electrical conductivity of SS304, SS3016L passive layer. Wang et al [52, 53] found that both austenitic SS349TM and ferritic AISI446 stainless steel with higher chromium content showed better corrosion resistance and they also verified the formation of a chromium oxide passive layer which increases the ICR in the long run. Wang et al [54] developed a light weight BP using titanium sheet as a base metal due to its low cost. Soma et al [55] found that the charge transfer resistance and contact resistance of a titanium BP is high at the cathode potential of 0.64V, whereas it is opposite at anode potential of 0.36V for titanium bipolar plates in a simulated fuel cell working condition. The surface oxides layer of Al, Ti, Cr, Ni etc. form a passive layer which increases the corrosion resistance but increases the ICR with GDL. So a protective coating is essential for long run of stack without compromising the fuel cell performance.

2.6.2 Noble metal coating

Gold and platinum can be used as a protective coating for BP as they have superior corrosion resistance and high electrical conductivity, but they are expensive, and require sufficient thickness of the coating to protect against corrosion. Wang et al.[54]

reported that the resistivity of the oxide film formed on the gold (Au) coated titanium plate is significantly less for non-noble metal coatings and they highly recommended it for portable applications as it has weight of just 175gm per BPP and contact resistance of 0.0013 Ω. Li et al. [56] studied the electrochemical performance of a silver (Ag) coated SS316L plate in the acidic environment (0.5M sulphuric acid, 2ppm of hydrofluoric acid at 80°C) and concluded that the passive layer of the Ag coated plate is reduced by 1nm compared to uncoated SS316L plate. This coating showed stable performance and acts as a barrier to decrease the ion leaching into solution, whereas the bare plate leached a large quantity of Fe, Cr, and Ni into the solution. Yu Fu et al. [57] coated Ag-PTFE (silver-polytetrafluoroethylene) composite film on SS316L and reported that defects on Ag-PTFE surface are greatly reduced compared to pure Ag coating and the ICR, corrosion resistance are par with pure Ag. Yoon et al.[58] coated 2nm of gold as a top layer for zirconium nitride coating on SS316L substrate and it showed a significance decrease in the contact resistance, however the thickness of the gold coating has to be greater than 10nm to completely protect the surface against corrosion. Ihonen et al. [59] coated platinum on a SS substrate and noted that the ICR of the Pt coated sample was reduced drastically compared to bare SS. However, in the long-term test, corrosion was evident in the anode and the author noted that if the coating thickness is too low, it will lead to localised corrosion. Wind et al [60] compared the performance of the gold coated SS316L and graphite BP. Almost no deterioration of voltage has been found after running the fuel cell for 1000hrs, which shows that the oxide layer formed on the surface of sample is too thin to affect the ICR of the cell. Similar results for Ag coated substrate is reported by Hentall et al. [61]. Due to the high cost of coating with noble metal, researchers have focused on developing other non-noble coating for BPPs.

2.6.3 Nitride coating

Some of the widely studied nitride-based coatings for BPP applications are titanium nitride, chromium nitride, zirconium and tantalum nitride, and multi layer coatings consisting of a combination of two or more coatings. Metal nitrides are known for superior chemical inertness, superior thermal conductivity and metal-like electrical conduction, which make them a promising coating for BPP applications. Chromium nitride (CrN) has been widely studied for cutting tools, stamping dies and moving

parts due to its excellent wear resistance, adhesion to substrate and toughness [62]. It can be produced through PVD [63] and arc ion plating [64] and it has been widely studied as BPP coating material. Pozio et al. [65] coated SS 304 and its lower carbon version, SS 316L, with CrN film using the PVD process and its performance in acidic environment was compared with the DOE target for corrosion resistance and electrical conductivity. It was found that CrN did not satisfy the DOE target of less than 1 µA /cm^2 for corrosion current density and electrical resistance of 10 mΩ cm^2 [66]. Cr_2N was coated on a polished SS316L sheet of 2mm thickness by the thermal nitriding process and an ICR of 50 mΩ cm^2 at 1.5Mpa and corrosion current density of 1.77 µA /cm^2 at 0.60V was determined by Nam and Lee [67]. Fu et al. coated and tested three different types of Cr_xN ($Cr_{0.49}N_{0.51}$ to $Cr_{0.43}N_{0.57}$) in a simulated PEMFC environment. The resulting corrosion current density in the electrolytic bath of 0.5M H_2SO_4 + 5ppm HF at 70˚C was 5 µA /cm^2 and the contact resistance 10 mΩ cm^2 at 1.2MPa compression force. Wang et al. [68] used the EBPVD process to coat TiN, CrN and TiAlN onto SS316L. From the results they claimed that of all the coatings TiAlN shows low contact resistance and poor corrosion resistance. The performance of coating in the order of contact resistance are TiAlN < CrN < TiN < SS316L and in the order of corrosion resistance in anode environment are TiN > CrN > SS316L > TiAlN and at cathode environment are SS316 > CrN > TiN > TiAlN. Park et al. [69] examined a multilayer CrN/Cr coating on STS 430 for DMFC. The performance of the coated sample showed superior corrosion resistance and higher protective efficiency under various simulated conditions. The ICR of CrN/Cr layer showed a significant decrease which indicates that CrN/Cr coated is a suitable DMFC BPP coated material. However, after recirculation the performance of coating degraded due to pitting corrosion induced by corrosion media through pinholes. Changhee et al. [70] coated a thin layer of tantalum nitride (TaN) onto the surface of SS316L by ICP (Inductively Coupled Plasma) assisted reactive magnetron sputtering at various nitrogen flow rates. The corrosion and electrical properties of the coating was examined in simulated fuel cell environment. The outcome of potentio-dynamic polarisation tests in cathodic and anodic conditions showed that the corrosion current density at anodic condition (-0.1 V) is 10^{-8} A cm^{-2} and at the cathode (0.6V) 10^{-7} A cm^{-2}, while the ICR at 150 N cm^{-2} is 11 mΩ cm^2 which is better than for bare SS316L. Zirconium nitride (ZrN) has several interesting properties like hard wearing

resistance, and high corrosion resistance. Coating ZrN through the PVD process is difficult since Zr has higher melting point, is sensitive to contamination and has a lower vapour pressure. Larijani et al.[71] coated ZrN by varying the nitrogen flow rate and suggested that corrosion resistance increases with formation of preferred (111) crystalline orientation which is predominant at higher nitrogen flow rate $F(N_2)$(80% Vol). At this high flow rate, the thickness of the formed film will be thin and it will lead to pitting or localised corrosion.

Titanium nitride (TiN) is one of the widely studied coatings for PEMFC applications due to its superior chemical inertness, high electrical conductivity and cost effective coating process. Yashiro et al. [72] coated TiN onto a SS310 surface to protect against corrosion. From the result it is understood that the corrosion current density and ICR were improved compared with bare SS substrate. Jin et al. [73] coated approximately 0.20 µm of TiN onto different types of aluminium BPPs using the DCRMS (DC reactive magnetron sputtering) PVD process and their result validated that TiN coated on A356 (aluminium) BPP shows better surface qualities such as smaller ICR and superior corrosion resistance than for bare BP. Zhang et al. [74] deposited TiN on SS304 through two different coating processes, pulsed bias arc ion plating and magnetron sputtering. The ICR of TiN and Ti_2N/TiN were 25 mΩ cm^2 and 26 mΩ cm^2 respectively and the corresponding corrosion current densities were 0.0131 µA /cm^2 and 0.0145 µA /cm^2.

Similar research by Jin et al. [75] used SS304 bipolar plate as substrate and coated with TiN, CrN and CrN/TiN. The flow channel on the SS plate is formed through the rubber forming process and channel depths greater than 0.3mm are formed through this process. The ICR of CrN/TiN, TiN, CrN and were 23.5 mΩ cm^2 , 10.2 mΩ cm^2, and 26.4 mΩ cm^2 respectively at compaction force of 145 Ncm^{-2}, while the respective current densities in a single cell setup were 0.670 mA /cm^2, 0.623 mA /cm^2 and 0.656 mA /cm^2. This shows that TiN has higher corrosion potential and lower corrosion current density than other nitride-based coatings.

2.6.4 Carbon-based coatings

Graphite has been used as a BPP material for the past few decades due to its exceptional high electrical conductivity and chemical inertness. But against that, there are the properties of gas permeability, brittleness, heavy weight, poor machinability and high cost which make it a poor choice for fuel cell. Therefore, depositing carbon/carbon-based material onto metal substrate can be a good alternative for graphite based BPP, as metal has superior electrical conductivity and higher strength. Formation of an oxide layer on the surface is the only problem associated with metal plate, which can be overcome using a carbon based coating. The electrical conductivity and chemical inertness of the carbon is completely dependent on the hybridisation. Carbon atoms can exhibit in one of three types of hybrid orbitals ($sp/sp^2/sp^3$). Out of its six electrons, four occupy the outer shell, two in s and two in p orbital, which bind in three different ways as mentioned above. In sp^1 hybrid orbital, two of four outer electrons enter σ orbital's, each forming a σ bond and the other two enters the 2p orbital to form weak π bond in the y and z directions. In the threefold coordinated sp^2 hybridisation, three of the four valance electron in s, p_x and p_y orbital form a hybrid orbital and the angle between orbital's is 120˚, which forms three σ bonds in plane and one π bond perpendicular to the plane. In the sp^3 hybrid orbital, all four valence electron participate in sp^3 hybridisation tetragonally leaving no π bond formation, which makes diamond a bad electrical conductor. The electrical conductivity of a bipolar plate can be enhanced by depositing carbon with more sp^2 hybridised carbon atoms.

In the aspect of carbon based coating, carbon polymer composite, pure carbon coating, metal carbide coatings like TiC (titanium carbide, Cr-C (chromium carbide), ZrC (zirconium carbide) and NbC (niobium carbide) are widely investigated coating for BPP applications. The carbon polymer composite coating on metal substrate protects the metal from corrosion but the polymer increases the ICR. Lee et al. [76] deposited polypropylene (PP) composite on the aluminium substrate to protect the plate from corrosion. The PP act as barrier between the acidic electrolyte and substrate, but its electrical conductive is reduced drastically due to its contact resistance. Even if carbon black and carbon paper are added to the interface, the ICR is still far from satisfying DOE target due to the PP addition. This makes pure carbon

or carbide coating a better choice for bipolar plate coating. There are few carbon composite bipolar plate materials that can satisfy the DOE targets for ICR and corrosion resistance. Du et al. [77] used compression moulding technique to fabricate a bipolar plate which comprises 50 wt% epoxy resin + 50 wt% expanded graphite which satisfies the DOE target. Huang [78] and Liao [79] developed carbon composite plates using a mixture 23 wt% polyphenylene sulphide + 70 wt% graphite + 7.0 wt% carbon fiber and 30 wt% vinyl ester resin + 70 wt% graphite + 2 phr multi-walled carbon nanotubes respectively which satisfies the DOE target for ICR and corrosion resistance but metal based BPPs are still considered as a better alternative to graphite due to the ease of manufacturing.

Chung et al. [80] deposited carbon film on a SS304 substrate by CVD (Chemical Vapour Deposition) at 680°C using an acetylene/hydrogen mixture. The fuel cell performance, ICR and corrosion resistance of the coated carbon are similar to graphite plate. This shows that coated carbon has excellent corrosion resistance and less electrical resistance. Fukutsuka et al. [81] used SS304 substrate and coated the surface with pure carbon using PACVD (Plasma Assisted Chemical Vapour Deposition). The coated plate shows high electrical conductivity and superior corrosion resistance compared to bare substrate. Feng et al. [82] deposited a CrN/C multi layer coating using CFUMSIP (close-field unbalanced magnetron sputtering ion plating) to protect the surface of the substrate corrosion. The coated film showed superior chemical inertness and had a very low ICR value of 2.6-2.9 $m\Omega\text{-}cm^2$ at a compression force of $150N/cm^2$ which is better than graphite plates. Bi et al. [83] synthesised a multilayer coating ZrC/a-C using magnetron sputtering to increase corrosion resistance and decrease the contact resistance. The ICR value can be decreased by coating pure carbon on the outer surface, which is due to the similar physical property of GDL. The corrosion density was measured as 0.49 $\mu A\ cm^{-2}$ at cathode potential 0.6V (vs SCE) which is within the DOE target of 1 $\mu A\ cm^{-2}$. The ICR value was measured after potentio-static test under both anode and cathode conditions; the values were 3.82 $m\Omega\text{-}cm^2$ and 3.92 $m\Omega\text{-}cm^2$ respectively. Bi et al. [84] tested three different seed layers, Cr, Ti and Nb to increase the a-C coating adhesion. From their results it was shown that Cr seed layer promotes sp^2 hybridised carbon growth on the outer layer. Gou et al. [85] successfully coated a ternary coating consisting of Nb-Cr-C using arc ion plating on titanium substrate. The coating obtained was 500 nm thick and the

corrosion current density was 0.022 µA cm^{-2} and 0.051 µA cm^{-2} at the cathode and anode environments respectively. The ICR value is lower at 1.15 mΩcm^2, which shows that the coating is superior to bare Ti. One of the interesting analyses which has not been done in most of journal papers on substrate coating is the fuel cell performance in single cell setup. The results show the peak power density of 1.167W/cm^2 is obtained with the Nb-Cr-C coating. Wang et al. doped tungsten metal in the cluster of carbon to increase the corrosion resistance by passivating the surface. The coated plate performs better than SS316L bare substrate and the corrosion increases linearly for coating with more tungsten element. Even though most of the coatings satisfy the DOE target, the actual fuel cell performance of the coating was not tested in a single cell fixture to validate the result over the long term. Yi et al. [86] studied the performance of a-C coated SS substrate; studied the ICR, corrosion current density, fuel cell performance and life cycle analysis of 200hrs. Compared with bare substrate the coated plate showed superior performance and it satisfies the DOE target for ICR and corrosion current density.

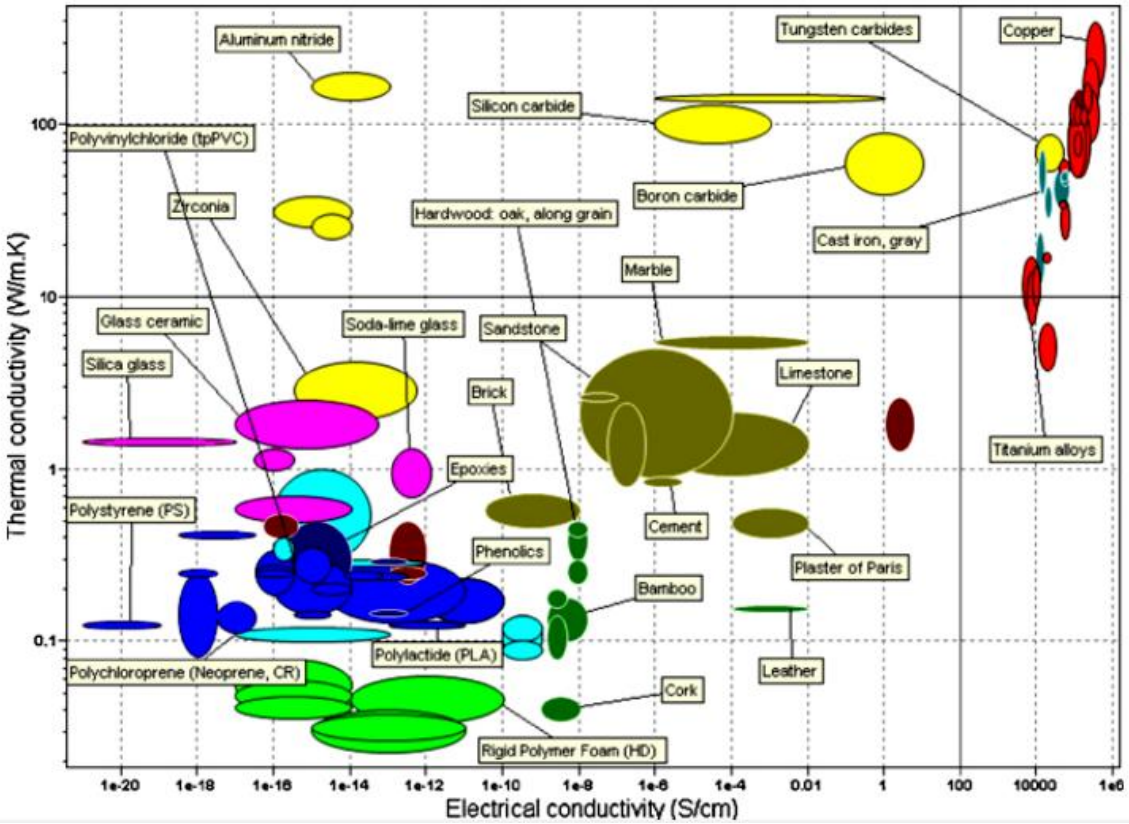

Figure 11: The thermal and electrical conductivity chart of different materials using Cambridge Engineering System software [87]

One of the basic requirements for a material to use as bipolar plate either by itself or as coating is to have high electrical and thermal conductivity. Oliveira et al. [87], used the Ashby chart to categorise material with high electrical and thermal conductivity as shown in Figure 11. Tungsten carbide is one of the exceptional ceramic materials which has high electrical and corrosion resistance and has the potential to satisfy the DOE target for BPP coatings.

In this research, Titanium Nitride, pure a-C carbon and Tungsten carbide carbon are coated using physical vapour deposition and their ICR, corrosion resistance in acidic medium and surface morphology are compared. From the peer review, it is understood that only a handful of literature is available on carbide or carbon based coating while no report on tungsten carbide carbon as bipolar plate coating in fuel cell environment has been identified.

2.7 Coating Methodology

The desired material can be coated using different coating techniques. Some of the commonly used techniques for coating BP are discussed below. The properties of the coatings are strongly influenced by number of microstructural factors like size and shape of grains, defects, porosity, presence of pin holes and cracks.

2.7.1 Electrodeposition

Electrodeposition is based on the principle of electrolysis, where the substrate or metal to be coated is connected to negative terminal of the power supply (cathode) and the plating metal is connected to the positive terminal (anode) of the power supply. During the deposition process, the metal ion in the salt bath is used up. If the plating metal is used as anode, the metal dissolves at the same rate as metal deposited to substrate at the cathode. The bath must be refilled with metal salt if the anode is made of different metal and the thickness of the coating is depending on the coating duration. Li et al. [88] coated TiN electrochemically on SS316L substrate for a PEM fuel cell. The coated sample shows promising interfacial contact resistance and corrosion resistance compared with bare substrate in the simulated acid environment, but a slight increase

in the ICR was observed after the potentio-static test, which is due to the passive layer formed on the surface of TiN-SS316L. Wang et al. [89] electroplated Chromium-Carbon on SS304 which offers excellent corrosion resistance and electrical conductivity. The deposition was conducted under different current densities and it was found that the carbon content in the composite decreased with increasing current density. Micro cracks were observed for samples coated for long duration. Jiang et al. [90] successfully deposited PPY (Polypyrrole) with different GO (Graphene oxide) contents on SS304 to enhance the coating adhesion and corrosion resistance in the simulated fuel cell environment. It was found that the composite coating with 1 $mgmL^{-1}$ of GO had better compact structure with few micro cracks. Garcia et al. [91] coated polypyrrole electrochemically on SS304 to study the corrosion protection provided by a conductive coating. The polarisation curve for the coated sample after immersing it for 1, 3 and 24 hrs in 0.1M sulphuric acid at 60°C and room temperature was determined. The corrosion current density diminished up to 2 orders of magnitude and 4 orders of magnitude for sample tested at room temperature and 60°C. However, the coated sample shows same level or less resistance to corrosion as bare SS304 due the loss of passivity. The major disadvantage of electrodeposition is the concentration gradient at the reaction which leads to the unequal loading, and the disposal of waste generated during the process is difficult and a risk to the environment [92].

2.7.2 Spray coating

Air brushing and thermal spray are two different coating techniques using similar devices, except combustion or an electric arc is used in the latter as a source to melt and fuse the coating material to the substrate. Air brushing is capable of self-cleaning, is suitable for large size substrate and has low cost. Susanna et al. [93] obtained very thin coatings of 270nm thickness and 80nm of surface roughness using the air brushing method. The pressure was maintained between 70kpa and 125kpa and the target distance was maintained between 100 and 180mm with temperature varying from ambient to 70°C and duration of spraying 30sec. Husby [94] used air brushing to coat graphite and carbon black mixed with epoxy with the hydrophobicity of the coating being improved by adding Teflon. The air brush is used to spray the coating which is thinned with xylene and the substrate was pressed in a Carver hot press to decrease the porosity. The contact resistances measured at compression pressure 145N/cm^2 was

11.3 and 10.6 mΩ cm^2 respectively and the resistance increases drastically after electrochemical testing.

Madadi et al. [95] used HVOF (High velocity oxygen-fuel) coating technique to produce NiCrBSi, NiCr, and (Co,Ni)CrAlY. Potentiaodynamic test and ICR of material was studied to find the best performing coating. The ICR value of NiCrBSi is on a par with graphite plate and EIS (Electrochemical Impedance Spectroscopy) value is higher than the other two coating. Gago et al.[96] coated pure Ti on SS bipolar plate to use in a PEM electrolyser. The vacuum plasma spraying technique is employed to coat a dense titanium coating using 21.27MJ of plasma enthalpy and obtained a corrosion current density of $1.10x10^{-5}$ A cm^{-2} which is a better value but still didn't reach the DOE target. Rendon-Belmonte et al [97] deposited Cr_3C_2(NiCr) on S4400 using HVOF thermal spraying. The corrosion resistance of the plate increased due to the presence of chromium in high content. One of the important criteria to consider for any coating for PEMFC is the behaviour of the coating in cathode environment. Even though Cr_3C_2(NiCr) corrosion performance is encouraging, the surface analysis made after corrosion test shows that the coating depletes in the long run, which in turn affects the fuel cell performance. Spray coating has various advantages like being environmentally friendly with a wide selection of substrate and coating materials, but its major disadvantage is porosity which exposes the base metal in acidic environments [98].

2.7.3 Vapour Deposition

The technique by which the coating material is vapourised and coated onto the substrate can be classified as a vapour deposition method but each of those differs in terms of physical process. The PVD is one of the widely used techniques which uses solid coating material (target) and the temperature of the substrate is maintained low (<300°C). The coating process is carried out in high vacuum and the sputtering source is maintained at a high negative potential. The metal to be coated is evaporated by heating or bombarded using Argon gas. The ejected ions form a compound with reactive gas and condense on the substrate and the coating uniformity is maintained by rotating the substrate holder. Sputtering, Ion plating and Arc evaporation are some of the PVD processes. CVD is similar to the PVD process, but the coating material is

introduced in the form of liquid or gas into the coating chamber and the deposition happens at high temperature (500-1000°C). Zhang et al. [99] used Arc ion plating to coat Ti-Ag-N nanocomposite onto SS plate and found that corrosion resistance and conductivity of the plate were improved. The coated plate had corrosion resistance of 2 $m\Omega cm^{-2}$ and lower ICR at 140 Ncm^{-2}. Zhang et al. [99] also conducted another investigation to enhance the performance of SS316L by coating $CrN_{0.86}$ film which has limited the ICR to 8.8$m\Omega$ cm^{-2} and corrosion current density to 0.1 μAcm^{-2} [100, 101]. From this study, it can be concluded that high film density produced using arc ion plating was the major factor that improved the performance of the bipolar plate.

The coating resulting from PVD processes are harder and have superior corrosion resistance to electroplating [51]. The corrosion current density of the vapour deposited coated sample was 0.00029 μA cm^{-2} which is very much less than the electroplated coating at 1.9 μA cm^{-2}. The vapour deposited process is more environmentally friendly and the coating properties like adhesion and uniformity are better than for other processes [39].

Due to these advantages all the coatings in this research work are coated through vapour deposition. There are two types of manufacturing possibility to produce finished BPP. One is through pre-coating and other is post-coating. In pre-coating, the protective layer is coated before stamping process, whereas, in post-coating, the coating is deposited after stamping. Pre-coated plates are the preferred material by tier 1 automotive manufacturers due to simplicity and cost reduction in handling. Sandvik and Impact coatings are the some of the companies supplying pre coated bipolar plates. Even though this technique reduces the complexity, the main concern about pre-coated plates is that they are more likely to get damaged during the stamping process. Another disadvantage of pre-coated material is the exposure of base metal while cutting bipolar plate to desired shape and punching input/outlet holes for allowing reactant gas to the reaction site. The post coated plates are less likely to suffer from the above issues and the cost of production can be improved by large scale coating [102]. In this study the desired coating is coated on the monopolar plate which has passed through forming process.

2.8 Focus of this research

From the literature review it is understood that fuel cells can be a promising alternative source of power for the transportation sector and the major limitation for the wider adoption is also discussed. This research work is focused on development and characterisation of coating material for current collector/separator/bipolar plate for PEMFC.

Conventionally used graphite plates have major disadvantages like high cost, low mechanical strength, and poor machinability. Metal BP can be a better alternative to graphite due to good electrical and thermal conductivity, formability, and mechanical stability. But metal plates are prone to corrosion in the PEM fuel cell condition which leads to leaching of metal into MEA. This will impact the electrochemical reaction and also forms a passive layer on the metal surface, eventually affecting the fuel cell performance. Therefore, metal plates need a protective coating to resist the corrosion and increase the electrical conductivity.

In this dissertation, titanium plate is used as a base metal/substrate and three different coatings TiN (Titanium Nitride), Amorphous Carbon coating (a-C) and metal carbide carbon coating (WCC-Tungsten Carbide Carbon) are investigated to find its potential as bipolar plate coating for PEMFC. Surface Electrical conductivity and corrosion performance of both the metal free and metal carbide coatings are compared with TiN, one of the most popular coatings studied in the FC research community. All three coatings are deposited through PVD process, and their surface properties are analysed using SEM, EDX, XRD and XPS. The electrochemical behaviour of the coating is studied through a potentiostatic test which is conducted in a highly acidic electrolyte to accelerate the corrosion. The contact resistances between electrode and coated plates are obtained through the ICR measurement setup. The protective coating which performs better in the above-mentioned analysis is coated on the stamped plate and the actual fuel cell performance is measured using fuel cell test station.

Research Gap:

1. The need for non-noble metal coating is immense as most of the major automakers use noble metal coatings as BPP material.
2. It is understood that not much study involved using carbon or carbon-based material as coating for BPP.
3. Only few reports discuss the performance of the coating in actual fuel cell environment apart from performance at simulated condition.
4. Very few literatures are available which discuss the long-term performance of BP in fuel cell environment.

Objectives of this research are to:

1. Find a novel non-noble coating material for bipolar plate
2. Produce a coated metal plate that satisfies the DOE-2025 target for corrosion resistance and ICR of bipolar plate
3. Compare the corrosion resistance and electrical conductivity of Titanium Nitride, Tungsten carbide carbon and pure carbon coated plates to find the suitable coating for fuel cell application
4. Design forming tools and fabricate a monopolar plate successfully without cracking
5. Analyse the long-term fuel cell performance of the coated material.

2.9 Closure

This literature review helps to understand that bulky, costly, brittle graphite plates need to be replaced with thin stamped metal plates. As the metal plates are prone to corrosion in fuel cell environment, a protective coating is necessary to increase the surface electrical conductivity. The nitrides, carbides and carbon based coatings are widely studied due to the superior corrosion resistance and high electrical conductivity compared with composite and pure metal based bipolar plate. In this study, TiN is coated on the titanium substrate rather than on SS to avoid the crystal mismatch. The technique used is cathodic arc deposition. Due to the reason that TiN is commonly studied nitride coating; its performance in highly acidic environment

through potentiostatic corrosion resistance test and ICR at 145 N/cm^2 is compared with other carbon based coatings.

Tungsten carbide carbon (WCC) is chosen as another coating material which is known for its hardness and widely used as cutting tool material. Its electrochemical performance, elemental composition and contact resistance are compared with pure amorphous carbon coating. Even though carbon based coatings have been studied before, most of the papers report the performance evaluated in a simulated fuel cell environment using small sized sample. It is worthwhile to study the performance of coatings in an actual fuel cell environment and test the lifetime in a single cell stack.

CHAPTER 3: RESEARCH METHODOLOGY

3.1 Introduction

From the previous Chapters, it is understood that PVD is an efficient method that can be used to coat the desired material for fuel cell application. In this chapter, the procedure and technique to deposit TiN, WCC and C are discussed, along with the methods to analyse the performance of the coating. The method of fabricating the stamped plate using forming tool is discussed in the last part of this chapter. The whole process from sample preparation to fuel cell performance is diagrammatically represented in Figure 12.

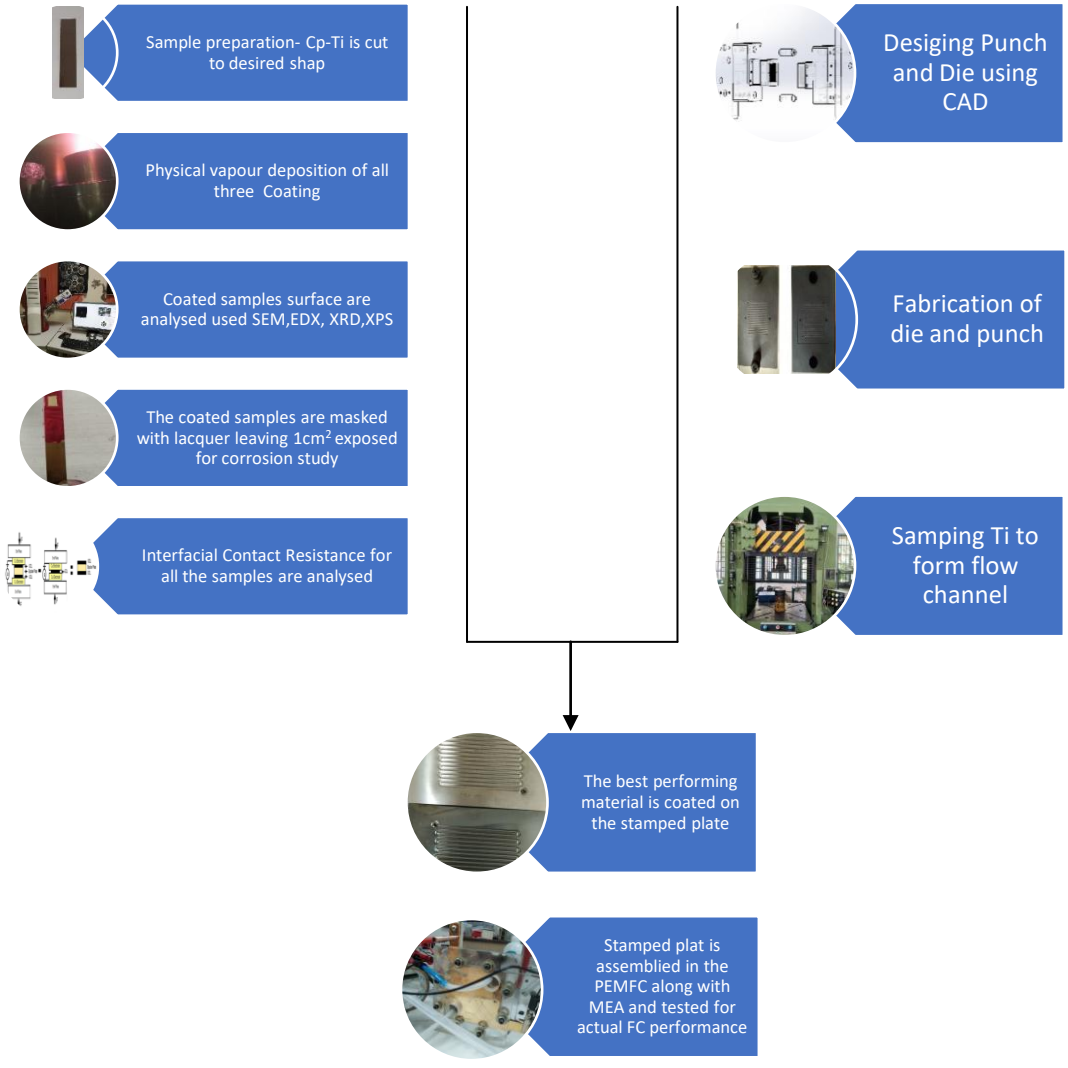

Figure 12: Schematic representation of process flow

The flow chart illustrates the process carried out to produce a coated monopolar plate

with a serpentine flow channel. Before coating and testing the stamped plate, a small sample of Cp-Ti (Base metal) is cut to 100mm*20mm*0.50 mm and tested in simulated fuel cell environment. Once the sample is prepared, it is loaded in the coating chamber and the desired material is coated through physical vapour deposition. SEM, XRD, XPS and Raman spectroscopy are used to analyse the surface of the coated sample. The corrosion current density of the coated sample is measured by masking the entire sample but leaving $1cm^2$ exposed to electrolyte. Once the corrosion study is completed, the examined area ($1cm^2$) is removed from the sample using a wire cutting method and the surface after corrosion test is studied. The ICR of the sample is measured before and after the corrosion test to determine the electrical resistance of the coated surface. In parallel, a forming tool is designed and fabricated. The design parameter for the die and punch is selected using ANSYS simulation. The monopolar plate with serpentine flow channel is produced by stamping a thin titanium sheet of 0.15mm thickness. The stamped plate is than coated with the coating that passes the DOE target for corrosion current density and ICR. The fuel cell performance of the coated monopolar plate is measured at the test station and also metal leaching into the MEA is determined after determining the long term performance of the BP in a fuel cell environment.

3.2 Base Metal preparation

The base metal for all the coatings is a Grade 1 Titanium (Cp-Ti) sheet of 0.50 mm*100mm*20mm. Before coating the material, the sheets are cleaned ultrasonically and blasted using Al_2O_3 to increase the coating adhesion by removing surface oxides. This helps to achieve uniform surface quality with fewer surface defects from the coating. The cleaned samples are mounted on a rotating stand inside the coating chamber. This process is repeated for all the different types of coatings.

3.3 TiN coated by PVD Arc method

The TiN is coated onto the sample using a cathodic arc deposition system. The whole coating process involves five stages: 1. Evacuating the coating chamber with a vacuum pump, 2.substrate heating to the required temperature, 3. substrate etching using Arc enhanced glow discharge (AEGD), 4. Depositing required coating and 5. Cooling the chamber before taking out samples. Once the desired vacuum pressure of $1x10^{-3}$ Pa was attained, the substrate was heated to 400°C. The negatively biased substrate is struck by positively ionised Argon gas which is accelerated at high voltage. This method of cleaning the substrate is AEGD (see above), and it helps to remove surface oxides, oils, and other surface impurities. Pure titanium (99.99%) is used as a target material. Before introducing the reactive gas into the chamber, a thin layer of titanium is coated onto the surface to improve the coating adhesion to the substrate. Nitrogen is used as a reactive gas, and it is fed at 500cc/m into the chamber as shown in Figure 13.

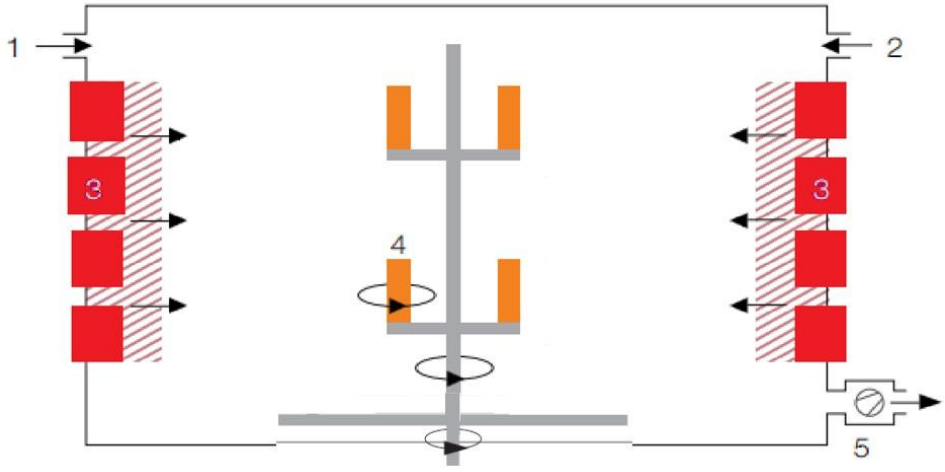

Figure 13: Cathodic Arc PVD coating setup (1. Argon gas input, 2. Reactive gas inlet, 3. Backing plate and coating material, 4. Substrate, 5. Vacuum pump)

3.4 WCC coated by PVD Sputtering method

Tungsten carbide carbon coating is prepared by DC magnetron sputtering. The cleaned sample is loaded to the rotation holder and the residual pressure in the chamber is set at 10^{-3} Pa. Unlike arc PVD coating, here the coating temperature maintained at low temperature i.e. below 250°C and the substrate holder is permitted for two-fold rotation. As a first step, the sample is cleaned using the AEGD process

and the chamber is flushed with argon gas for depositing the WCC coating. During the WCC coating process, both the argon and acetylene were allowed inside the chamber, and the DC power is applied to tungsten carbide targets to coat a 2.5µm thick WCC. Towards the end of coating the current to the tungsten carbide target is reduced to increase the carbon content on the surface which will helps to reduce the columnar defect/pinholes and also this helps to produce more WC than W_2C. The resulting coating is made up of carbon-hydrogen matrix with an infusion of tungsten carbide.

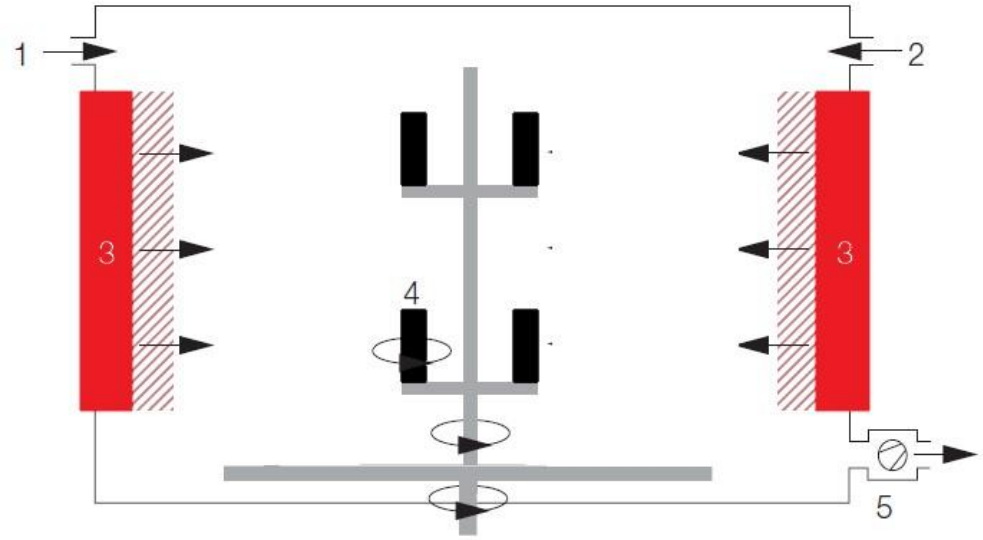

Figure 14: Sputtering PVD coating setup (1. Argon gas input, 2. Acetylene gas inlet, 3. Planar magnetron evaporation source and coating material, 4. Substrate, 5. Vacuum pump)

3.5 Pure Carbon deposited by PVD Arc method

Metal-free carbon is coated through a cathodic arc vapouriser PVD setup just like that used for TiN but the temperature of the chamber is maintained at less than 200°C. After the initial wet cleaning process, the samples are ion cleaned by the AEGD process. Due to the difference in the material property of a-C and titanium metal substrate, a thin layer of chromium is coated to increase the coating adhesion. The carbon coatings that were deposited without chromium interlayer fail the scratch test (done using tweezers). This poor adhesion of a-C on titanium substrate is due to

high internal stress developed by carbon coating. During the coating process, the high-energy ion bombardment can lead to the development of internal stress in the coating, which can cause the formation of microcracks and poor adhesion of the coating to the substrate. As a consequence, this can ultimately result in the failure of the coating [103, 104].

3.6 Potentiostatic Corrosion resistance measurement

The coated samples are masked with lacquer solution leaving 1cm^2 exposed as shown in the Figure 15. The corrosion resistance of the coating is assessed by conducting a potentiostaic test using an electrochemical test station (BioLogic Potentiostat-EC LAB). To mimic the fuel cell environment' the experiment is conducted using the electrolyte solution of 1M H_2SO_4 and 2ppm HF at 70°C; the pH of the electrolyte solution is made less than 1 to accelerate the corrosion rate. Since, the rate of oxide formation is more on the cathode than the anode [105], the test is conducted by maintaining the working electrode at 0.60V with reference to a calomel electrode and the oxygen is purged throughout the experiment. Figure 15 shows the setup for measuring the electrochemical corrosion resistance; the working electrode (1) is dipped into the electrolyte bath until the 1cm^2 exposed area is covered with electrolyte solution, the counter electrode (2) is a platinum wire and (3) is reference electrode (Ag/AgCl or calomel electrode). The temperature of the bath is maintained at 70°C using electronic hot plate. All the coated plates are subjected to corrosion test for 4 hrs, and their respective corrosion current densities are measured.

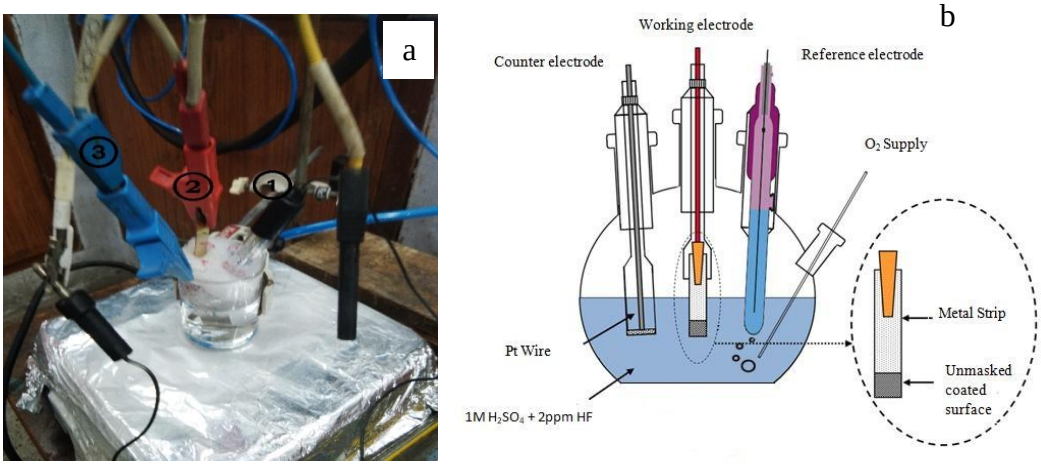

Figure 15 a.) Picture of Potentio-static test setup. b.) Schematic representation of Three Electrode System to find corrosion resistance of the coating (1. Reference electrode 2. Working electrode 3. Counter electrode)

3.7 Interfacial contact resistance measurement system

The ICR of the coated samples are determined using setup below shown in the figure 16, which is similar to that proposed by Wang et. al [52]. This experiment involves two setups, in setup 1 the metal sample is placed between the GDL (Carbon paper based Gas Diffusion Layer) and sandwiched between two polished copper plates, whereas in setup 2, only the carbon paper is placed between the copper plates which helps us to evaluate the contact resistance between the GDL and copper plates. A constant current of 1A is applied between the two-copper plates and the potential drop is recorded with respect to the increasing compacting force.

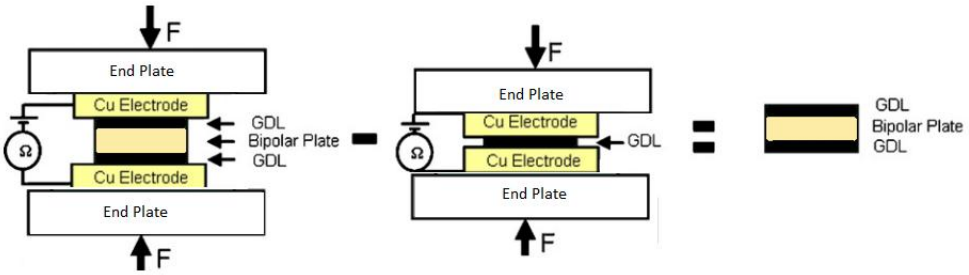

Figure 16: Calibration setup for finding interfacial contact resistance [106]

$$R_{Total} = [2R_{Cu} + 2R_{GDL} + R_{Bp} + 2R_{(Cu-GDL)}) + 2R_{(Bp-GDL)})] \ldots\ldots\ldots\ldots\ldots\ldots(1)$$

$$R_{(Bp\text{-}GDL)} = 0.5\ [R_{Total} - 2R_{Cu} - 2R_{GDL} - R_{Bp} - 2R_{(Cu\text{-}GDL)}\ ] \ldots\ldots\ldots\ldots\ldots\ldots (2)$$

R_{Total} = Total resistance

R_{Cu} = Bulk resistance of copper plate

R_{Bp} = Bulk resistance of BP

R_{GDL} = Bulk resistance of GDL

$R_{(Cu\text{-}GDL)}$ = Contact resistance between copper plate and GDL.

$R_{(Bp\text{-}GDL)}$ = Contact resistance between BP and GDL

In the setup 2, GDL is placed in-between the copper plates and calibration is repeated.

$$R'_{Total} = [2R_{cu} + R_{GDL} + 2R_{(Cu\text{-}GDL)}] \ldots\ldots\ldots\ldots\ldots\ldots (3)$$

$$R_{(Cu\text{-}GDL)} = 0.5\,[R'_{Total} - 2R_{Cu} - R_{GDL}] \ldots\ldots\ldots\ldots (4)$$

Substituting the value of $R_{(Cu\text{-}GDL)}$ in the equation 2 will give the interfacial contact resistance between GDL and BP.

3.8 Base material selection and Flow Channel Fabrication on metal plate for fuel cell testing

A bipolar plate requires several features to perform its function It needs to have a high electrical conductivity to reduce the ohmic loss and reduce the voltage drop across electrodes, high corrosion resistance, low gas permeability of reactive gases as the oxygen and hydrogen are supplied to opposite sides and should not get mixed inside the cell. The by-product of the exothermic chemical reaction in the fuel cell is water vapour. The overall efficiency of the fuel cell can be improved by rejecting heat from the system and this can be achieved through BP having high thermal conductivity.

Titanium (Ti) was chosen as the base metal for this study as it satisfies most of the qualities mentioned above. The formation of a passive layer on its surface under acidic conditions makes titanium a best choice for any corrosive environment however this oxide layer will drastically increase the ICR. For this reason a thin layer of conducting material is coated onto the titanium sheet to protect the surface from forming an oxide layer after the stamping process.

The Ti sheet used to produce flow channel is grade 1 (99.99%) Cp-Ti sheet, 0.15mm thick. The bipolar plate is formed by laser welding two monopolar plates back-to-back. Since this study is related to finding best surface coating for base metal, only the monopolar plate was fabricated, and the method to form the flow field on the titanium sheet was through a stamping process. From the literature it is evident that serpentine flow channel has better pressure drop and gas distribution to electrode than other flow field designs. In this work, a die and punch was designed to form serpentine channels covering the 50mm*50mm active area. The punch and die was designed using CAD (Computer Aided Design) and fabricated using the VMC (Vertical Machining Centres) and the radius on tools are achieved using the EDM

(Electron Discharge Machining). Figure 17 shows schematic representation of the stamped plate.

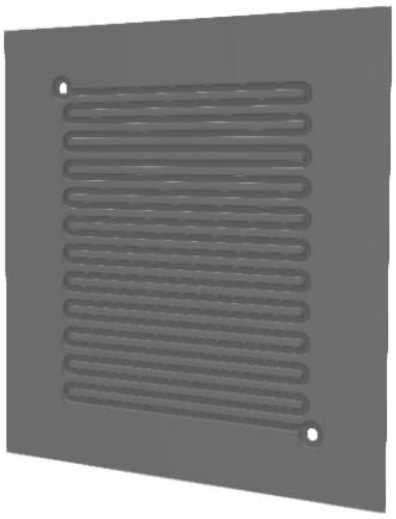

Figure 17: Schematic representation of Stamped monopolar plate

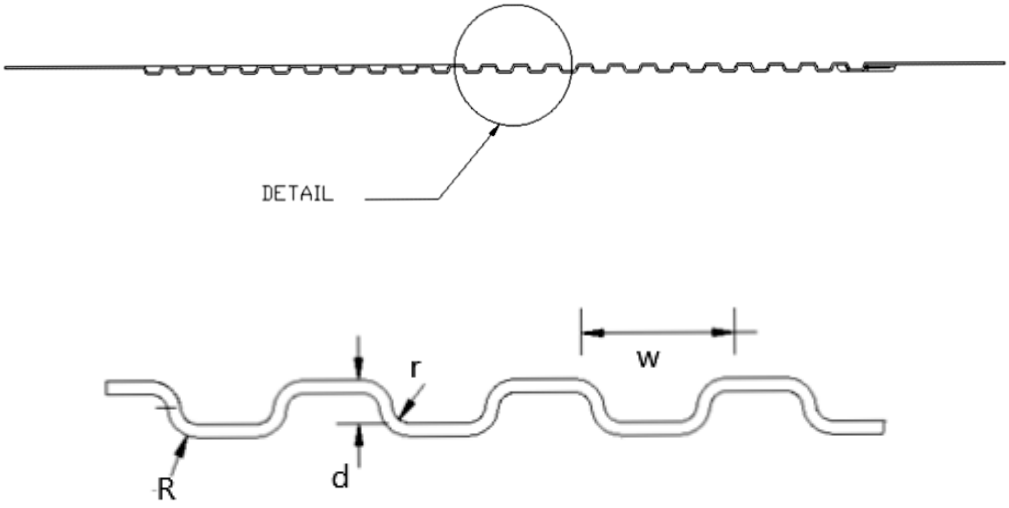

Figure 18: Diagrammatic representation of Cross-section view of Stamped metal plate

The geometry of the stamped monopolar plate is dependent on the parameters such as channel depth (d), width (w) and fillet radii (r and R). The dimensions of these parameters are dictated by the geometry of punch and die and the forming condition (pressure and lubrication). Hence the influence of the die and punch tool geometry on the sheet formability is assessed through metal thinning and equivalent strain. The equivalent strain of a monopolar plate fabricated with different tool geometries was

analysed through simulation and the design with lowest average strain at the critical spots (bends) considered for fabrication. The thickness of plate in the channel after stamping process has to be compared with simulation result.

3.9 Fuel cell Assembly and testing

The conventional fuel cell set up consists of graphite as mono- or bi- polar plates which sandwich the MEA. The fuel cell performs better when the MEA is compressed at 140 N/cm^2 [107]. The single cell stack is compressed using torsional force applied by the nut and bolt, which also helps to avoid leaking of reactant gases. The carbon electrodes on both the anode and cathode sides are 39BC SGL Gas Diffusion Layer (GDL) coated with platinum of $0.20mg/cm^2$ and $0.40mg/cm^2$ respectively. Nafion 211 membrane is sandwiched between the two electrodes and pressed in hydraulic press at 20bar at 130°C to form a complete Membrane Electrode Assembly (MEA).

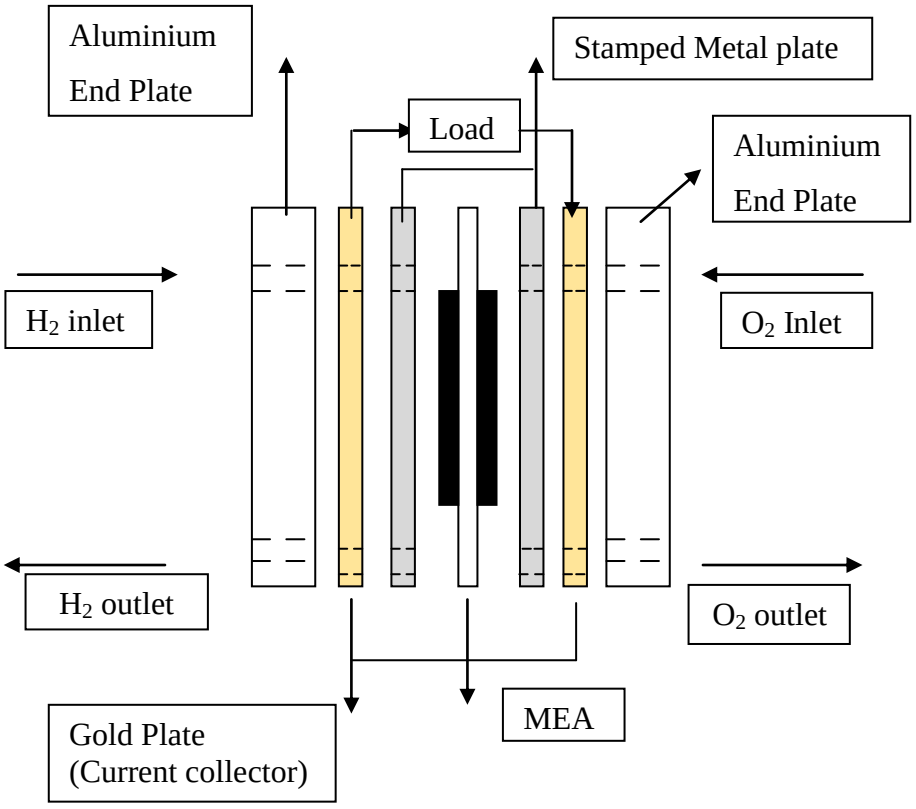

Figure 19: Schematic representation of Single Fuel cell assembly

Silicon gaskets are used on either side to seal the cell. The Teflon coated carbon papers are cut to the active area size of 50mm*50mm and the platinum on carbon catalyst is spray coated on the carbon paper using spray gun. The catalyst coated

electrodes are dried in the nitrogen environment at 100°C before hot pressing the membrane and electrode. The hydraulic hot press is preheated to 130°C and the pressure is set at 20bar [108]. The Nafion 211 membrane is sandwiched between the electrode and pressed for 3min at the set temperature and pressure. The prepared MEA was assembled into the fuel cell as shown in the figure 19 by placing it in between the stamped metal plate/Graphite plate and the gold coated copper plates are used to collect the electrons released from the system. Hydrogen is oxidised at the anode and the released electrons reaches cathode via the load.

The single cell testing of both metal and graphite plates was carried out on a Fuel cell technologies Inc. test station which has a built-in Agilent N3300A electronic load. This test station can control the relative humidity, pressure and gas flow rate of the reactant gas, and can measure and plot the current produced, and the corresponding voltage. The fuel cell performance is analysed using the test station and the MEA is activated before plotting the polarization curve.

3.10 Closure

The techniques and process involved in coating and stamping are discussed in this chapter. The TiN and Carbon coating was carried out using an arc deposition process, whereas WCC is coated by sputtering. The potentiostatic and ICR test show the ability of the materials to resist corrosion and conduct electrons in an acidic medium, respectively. All materials that are prepared in the above-mentioned process are subjected to surface characterisation, which will be discussed in Chapter 4.

CHAPTER 4: TITANIUM NITRIDE COATING

4.1 Introduction

Titanium nitride is one of the promising ceramic coatings for bipolar plate, as it has superior corrosion resistance and electrical conductivity. In this chapter, the physical and electrochemical properties of the TiN coatings are compared with those of bare titanium substrate. Crystal structure and particle size is analysed using XRD and SEM respectively. The electrochemical properties of the TiN coating is examined through potentiostatic corrosion tests and their contact resistance with GDL is determined using the interfacial contact resistance test. The size of the sample that undergoes all the testings (XRD, Corrosion, ICR, SEM, XPS) are 1cm^2.

4.2 XRD analysis of TiN coated substrate

The XRD analyses for all the samples are taken using D8 ADVANCE (Bruker) which uses a copper target as the X-ray source. The presence of TiN can easily be identified by the golden coloured coating layer above the titanium substrate. Figure 20 shows the XRD of bare Ti and TiN-coated substrate.

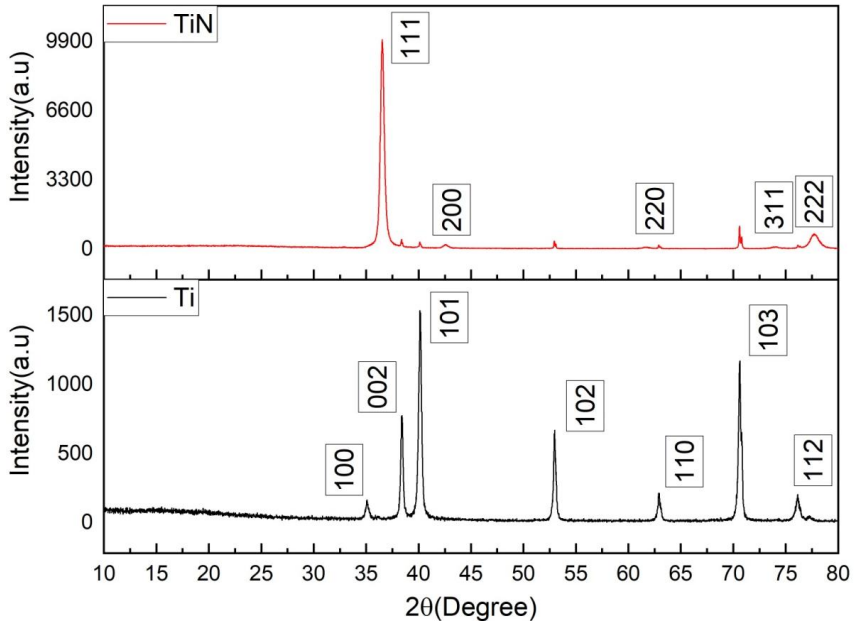

Figure 20: XRD pattern of Titanium (Ti) and Titanium Nitride (TiN)

The crystalline structure of formed TiN is FCC (Face Centred Cubic) and the major peak around 36.65° corresponds to (111) orientation and the other peaks at 42.57°/61.77°/74°/77.9° correspond to (200)/ (220)/ (311)/ (222) orientations respectively. The lattice parameter of the coated film is 0.424nm which is in agreement with JCPDS 38-1420 and other reports [109-111].

4.3 Potentiostatic corrosion resistance test for Bare Ti and TiN coated substrate

Figure 21, presents the potentiostatic polarisation curve for bare titanium substrate (black line) and TiN coated substrate (red line). Within few minutes of exposure in cathodic conditions the corrosion current density of the bare titanium strip is stabilised due to the titanium oxide passive layer. Due to the passive layer, the corrosion current of the substrate decreases rapidly and is relatively stable. The corrosion current density of the titanium plate is 38µA/cm^2 after 4hrs corrosion test in the simulated environment of PEMFC at the cathode potential 0.60V vs Ag/AgCl and the solution is purged with oxygen and the electrolyte at 70°C.

The titanium nitride shows stable and low corrosion current compared with bare titanium substrate which confirms that the corrosion resistance of TiN is better than pure titanium. After 4 hrs corrosion testing the golden colour sample turns a light

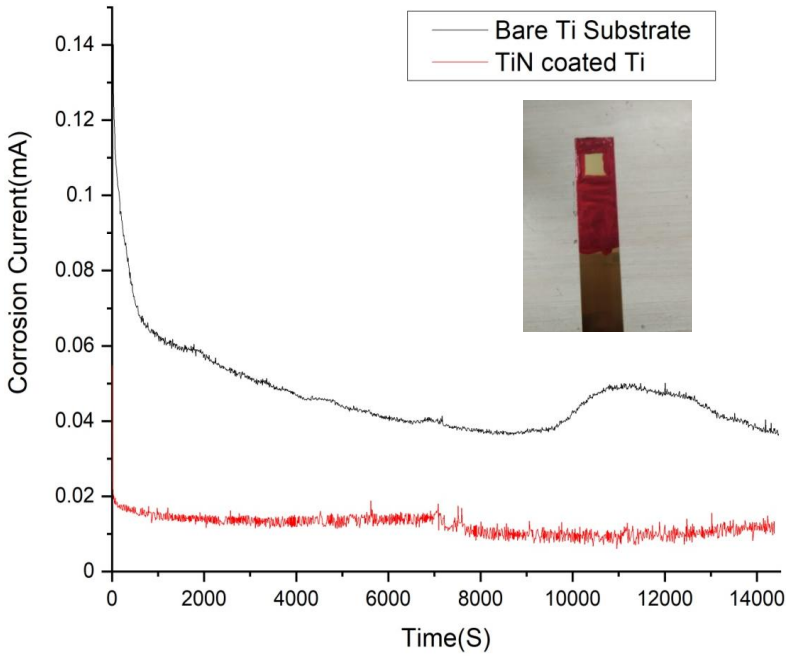

Figure 21: Potentiostatic corrosion resistance test, inset Masked TiN coated substrate

brown colour due to the formation of passive oxide layer above the coating and the corrosion current density is 12 µA/cm^2. The necessary current required to maintain the surface inertness is very low, as the passive film is uniformly formed on the coated surface. Avasarala et al [112] observed a similar passive layer formation of oxynitride/oxide at the potential range between 0.50-0.90V vs SHE. The deterioration of the coating surface and the oxidation of TiN in an O_2 purged acidic environment is accelerated by the rapid diffusion of oxygen by oxynitride. Similar research by Zhang et al [74] compared the corrosion resistances of TiN coating on titanium sheet and stainless steel. It was found that corrosion current for the TiN coated on titanium substrate is less than TiN coated on SS, which is due to less crystal mismatching between the coating surface (Ti) and TiN.

4.4 Scanning electron microscope analysis

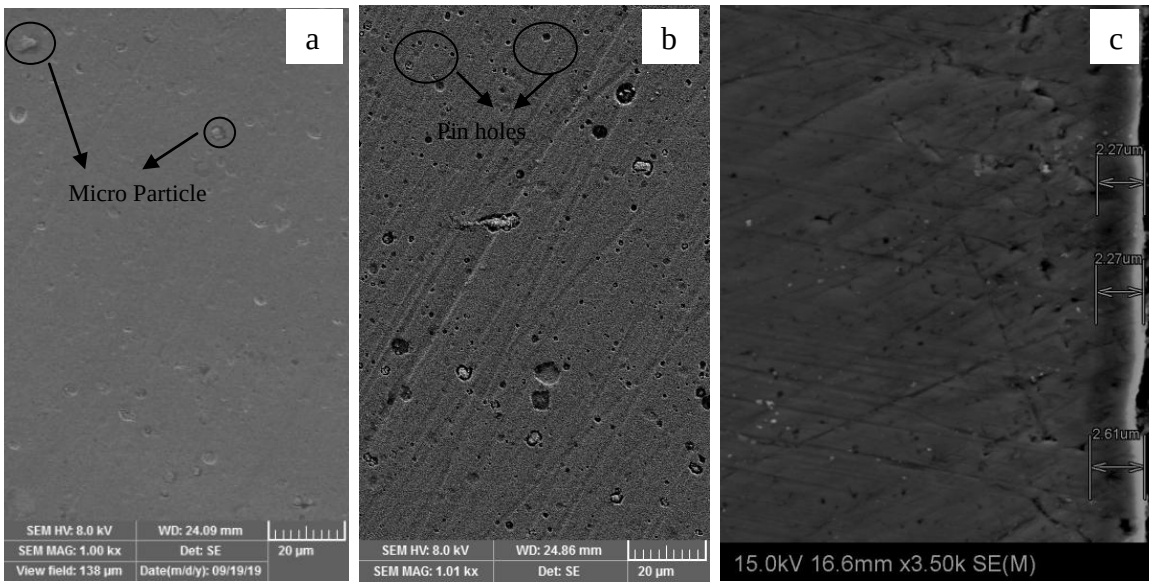

Figure 22: Field emission SEM images of a TiN coated sample

a.) Before corrosion test b.) After corrosion test c.) Cross section image

SEM micrographs for all the samples are taken using Tescan Vega 3SBH with Brukereasy EDS. Figure 22 (a & b) shows the surface morphology of the coating before and after 4hrs of corrosion testing. It is observed, that some micro particles are formed on the surface of the coated film. These macro particles are attached weakly to the TiN surface and peel off after the corrosion resistance test. Macro particles formation are inherent to PVD process[113]. When Ar arc with high-intensity current

is applied, it causes small portions of the target to melt and produce liquid droplets of titanium (Ti) and this settle on the substrate to form macro particle[111]. This can be observed in the figure 22b along with pin holes formed during the deposition process. The coated substrate is cut into small pieces using a wire cutting machine and the surface is polished to scan the cross section for measuring the thickness of the coating. From the figure 22 c, the thickness of the coating is found to be 2.45±0.2µm.

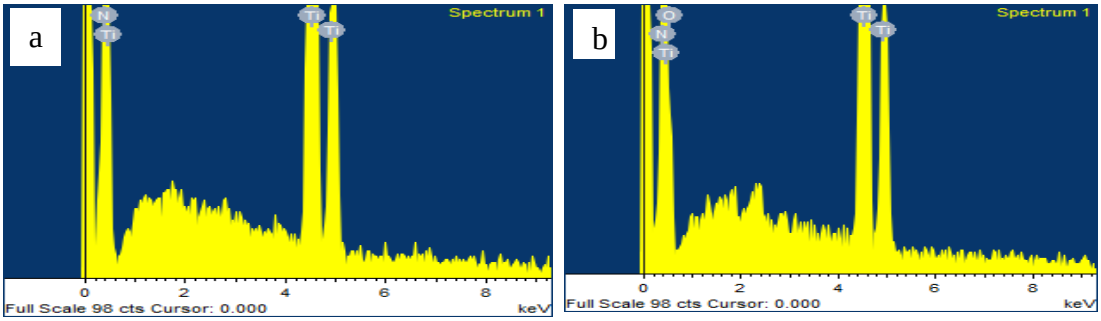

Figure 23: EDX of TiN before (a) and after (b) corrosion test

The surface EDX for both samples before and after corrosion test is shown in Figure 23. It is evident from the presence of oxygen element in the EDX, that the surface of the tested sample forms a passive oxide layer. Omrani et al [114] observed similar kind on pitting corrosion on coated TiN.

4.6 Interfacial contact resistance of TiN coating

Figure 24 shows interfacial contact resistance of TiN and Ti. It is clear that contact resistance decreases with increase in compaction pressure from 20 to 220N/cm^2 for all the samples. This is due to the increase in surface area of carbon paper in contact with metal substrate. At higher compression pressures, the ICR value becomes stabilised as there is no further increase in effective contact area, therefore no path for more electron flow through the interface. The ICR value for Bare-Ti coated sample before corrosion test at typical fuel cell stack compression force of 140N/cm^2 is 81.72 mΩ.cm^2 and for TiN coated film ICR value 10.43 mΩ.cm^2 which is slightly above the DOE target (10mΩ.cm^2). This shows that electrical conductivity is improved by coating TiN. But the ICR value of TiN after potentiostatic test increases to 40.80 mΩ.cm^2. This increase in ICR is due to the formation of an electrically resistive oxide layer and the other factor which also contributes to higher ICR is the pin hole which decreases the effective contact area with GDL[115]. Even though the value is less

than the bare titanium, it's still higher than the DOE target and similar increase in ICR under potentiostatic polarisation is observed by Shi et al [116].

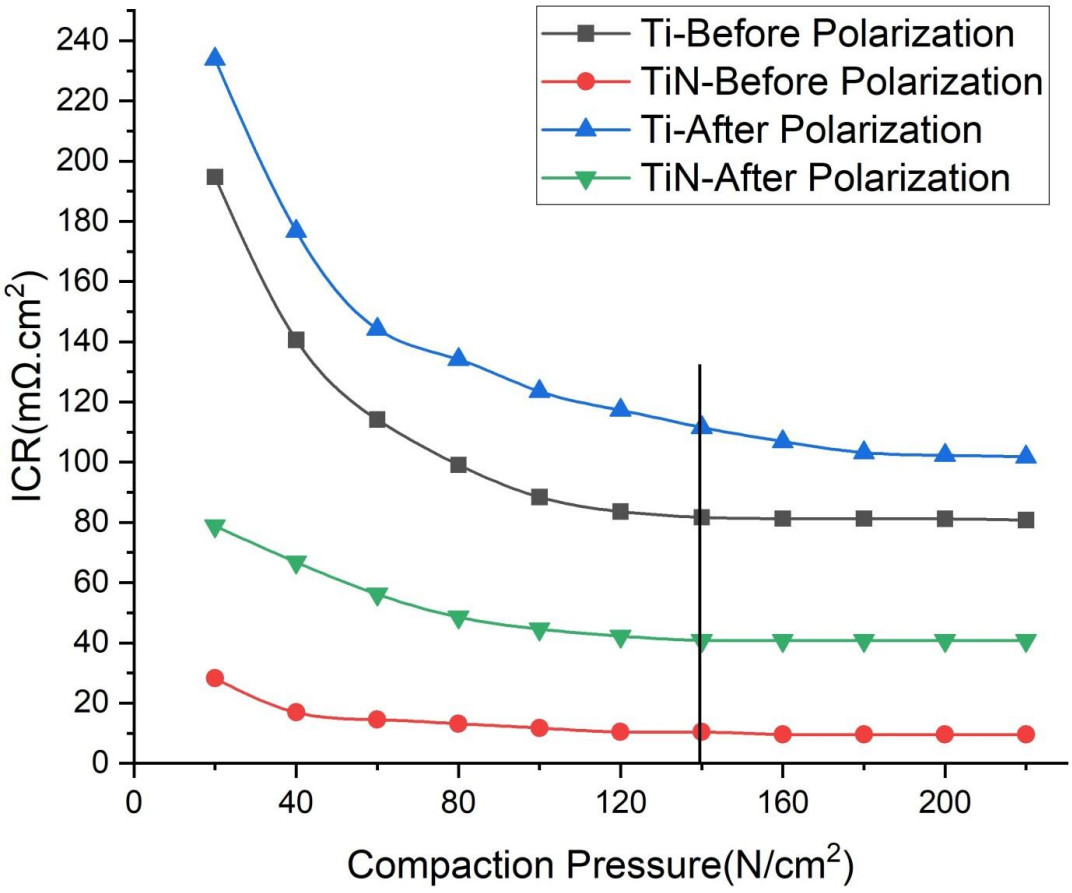

Figure 24: ICR of bare Ti and TiN coated sample at different compaction pressure

4.7 Closure

The results obtained by xrd and sem test confirm the formation of tin on the surface of titanium substrate. the corrosion current density for the tin coated sample is 12 µA/cm2 which is lower than the value of bare-ti sample (38 µA/cm2), but the coated substrate is still higher than the doe target of <1 µA/cm2. it is clearly understood that the formation of passive oxide layer in the highly acidic environment under cathodic potential (0.60v) reduces the surface electrical conductivity.

CHAPTER 5: CARBON BASED COATING

5.1 Introduction

In the previous chapter, TiN as protective coating for bare Ti is discussed and it was found that TiN is not a suitable coating for PEMFC environment. In this chapter, the corrosion resistance and surface electrical resistance of the (amorphous carbon) a-C and Tungsten carbide carbon (WCC) coating is investigated. The performance of these coatings in the simulated environment is examined and the DOE target for bipolar plate is taken as reference for selecting a coating for actual fuel cell testing. Similar to Chapter 4, both the carbon coatings undergo SEM analysis to identify the surface morphology before and after the corrosion test. The XRD is used to extract the crystallographic information of the coated and uncoated sample. To accelerate the corrosion rate, the pH of the electrolyte used in the potentiostatic corrosion test is close to 1, whereas the water drained from a fuel cell has pH between 2 and 3. The ICR test is conducted in the same set up for all the samples and the copper plate is polished for each experiments.

Pure carbon and metal infused carbon coating are evaluated as both of them have good electrical and mechanical properties. It is worthwhile to study the hybridization of the carbon atom to understand the properties in detail. The outermost *s* and *p* orbital of carbon hybridise into sp^2 and sp^3 to form π and σ bonds. Where, the σ bond governs hardness and chemical inertness of the material, and π bonds are formed only between the sp^2 hybrids which are responsible for electrical conductivity. To understand the coatings property it is desirable to evaluate the sp^2 and sp^3 hybrid concentration in a-Carbon. In general, more sp^2 hybridised carbon promotes graphite like properties, while higher sp^3 content promotes diamond like properties. Raman spectroscopy and XPS are used to analyse the hybridisation of carbon.

The best performing coating material in the simulated condition is tested in the actual fuel cell working condition. This will give a better understanding how the coated plate works in the fuel cell stack.

5.2 XRD of two different carbon based coating

XRD peak for both a-C and WCC is shown in Figure 25. Due to the extremely amorphous nature and thinness of the coating, only titanium peaks are observed along with minor peak at 43.93° which is attributed to a (110) phase of chromium [117]. The absence of a carbon peak might be due to the extreme irregularity (amorphousness) in the carbon structure [118, 119].

For WCC, the presence of broad at 38.50° shows weak crystallinity or amorphous nature of the C and WC coating [120] and the peak corresponds to diffraction at 64.1° is due to WC (110) phase, while the peak at 39.93° and 38.10° represent W_2C phase [121]. This shows the prepared coating is the mixture of Hexagonal Close Packed (HCP) and Face Centered Cubic (FCC) structure [122]

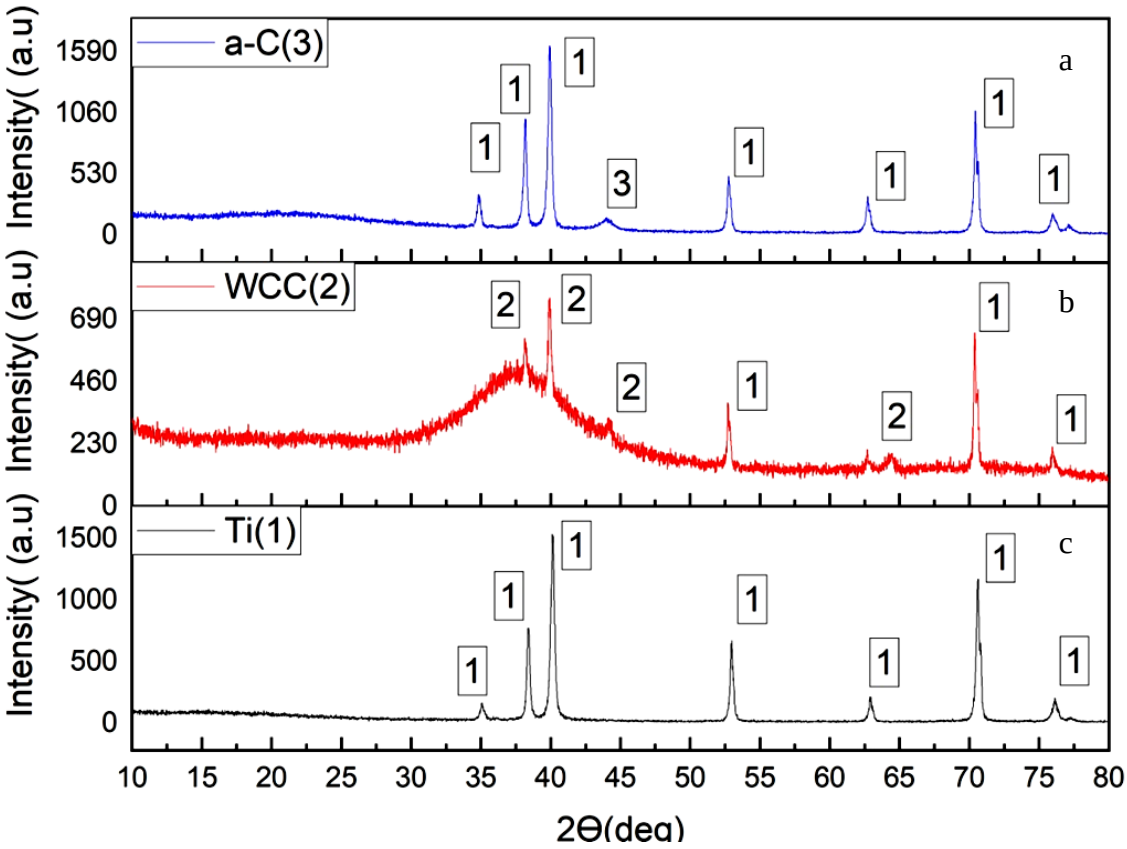

Figure 25: XRD of different carbon based coatings a-C (a), WCC(b), Bare-Ti(c)

5.3 SEM micrograph and EDX analysis of a-C and WCC

Figure 26 corresponds to the SEM micrograph of WCC coating before and after the potentiostatic corrosion test. Thicknesses of the coatings are measured through the cross section image. The surface of WCC shows no changes in the morphology or any damage to surface after potentiostatic corrosion test, apart from observing a few corrosion products in the SEM image.

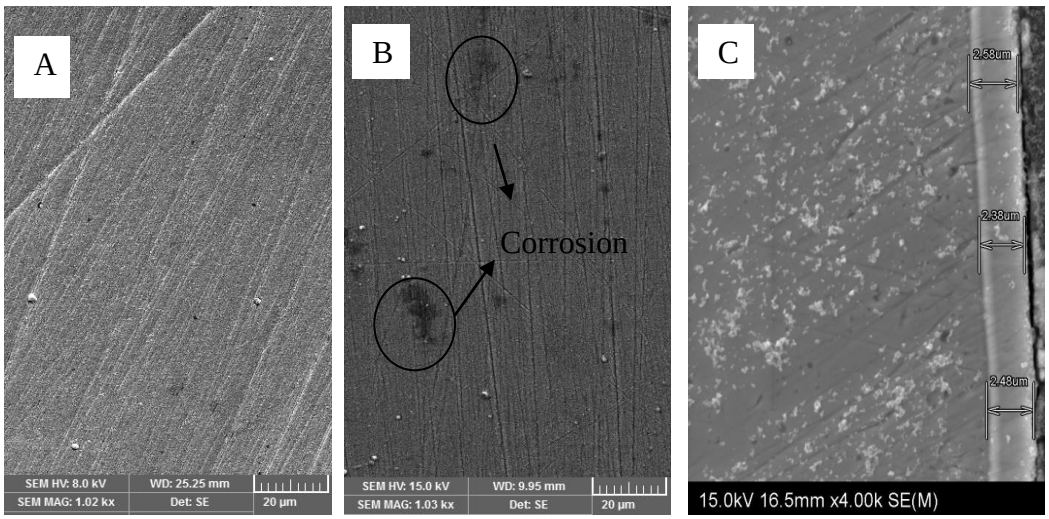

Figure 26: SEM images of WCC coated corrosion sample A.)Before corrosion test B.) After corrosion test C.) Cross section image

Figure 27 corresponds to the SEM image of a-C before and after the corrosion test. The deposited amorphous carbon film shows a high level of granularity and no sign of visible corrosion is observed on both of the coated samples.

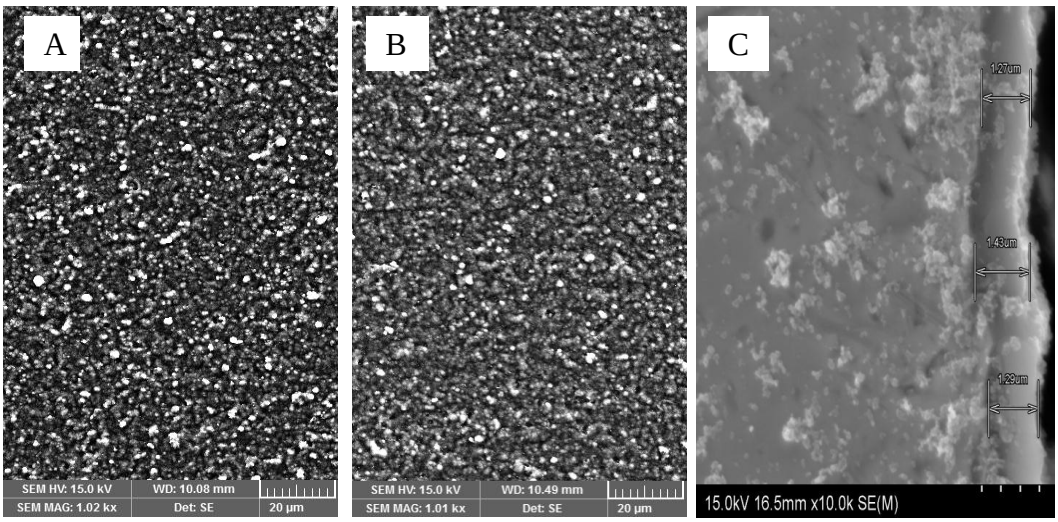

Figure 27: SEM images of a-C coated corrosion sample A.) Before corrosion test B.) After corrosion test C.) Cross section image

Figure 28 shows high magnification images of both coatings. It is clearly seen that surface particle size of WCC is in few hundred nanometre, while the particle size of a-C are in form of micro granules. The excess carbon coated on the surface of WCC coating is in the form of spherical shapes. This forms a highly conductive contact with GDL (carbon paper) which has similar property.

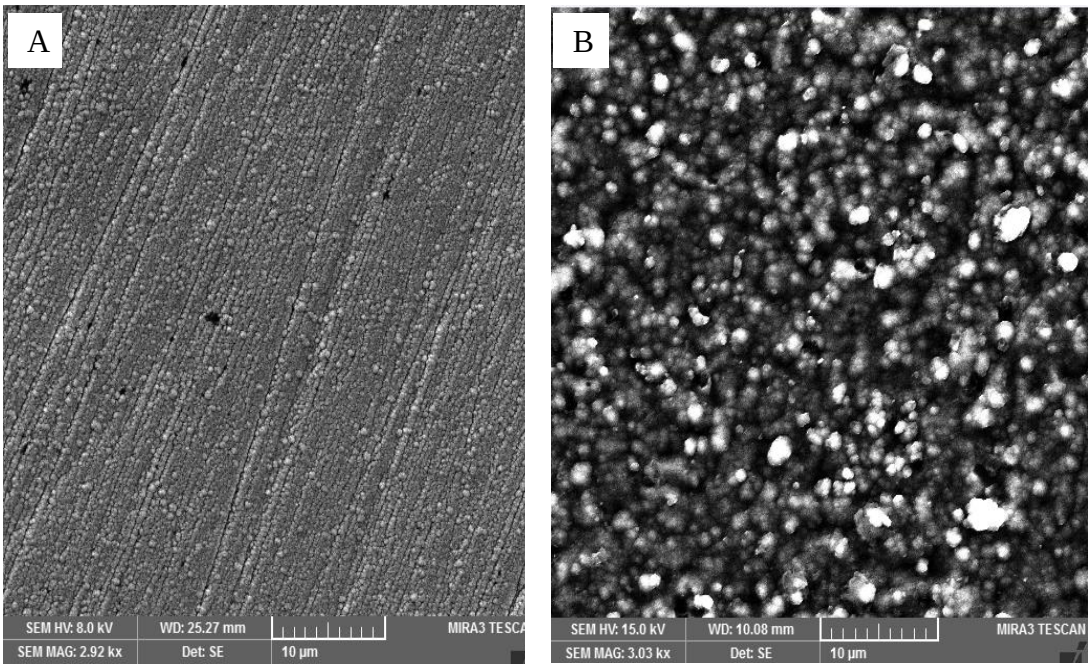

Figure 28: High magnification SEM images of corrosion samples A.) WCC B.) a-C

Figure 29 presents the EDX analysis report for WCC and a-C coating taken before and after corrosion testing. Few minor peaks correspond to titanium elements are observed and this shows the substrate is not covered completely. The presence of chromium elements in the a-C coating examined after the corrosion resistance test shows signs of corrosion whereas the substrate coated with WCC coating shows no peak for titanium but the presence of oxygen might be due to surface contamination.

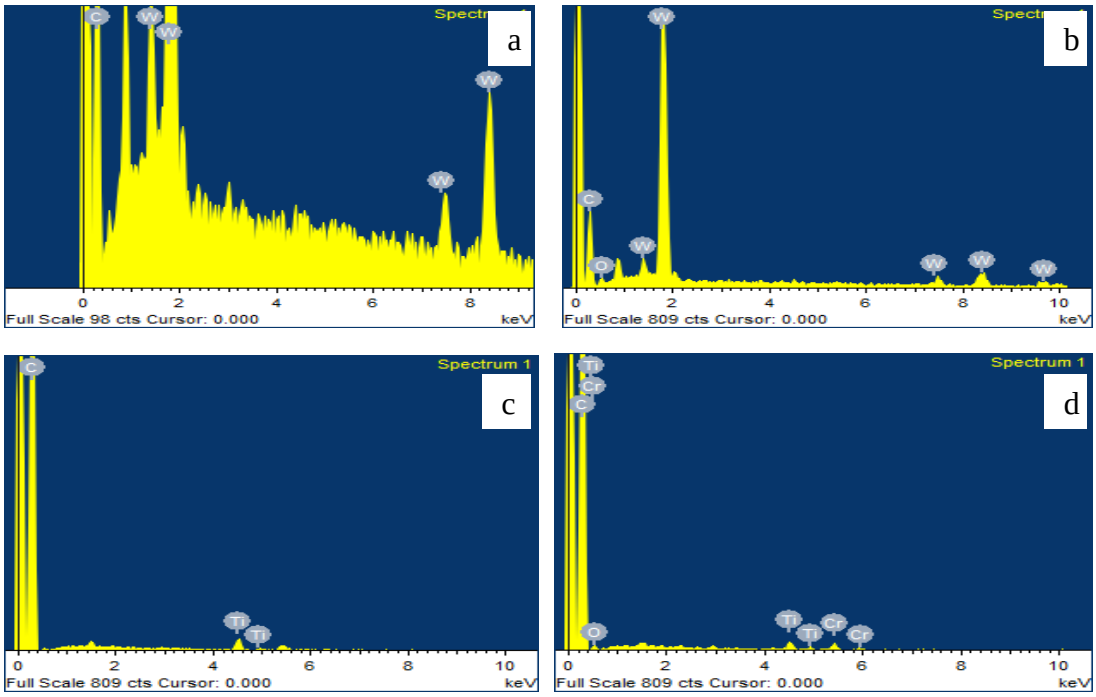

Figure 29: EDX for WCC and a-C corrosion samples (a. WCC-before corrosion test, b. WCC-After corrosion test c. a-C before corrosion test d. a-C-After corrosion test)

5.4 Corrosion resistance test

Two things that corrode the titanium substrate in the fuel cell environment are its acidic environment and the polarization potential. In the corrosion resistance test, the 1cm^2 exposed samples are tested for 4hrs in the electrolytic bath as mentioned in the Chapter 3.

Figure 30 shows the potentiostatic corrosion current for both the carbon based coating and bare titanium substrate. The figure inset shows the magnified region of the corrosion current density data for three coatings (bare Ti, a-C and WCC). The active peaks in the first half of the corrosion test for a-C shows the sign of corrosion. These

active peaks disappeared during the second half of the experiment and the corrosion current stabilises at around 2.54 µA/cm^2 towards the end of the test. These strong peaks are due to the corrosion of titanium substrate which got exposed to the electrolyte. This Supports the EDX interpretation, that the substrate is not completely covered with carbon. The formation of macro granular particles during the arc deposition process might be reason for the electrolyte to reach the substrate metal [123, 124].

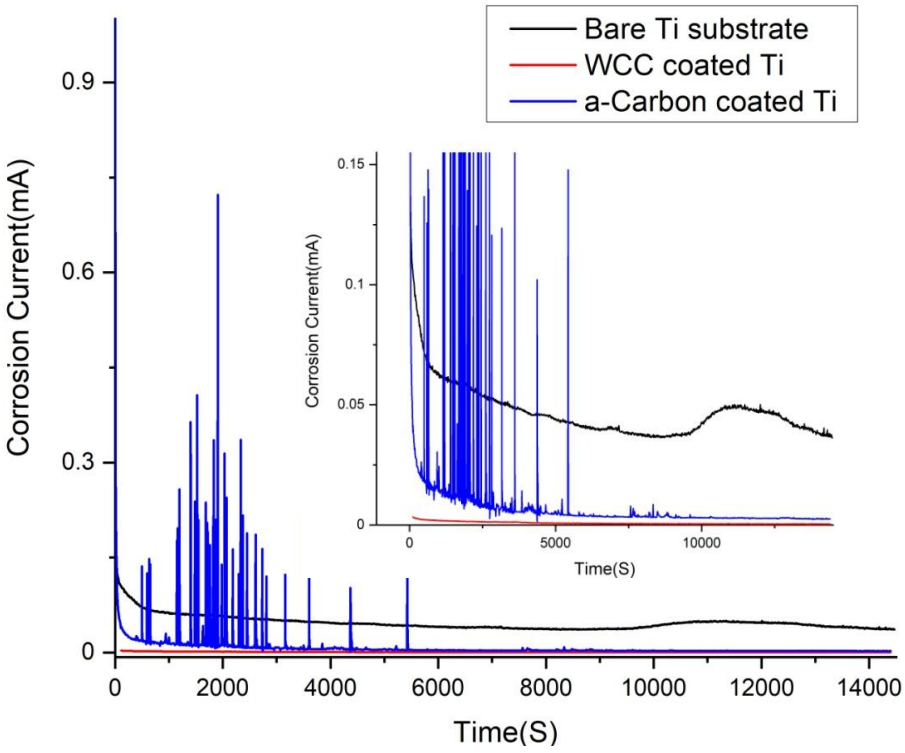

Figure 30: Corrosion current density comparison with respect to time

In the case of WCC coating no active peaks are observed and the corrosion current density is stabilised right through from the beginning to the end of the 4hrs test. The corrosion current density is 0.361 µA/cm^2 which is well within DOE 2025 target of <1 µA/cm^2. Out of the all the coatings, WCC is the one which satisfies the DOE target [125] with the corrosion current density being on a par with a noble metal coating [56, 126].

5.5 Interfacial Facial Contact Resistance

Figure 31 shows the ICR of a-C and WCC coating compared with bare Ti substrate. For all the samples the ICR value decreases with increasing compressive pressure. At a pressure of 140N/cm^2, the ICR value of a-C before and after corrosion test is 34.37mΩ.cm^2 and 43.76mΩ.cm^2 respectively. Whereas, the WCC coated sample has ICR of 5.70mΩ.cm^2 and 6.59mΩ.cm^2 respectively. The surface electrical conductivity of the WCC coating shows exceptional performance similar to noble metal coating[39]

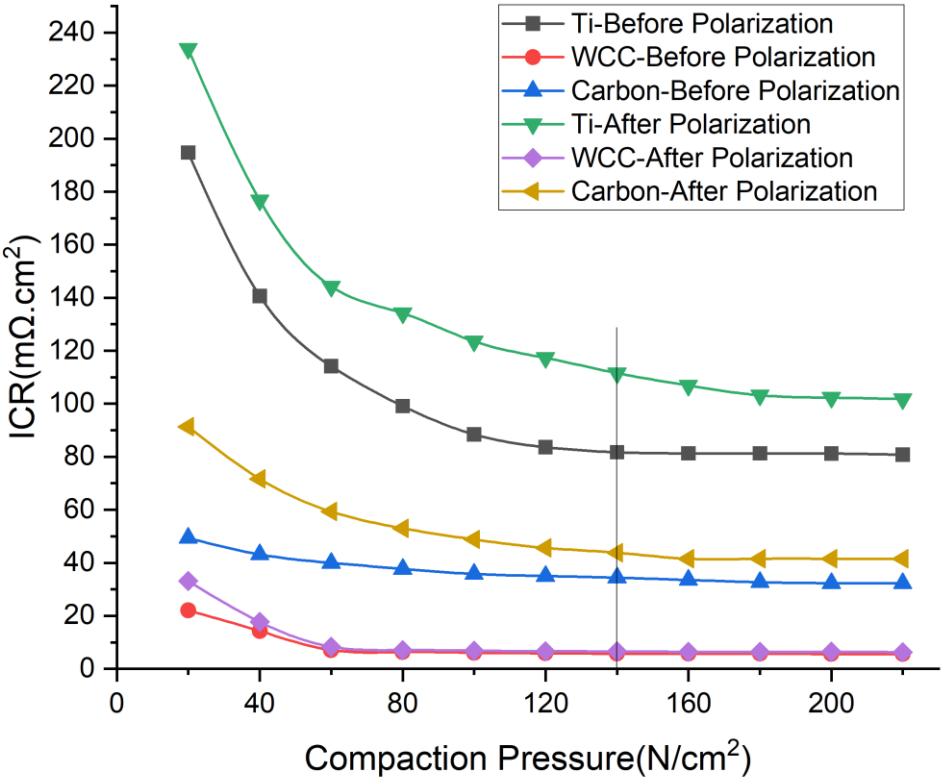

Figure 31: ICR of a-C and WCC with respect to compression force

The WCC coating satisfies the DOE 2025 target of <10 mΩ.cm^2. Generally the amorphous carbon based coating consists of different hybridisations. The electrical conductivity and corrosion resistance depends on the hybridisation. The most predominate carbon is sp^2 and sp^3 hybridized carbon which represent the electrical

conductivity and corrosion resistance respectively. Larger sp^2 content leads to better electrical conductivity. The further insight on the hybridisation of the carbon based coating is studied using Raman spectroscopy and XPS. The ICR for most of the metal coatings can be determined analytically but the limited data's on surface properties of carbon based multi layer coating makes it difficult to find through simulation.

5.6 Raman Spectroscopy

This analysis is done using Shimadzu, 3600 Plus (ultraviolet-visible) spectrophotometer. Figure 32 shows Raman spectroscopy of a-C and WCC coated on Ti substrate. The typical carbon coated films are characterised using the peaks observed between 1000 cm^{-1} and 2000cm^{-1}. The peak at low wave number 1334 cm^{-1} is called D peak which is corresponds to disorder or defects in the carbon crystal and the one at high wave number 1568cm^{-1} is called G peak which corresponds to graphitic lattices. The intensity of G and D peak is represented as I_G and I_D and it is observed from the figure that the I_D / I_G ratio of WCC is more than a-C. Ferrari et al. [127] observed similar increases in the I_D / I_G ratio and concluded that it is attributable to increase in sp^2 content. This increase in defect level increases the density of unpaired electron which eventually decreases the resistivity of the WCC film [128, 129]. Though Raman spectroscopy gives a qualitative result, only XPS analysis gives insight to the content of sp^2 and sp^3 carbon as it excite electrons differently in σ band (sp3 hybridised orbital) using visible light energy, which makes Raman scattering effect to characterise more of sp^2 than sp^3 carbon [130].

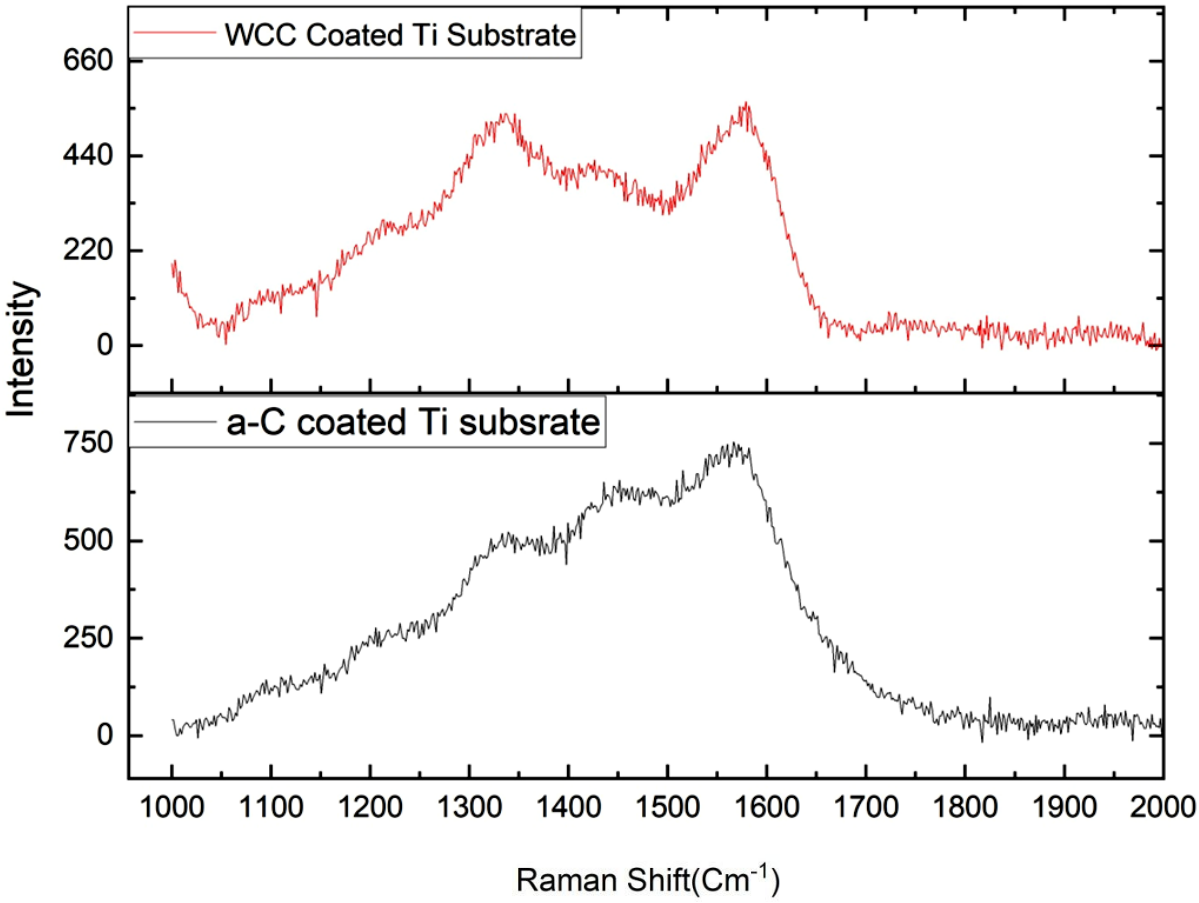

Figure 32: Raman Spectroscopy of a-C and WCC coated Ti Substrate

5.7 XPS analysis on a-C and WCC

The chemical state of both WCC and a-C coatings are investigated using XPS analysis (Physical Electronics (PHI VersaProbe III)) with an X-ray source of Al Kα 1486.6 eV.

For a-C, the only major peak is for C1s which is observed at higher binding energy of 285.05 eV and this shows that the major carbon content is sp^3 hybridised [131]. As shown in Figure 33, the C1s is deconvoluted into two peaks which gives an insight to the composition of the carbon coating. The graphitic nature of carbon in C1s is reflected at lower binding energy and it is attributed to sp^2 hybridisation while the binding energy of diamond-like carbon is reflected at the higher binding energy which is attributed to sp^3 hybridisation. The binding energies of graphite pristine C=C sp^2

and diamond pristine C-C sp^3 are 284.4±0.1 eV and 285.2±0.1 eV respectively and the peaks are deconvoluted accordingly [132]. The peak area ratio of deconvoluted C1s is 0.86(sp2/sp3) which shows the presence of higher concentration of sp3 carbon which is the reason for poor electrical conduction of a-C and better corrosion resistance. This arrangement of carbon is completely dependent on the deposition condition.

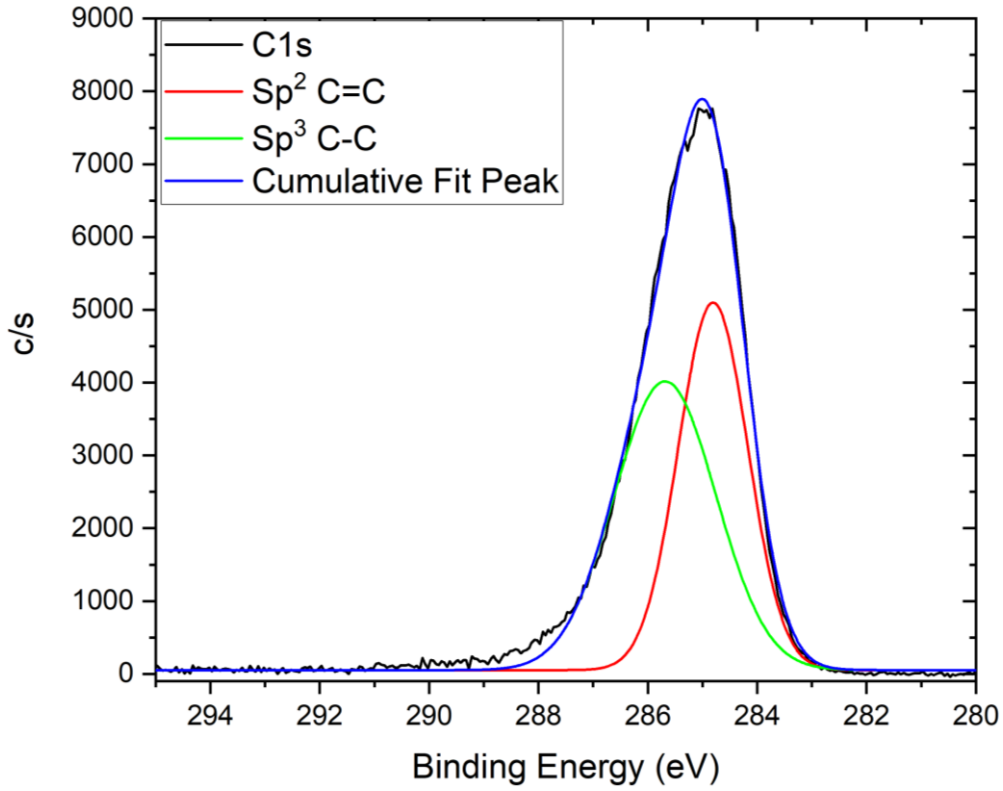

Figure 33: High resolution C1s peak of a-C coating

In the WCC coating, the carbon atoms are placed in the interstitial site of the host tungsten atom. The deposition at higher temperature (more than 200°C) helps to arrange the free carbon atoms on the surface of WCC coating to form an aromatic chain and also it is observed that introducing metal carbide into the carbon structure helps to improve the electrical conduction by clustering sp^2 carbon [133]. The surface properties and electronic status of WCC coating is revealed by high resolution C 1s and W4f spectra. Figure 34 shows XPS spectrum of C1S for both coatings, here the peaks are deconvoluted to find the nature of the bonding. The presence of carbidic C can be confirmed due to the shift in the binding energy of C1s peak from 285.05 (a-C) to lower binding energy of 284.72eV (WCC). Due to the excess carbonisation on the surface, the peak corresponding to W-C at the binding energy 282.6 eV is not

detected. This phenomenon is due to the overlap of carbon intensity over carbide intensity and the similar kind of overlap has been reported by Zhang et al. [134]. The high resolution spectra of W4f is split into a doublet W4f 5/2 and W4f 7/2 which corresponds to W^{4+} state of tungsten. The binding energy of peak W4f7/2 is 32.12 eV, whereas for the pure Tungsten metal the binding energy is 31.4 eV [122], which helps to confirm the formation of WC in the coating. The minor peak at 37.82 corresponds to W5p3/2($W6^{+}$) which might be due to the presence of surface contamination by oxygen [135].

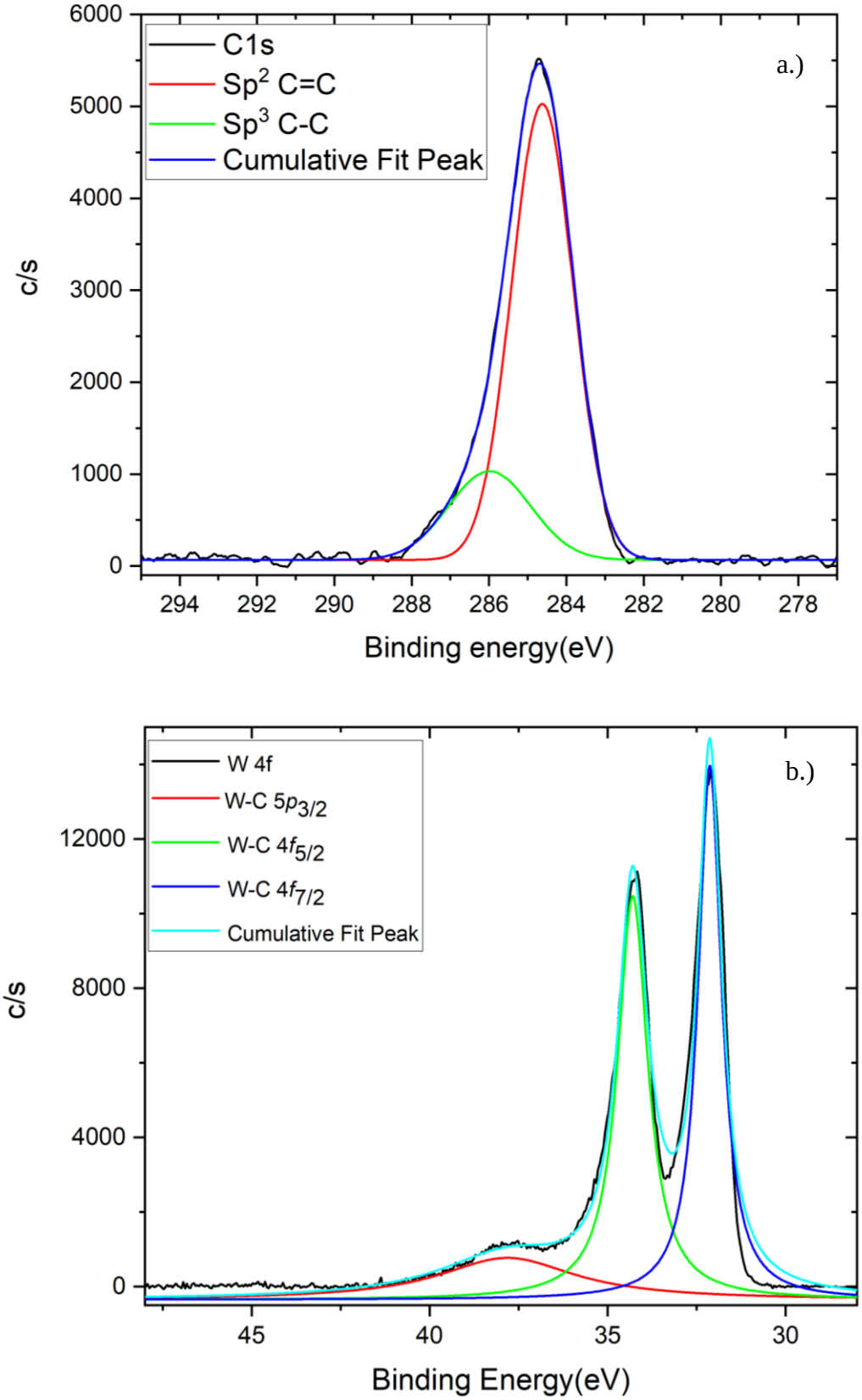

Figure 34: High resolution XPS spectra
a.) C1s and b.) W4f spectra of WCC coating

The excess carbonization towards the end of deposition process makes the WCC coating carbon rich with more than 63%. The C1s spectra is deconvoluted to evaluate the content of carbon in sp2 and sp3 hybridisation. The peak area ratio (sp2/sp3) for WCC coating is 3.83 which shows that the major carbon content present on the surface is double bonded carbon (sp2), which supports the results obtained through ICR test where the electrical conductivity of WCC coating outperformed the rest and satisfies the DOE target 2025.

5.8 Closure

The basic requirement for a material to consider as bipolar plate coating is to satisfy DOE target for ICR and corrosion resistance. From the above discussion it is understood that, only the WCC coating satisfies the DOE target 2025 for both the requirement, while carbon deposited through sputtering process produce big carbon particle which might have exposed the base metal in macro spots that causes sudden peaks in the corrosion resistance test for a-C coated titanium plate. The tungsten carbide coating increased the corrosion resistance and the surface contact resistance is reduced by increasing the sp^2 hybridised carbon content. This helps to make a good electrical contact with GDL which has similar electrical properties. Due to the superior performance of WCC coating in the simulated environment, its actual performance in single fuel cell is studied further. WCC is coated on the thin metal foil of 0.15mm thick plate after stamping it to form flow channel using die and punch tool. This will be discussed in detail in Chapter 6.

Table 3: Corrosion Current and ICR comparison of all different coatings studied

Coating	Un-coated Ti	TiN coated Ti	a-Carbon coated Ti	WCC coated Ti
Corrosion Current	38μA/cm^2	12 μA/cm^2	2.54 μA/cm^2	0.361 μA/cm^2
ICR	81.72 mΩ.cm^2	10.43 mΩ.cm2	34.37mΩ.cm^2	6.59mΩ.cm^2
DOE target 2025	X	X	X	✓

CHAPTER 6 DESIGN AND FABRICATION OF STAMPED MONOPOLAR PLATE COATED WITH WCC AND ITS FUEL CELL PERFORMANCE

6.1 Introduction

In the previous Chapters, the method of coating nitride, carbide and carbon coating, and their performance in simulated fuel cell environments were studied. In this Chapter, the process of designing a die and punch set for creating micro channel of titanium sheet is discussed in detail. A hydraulic press in used to stamp the metal plate. The plate is then coated and assembled in the fuel cell fixture following which its long term performance (500hrs) is analysed by running the fuel cell in constant current mode to determine the voltage drop. After the long term test, the MEA is disassembled from the fixture and ICP is done to reveal the concentration of metal leached into MEA.

To best of the Author's knowledge, this is the first report on the performance of the WCC coated monopolar plate in a fuel cell.

6.2 Flow channel Design

Due to the advantage of serpentine flow channel over others flow pattern in terms of less pressure drop cross the flow field, suitable contact area between BP and electrode [136], the single serpentine flow channel is used in this research It is formed on titanium sheet of thickness (t) 0.15mm and fabricated through forming tool method. The forming tool is designed and analysed with the aid of the ANSYS software.

In Figure 35, the cross section of a single flow channel is depicted along with the various parameters. The geometry of the stamped monopolar plate is dependent on parameters such as channel depth (d), width (w) and fillet radii (r and R). The dimensions of the stamped plate depend on the geometry of the punch and die and the forming conditions (pressure and lubrication). The aspect ratio (w/d) is maintained at around 0.5 by keeping width and depth value constant for all designs and the radius of

the fillets (r and R) is changed to find the design with less strain and better thickness distribution at the corners which are vulnerable to cracking.

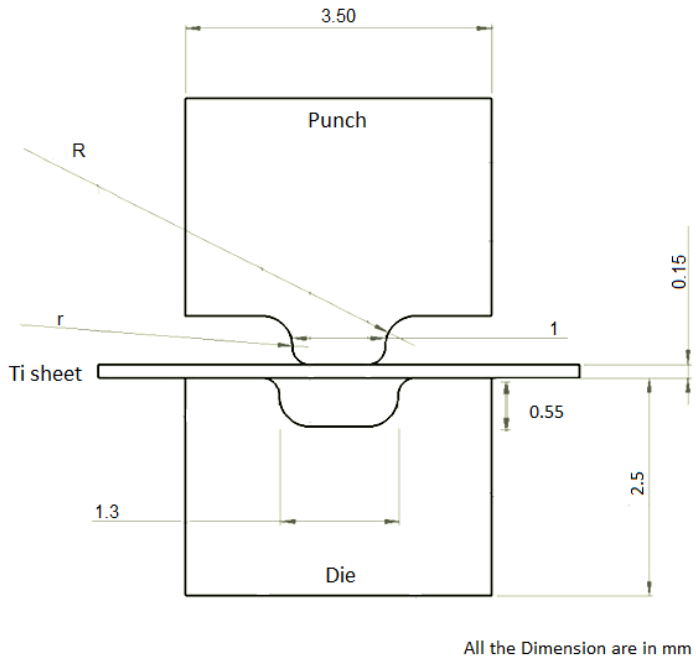

Figure 35: Schematic representation of a single tooth of die and punch

The equivalent strain on corners of single flow channel designed with different tool geometry will be analysed through simulation and the design with less average strain at the vulnerable spots will be considered for fabrication. The thickness of titanium sheet for all models is 0.15mm and the clearance between die and punch is kept constant at 0.15mm on each side. The actual thickness distribution in the channel after the stamping process will be compared with simulation result. The dimensions of the forming tool for all three designs are as follows

Table 4: Dimension of forming tool with different fillet radius

Model 1	Model 2	Model 3
R=0.15	R=0.25	R=0.35
r=0.25 mm	r=0.15	r=0.25
W=1mm, d=0.55mm	W=1mm, d=0.55mm	W=1mm, d=0.55mm
t=0.15mm	t=0.15mm	t=0.15mm

6.3 Method of Analysis

The first step of the analysis for determining the optimal radius of fillet to form channels without cracking is to create the geometry of all three models according to the above mentioned dimension constraints. After creating the geometry, the material for the forming tool (die and punch) and sheet metal is assigned as hardened steel and titanium respectively. The connections between the bodies are assigned in the next step. The die and punch set is selected as rigid body and the top surface of the titanium sheet is set with the surface of punch (target surface), while the bottom surface of titanium sheet is set with die (target surface). The sheet metal is supported by two blocks act as a roller support and prevents lifting of blank during the stamping process. As shown in Figure 36, the sheet metal (blank) undergoes whole body meshing and the tool surface that makes contact with blank is meshed too. A mesh can be described as a volume which has been disintegrated into a series of smaller elements to perform the analysis with boundary conditions. The fine mesh option is chosen to increase the number of nodes and element which will increase the precision of the simulation. For 2D geometry, the triangle and quadrilateral element or a combination of both can be selected. The skewness is defined as a deviation from the perfect element and it is measured in the scale 0 to 1. A skewness value closer to 0 is the best scale for maintaining greater accuracy[137]. The total numbers of elements are 2924, material of die, punch and holder is Structural steel, and the Sheet metal is Titanium.

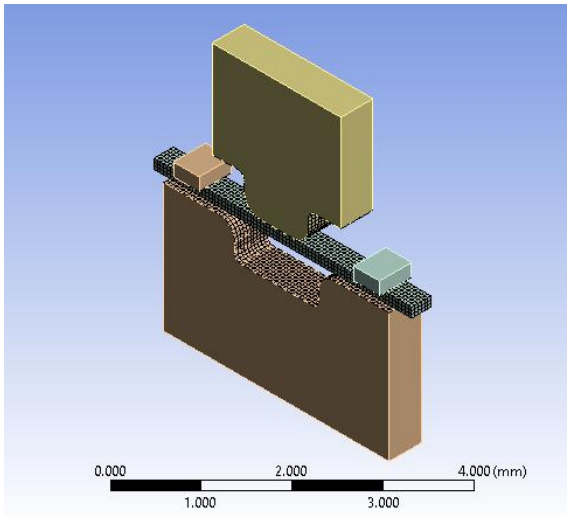

Figure 36: Mesh generated for blank and forming tool

After meshing the geometry, the model is set with boundary condition for analysis. The degree freedom of die is arrested in all directions while the punch is allowed to move only in the negative y axis. The total distance for the deformation of punch is set to achieve the filling of die with sheet metal and solved for equivalent strain(Von Mises). Figure 37, shows the strain contours for all three models.

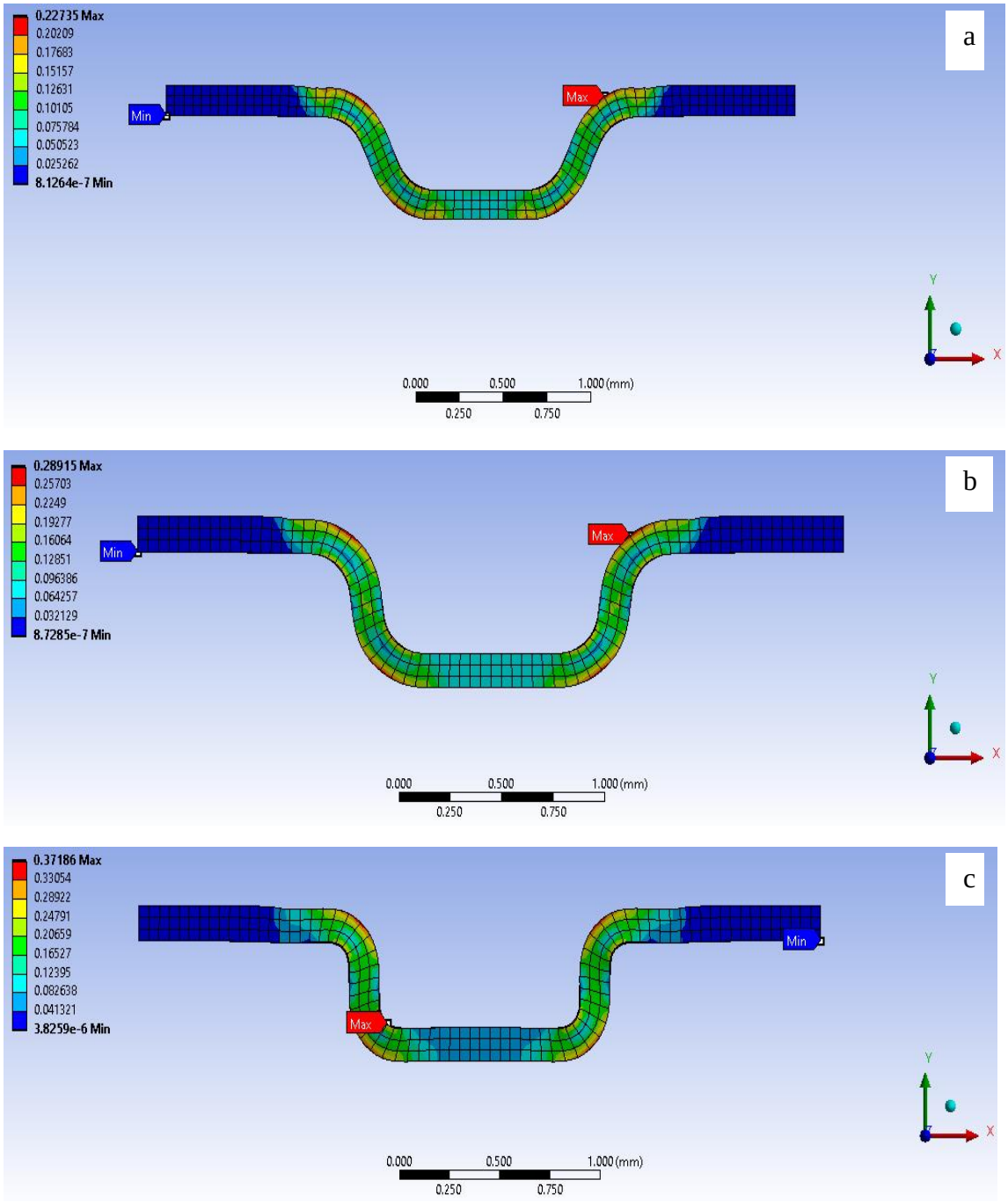

Figure 37: Equivalent Strain contours of all three die and punch models a. Model 1 b.) Model 2 c.) Model 3

The model with the least equivalent strain in the vulnerable corners is identified by calculating the average strain value in the elements occupying in the bends. These critical spots are divided into 10 segments and the equivalent strain in the cross section is identified. Figure 38a shows the position of segmented model and these locations were selected for all three models.

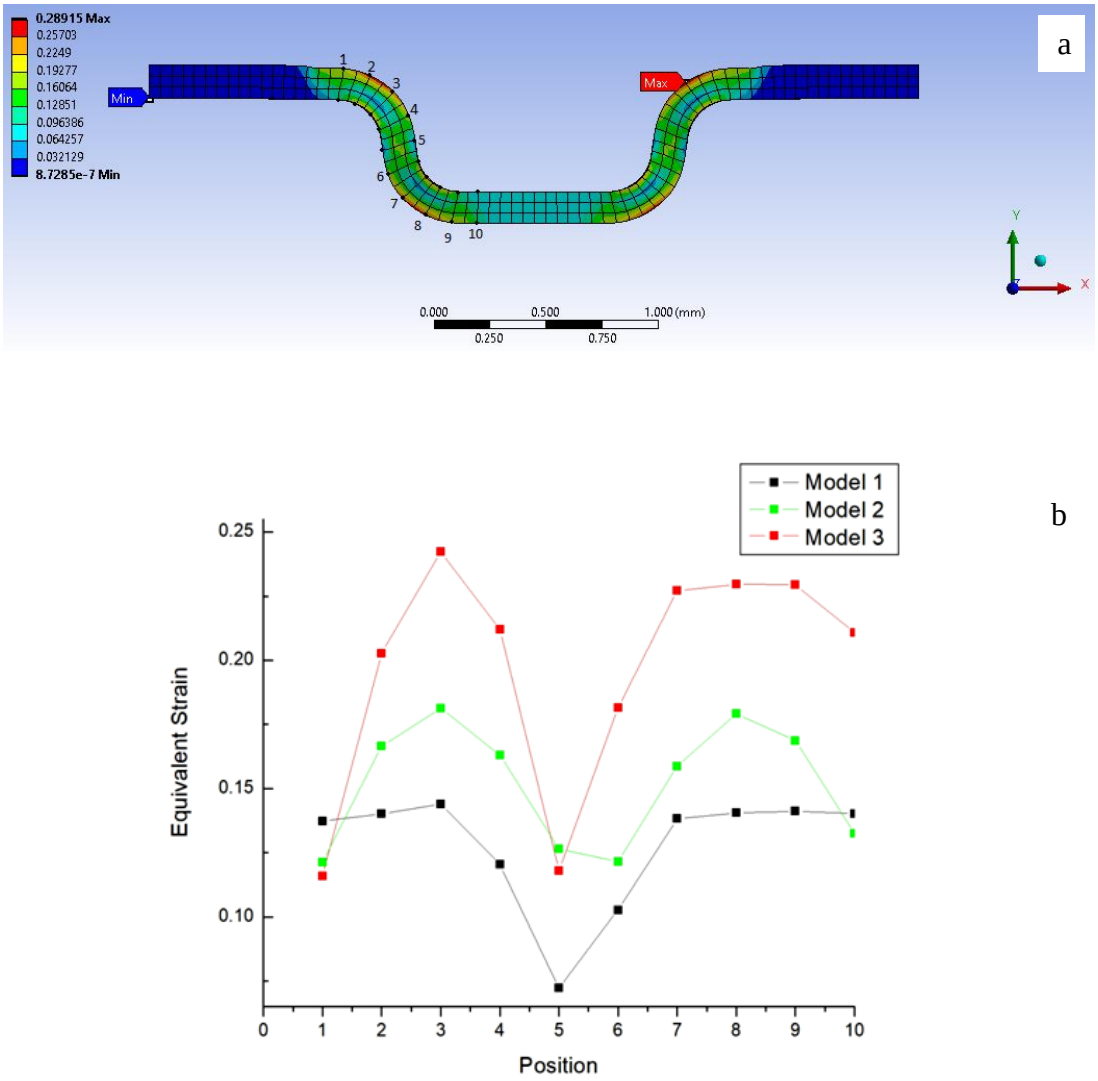

Figure 38: a.) Critical location marked in the deformed plate b.) Equivalent strain at critical location for all three models

Figure 38b shows the location of the critical spots and their respective strain values. From the simulation results it is clearly observable that the average strain value is high for model 3 and lowest for model 1. Another important factor to consider when selecting a model for fabrication is the draft angle (α) of the stamped plate. The formability of channel on the sheet, heat management and fuel cell performance depends on α. From the ANSYS study it is clear that the draft angle has major

influence on formability of the channel during the stamping process. In the open channel air cooled stack, the air used as both fuel and coolant. If the draft angle is larger, the volume fuel to electrode will be more and volume of air supplied to cool the stack will be smaller which will affect the heat management and consequently affecting the fuel cell performance[138]. Figure 39 shows the draft angle of all three simulation model. The higher the draft angle of the stamped plate, the lower is the pressure drop adversely affecting the fuel cell performance by causing poor water management [139].

Shimpalee et al. [139] studied the effect of channel tolerance on fuel cell performance in both stationary settings and portable settings, by changing the draft angle , depth and bending angle of the channel. It was concluded that higher draft provide lesser land length which limits the heat exchange and dehydrates the membrane which in turn reduces the ion exchange. In a limited space, a channel with a larger draft angle makes it difficult to accommodate more channels [140].

Model 3 has a channel with zero draft angle which is mostly studied in the case of graphite plates but in term of metal stamping it is highly inadvisable to consider a design with zero draft because the high possibility of tearing at the corner. Due to this reason, only model 2 is considered for fabrication and its thickness distribution at the corner is studied.

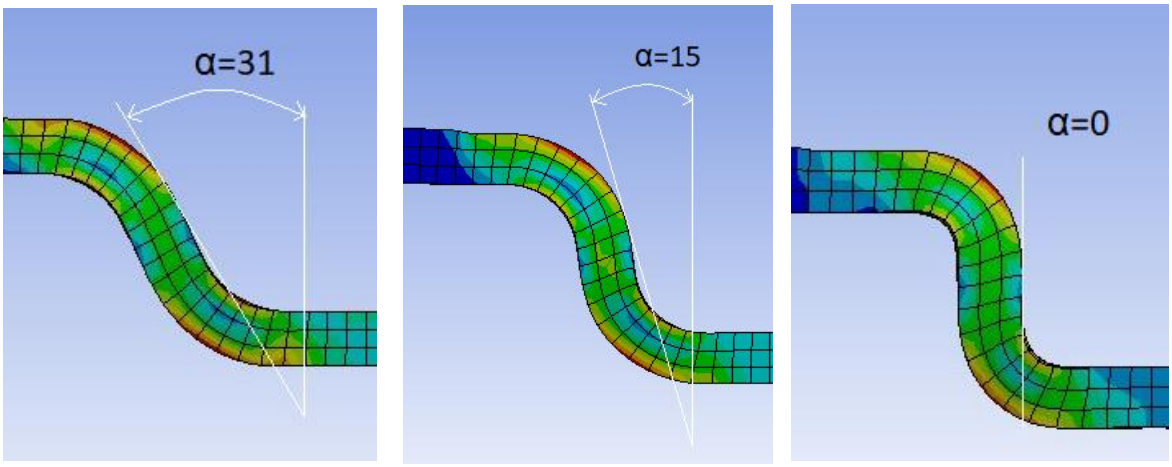

Figure 39: Draft angle of simulated models (From left: Model 1, Model 2, Model 3)

6.4 Fabrication of forming tool and stamping sheet metal

The dimensions of model 2 were chosen for fabricating forming tool. The stamping die is machined in a VMC and the corners are etched through EDM to get a high precision radius. Figures 40a shows the picture of die and punch along with the guide pin and figure 40b is the picture of Pressform hydraulic press.

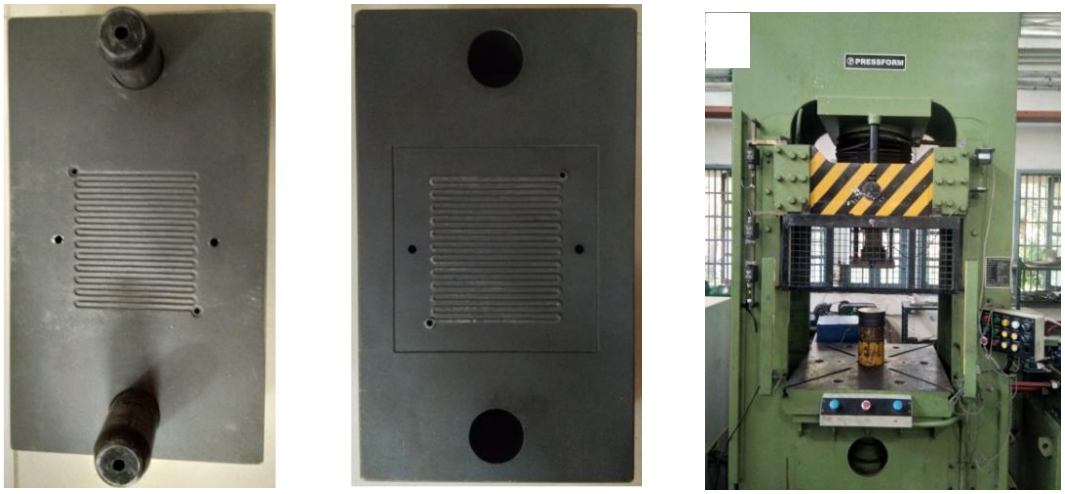

Figure 40: a) Forming tool and b) Hydraulic press

Pure titanium sheet of thickness of 0.15mm is placed in-between the forming tool and the hydraulic press (Pressform Industries) with 100MT capacity is used to stamp the sheet. The increased flow of material into the cavity and the thickness reduction at the corners can be better achieved by using oil as a lubricant. The other factor which affects the formation of channel is the force applied during stamping. The stamping force was increased from 60kN to 170kN and it was found that 115kN is the optimal force which produces a channel with a completely filled depth and no cracks are observed. Figure 41 shows cross section image of formed plate at different forces. The plate stamped at 60kN is not completely formed since the force is not sufficient to deform the titanium sheet, while the 170kN force fills the depth but also ruptures the titanium sheet developing cracks at the corner.

The formed plates are punched with holes at the each corner to facilitate the gas reaching the reaction site. To measure the thickness reduction of the formed plate, the samples pressed at different forces are sheared by wire cutting which doesn’t apply any additional force on the stamped plate.

a.

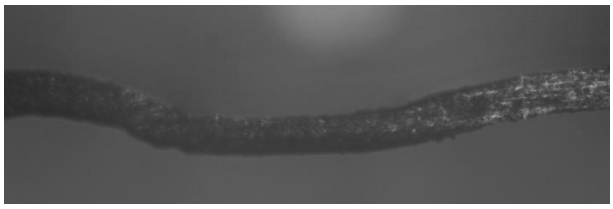

b.

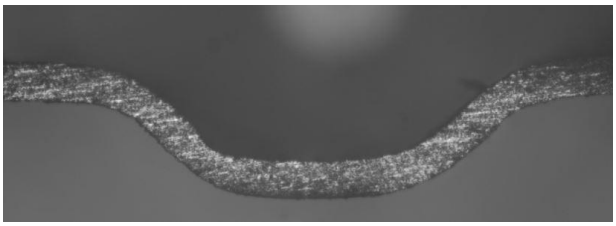

c.

Figure 41: Cross sections of the stamped plates at different forces a.) 60kN b.) 115kN c.)170kN

An optical microscope was used to capture the images of the cross sections. The sheet thickness at the corners of the stamped plate which is produced without crack is measured and compared with simulation result. It found that the stamped plate

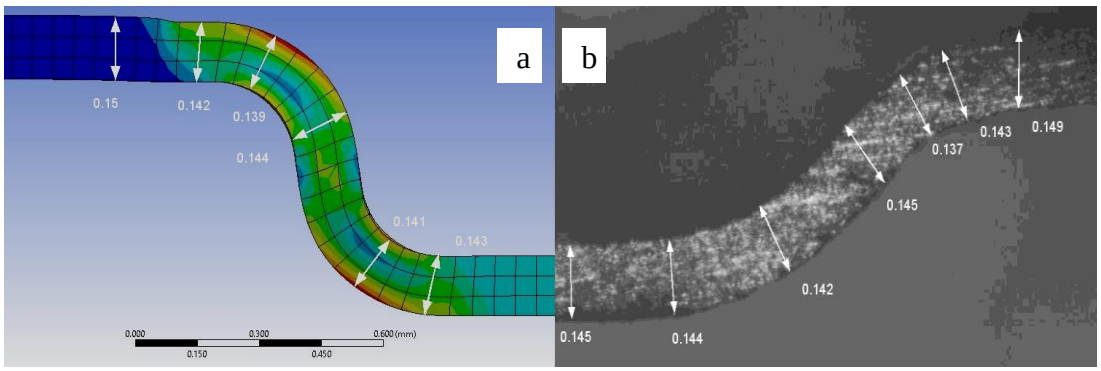

Figure 42: Simulated and experimental stamped plate thickness comparison a.) Simulation b.) Experiment

dimensions are in agreement with simulation results as shown in Figure 42, excepting the depth of the formed channel. The depth of the channel is observed as 0.45mm, which might be due to the spring back effect of the titanium sheet. The inaccuracy in the dimension can be improved by combining with hydro-forming method[141].

6.5 WCC coated stamped plate and its fuel cell performance

The stamped plate is trimmed to 80mm x 80mm size and coated with WCC using the same parameters used to coat the metal strip through physical vapour deposition. Figure 43, shows the picture of a bare titanium plate and a WCC coated plate. The colour of the coated plate appears as shiny black anthracite. The coated plate is assembled in the fuel cell along with the hot pressed MEA. A silicon gasket is used to arrest leakage of reactant gases and a pair of gold coated copper plates are used as a current collector as shown in Figure 44. The assembly is connected to the test station and the MEA is activated according to USFCC (US Fuel cell Council) procedure, where the hydrogen and oxygen is supplied at 100%RH and the fuel cell temperature is set at 80°C. The stoichiometric ratio between hydrogen and oxygen is maintained 1.2:2 ratio at a pressure of 150 kpa. Initially the fuel cell is kept under constant voltage mode at 0.6V for 1hr and then put under cyclic load holding at 0.7 V for 20min then at 0.5V for another 20min. This cycle is repeated nine times and then the actual performance is recorded [91].

Figure 43: Photograph of Bare Titanium (Left) and WCC coated titanium plate(Right)

After 20 hrs of maintaining the cell at constant voltage of 0.60V the fuel cell performance of both the coated titanium and bare titanium stamped plate is analysed and the polarisation curve plotted. The subsequent long-term performance analysis of the coated plate is examined by maintaining it in constant current mode. The test is conducted for 500hrs in fuel cell set up and the metal contamination in the MEA is obtained through ICP.

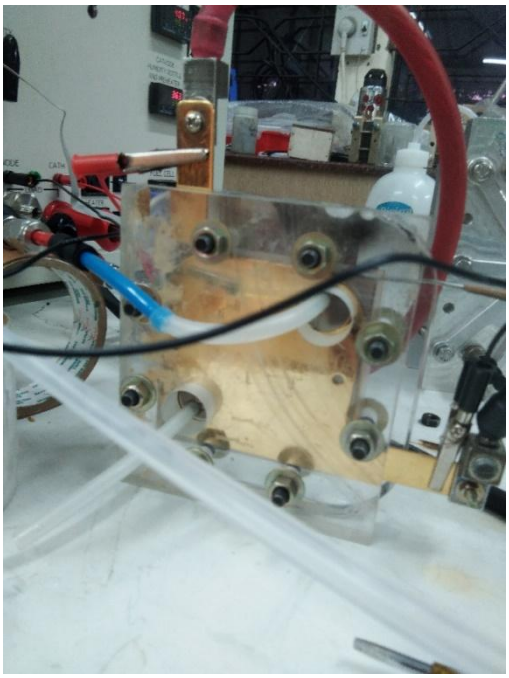

Figure 44: Assembled Single fuel

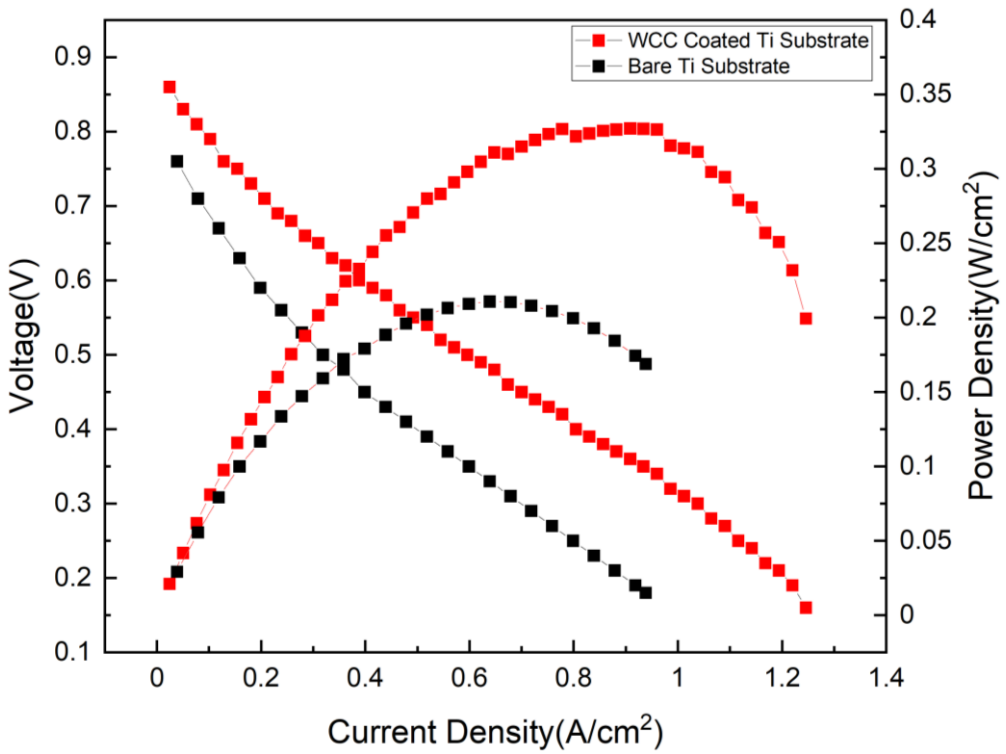

Figure 45: Fuel cell polarisation curve for Bare and WCC coated titanium substrate

The MEAs prepared for the two set-ups are stamped using same catalyst loaded electrode, membrane and stamping parameters (Pressure and temperature). The OCV (Open Circuit Voltages) of bare titanium plate and WCC coated plate are 0.88V and 0.92V respectively. Figure 45 shows the polarisation curve for both coated and uncoated titanium plate. The peak power density of WCC is 0.321W/cm^2 at 0.8 A/cm^2, while bare Ti shows a peak power of 0.21W/cm^2 at 0.63A/cm^2. For most applications it is recommended to operate the fuel cell at 0.60V for stable power output [142]. The current density at the operating voltage is 0.198A/cm^2 and 0.387 A/cm^2 for the uncoated Ti and WCC coated Ti plates respectively. It's clear that the coated plate shows superior performance to the uncoated Ti plate.

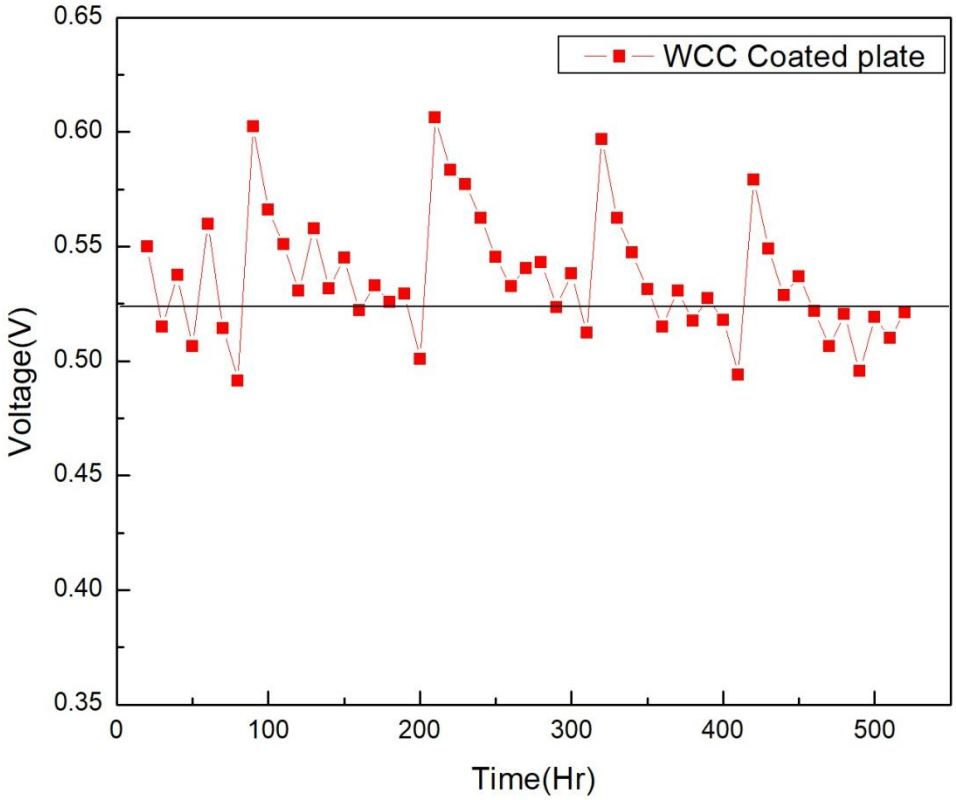

Figure 46: Long term fuel cell performance of WCC coated titanium plate

Figure 46 shows the long term performance of fuel cell using coated plate WCC. The performance is analysed by maintaining the load in the constant current mode at 0.50A/cm^2 (12.5A). The hydrogen and oxygen are supplied through an electrolyser and an electronic load is used to analyse the performance. The reading is taken once for every 10hrs. Nitrogen gas is purged through anode and cathode when the voltage drop exceeds 10%. When this occurs nitrogen gas is purged for 10 min at 2bar to stop the reaction and remove the excess water agglomerated in the channel and GDL. Restarting the fuel cell generates a spike in the performance and gradually the voltage settles at around 0.52V over most of the time, which is a potential drop of 5% during the 520 hrs test. To determine the amount of metal leached into the membrane, the fuel cell is disassembled and the MEA is tested using ICP. It has been found that the total contaminations of titanium and tungsten metal leached into the MEA are 6.55 ppm and 4.59 ppm respectively. Even though there are no reports available on the long term performance of WCC coated bipolar plates, it is noteworthy that this value is less than in most of the reports available for various other coatings [143, 144].

6.6 Closure

This Chapter describes how a die and punch is designed using data collected from ANSYS simulation and the results are compared with a stamped titanium plate. Titanium sheet metal of 0.15mm thickness is stamped using the forming tool in a hydraulic press. The stamped plates are coated with WCC coating and assembled in the fuel cell along with an in-house fabricated MEA. The fuel cell performance of the WCC coated plates show a superior performance of 0.321 W/cm^2 after activation, a long term corrosion test is conducted on the fuel cell and the quantity of metal leaches into the MEA is determined using the ICP test. A voltage drop of 5% was observed over the 500hrs constant current mode setting.

CHAPTER 7 CONCLUSIONS AND FUTURE WORK

7.1 Summary and discussion

This research investigated the suitability of different thin film coatings for PEMFC bipolar plates (BP). All the coatings were produced by the PVD technique due to its various advantages over other coating methods. It is advisable to consider all properties of the BP coating, as the bipolar plate is itself a multifunctional component in fuel cell. Let's consider polymer graphite composite material, it has impressive corrosion resistance in acidic environments but it has a higher ICR than graphite or metal BP. An extensive literature review has been done to find the most reliable, efficient, environmentally friendly and mass producible coating technique. It is understood that PVD has most of the required qualities but only few non-noble coatings have been well studied in the fuel cell environment. In this research, a comprehensive approach is used to study different properties of BP to find the most suitable coating. Three coatings were deposited on titanium substrate and put under test for one of the basic requirements of BP: corrosion resistance in a highly acidic electrolyte solution of 1M H_2SO_4 and 2ppm HF at 70°C. Unlike potential-free corrosion, BPs are exposed to a constant potential between -0.1 V vs RHE and 0.8 V vs RHE. So the corrosion resistance test is taken applying 0.60V with reference to the calomel electrode to mimic the actual fuel cell environment and the corrosion resistance of the coatings were determined in the following order of magnitude: Bare-Ti<TiN<a-C<WCC. The reason for TiN and a-C showing less resistance to corrosion is due to pinholes and granularity in the coating, which was confirmed through SEM micrography. Raman spectroscopy was used to analyse the disorder in the carbon based coating and it was found that WCC improved the clustering of sp2 hybridized carbon. Further quantitative analysis by XPS measured the content of sp2 and sp3 hybridised carbon by deconvoluting the C1s spectra. The excess carbon deposited on the surface of tungsten carbide favours the sp2 hybridisation which eventually increases the surface electrical conductivity. This sp2 hybridised carbon helps to reduce the ICR between the coated surface and GDL. The ICR test results for all coatings before and after potentiostatic corrosion test in the order of increasing resistance are as follows: WCC<TiN<a-C<Bare-Ti. Comparing these three different

coatings in the simulated environment, WCC is the one which satisfies DOE target 2025 for both corrosion resistance and ICR. Hence, it was studied further in the actual fuel cell.

A die and punch was designed based on the simulation results of the three designs have different fillet radii. The theoretical performance of the design was analysed through ANSYS to determine the strain at 10 critical points of the deformed plate and the angle between channel walls. The model 3 design with a draft angle of 15° had relatively less strain at the critical spots and that draft angle is not small enough for generating cracks in the corner nor so large as to affect the thermal property of the channel. The optimal force for forming the required channel dimension is 115kN above which the plate gets cracks at the corners. The thickness of the actual formed plate through the stamping process is in agreement with the simulation result. The stamped plate was coated with WCC. The fuel cell performance of the coated plate showed 95.5% more current density than uncoated titanium plate at 0.60V (the FC working potential). The 500hrs long term fuel cell testing shows little decrease in the performance with just 6.55 ppm and 4.59 ppm of titanium and tungsten metal respectively leaching into MEA. This shows overall performance of the WCC coated plate is on a par with noble metal coatings (Ag, Au) but at a fraction of their cost.

Findings of this research:

1. An extensive literature review has been done to find a novel coating material and a reliable, efficient, environmental friendly and mass producible coating technique.

2. The corrosion resistance of the three selected coatings were in the following order of magnitude: Bare-Ti<TiN<a-C<WCC.

3. The ICR test result for all coatings before and after the potentiostatic corrosion test in the order of increasing resistance were as follows: WCC<TiN<a-C<Bare-Ti.

4. The electrochemical performance of the WCC coating was studied in a simulated fuel cell environment and its corrosion current density after a 4 hr test was found to be 0.361 $\mu A/cm^2$ which is well within DOE target 2025 of <1 $\mu A/cm^2$

5. The ICR of WCC coating after potentiostatic test is 6.59$m\Omega.cm^2$ which is also within the DOE target 2025 of <10$m\Omega.cm^2$

6. A monopolar plate with a serpentine flow channel has been successfully designed and fabricated without crack.

7. The fuel cell performance of the WCC coated plate shows 95.5% more current density than uncoated titanium plate at 0.60V (FC working potential).

8. The long term fuel cell performance of the WCC coating has been studied and the quantity of material leached into the MEA is analysed.

From the above findings it is clear that all the objectives of this research have been achieved and the outcome of this research will help to increase the understanding about the performance of WCC coatings both in the simulated and actual fuel cell environment.

7.2 Future work

As mentioned in the early part of this thesis, titanium plate was chosen as a substrate due to the targeted application of this research work which is for the aviation sector, specifically drones. The best drone in the market can't fly for more than 30 min because they use batteries as their power source which have a poor energy density. A fuel cell with a lightweight stack can readily replace batteries and can extend the flight time from minutes to hours. Fuel cells have a great potential as an alternative power source for aviation industries, thanks to its exceptional power to weight ratio.

This has led to a successful design for a drone (Hexacopter) powered with a fuel cell stack made of uncoated commercial titanium plate and with a battery as secondary power source. The power output of the stack at 0.65V is 250W and the hydrogen is supplied from a cylinder which can store hydrogen at 200bar. As the uncoated plate's performance (wattage) deteriorates over time, it needs a protective coating to maintain the output power.

Figure 47: Hydrogen fuel cell powered UAV

An in-depth analysis to understand the life of the WCC coated plate in 5000hrs fuel cell testing will be conducted and a 36 cell stack coated with WCC will be used to evaluate its performance in the drone application.

REFERENCES

1. (WDI)database, W.d.i. *World Bank database*. 2021; Available from: https://data.worldbank.org/indicator/.
2. IEA, G.e.-r.C.e., 1990-2020, IEA, Paris. Available from: https://www.iea.org/data-and-statistics/charts/global-energy-related-co2-emissions-1990-2020.
3. Hussain, J., A. Khan, and K. Zhou, *The impact of natural resource depletion on energy use and CO2 emission in Belt & Road Initiative countries: a cross-country analysis.* Energy, 2020. **199**: p. 117409.
4. IEA (2021), G.E.R.C.E.i., IEA, Paris Available from: https://www.iea.org/articles/global-energy-review-co2-emissions-in-2020.
5. Rashid, M., et al., *Hydrogen production by water electrolysis: a review of alkaline water electrolysis, PEM water electrolysis and high temperature water electrolysis.* International Journal of Engineering and Advanced Technology, 2015.
6. Uemiya, S., et al., *Steam reforming of methane in a hydrogen-permeable membrane reactor.* Applied catalysis, 1990. **67**(1): p. 223-230.
7. Teets, T.S. and D.G. Nocera, *Photocatalytic hydrogen production.* Chemical communications, 2011. **47**(33): p. 9268-9274.
8. Romm, J.J., *The hype about hydrogen: fact and fiction in the race to save the climate*. 2004: Island Press.
9. Su, Y., et al., *Review of the Hydrogen Permeability of the Liner Material of Type IV On-Board Hydrogen Storage Tank.* World Electric Vehicle Journal, 2021. **12**(3): p. 130.
10. news, A.h. *Growing Australia's hydrogen industry*. Available from: https://www.industry.gov.au/policies-and-initiatives/growing-australias-hydrogen-industry.
11. Shamsul, N., et al., *An overview on the production of bio-methanol as potential renewable energy.* Renewable and Sustainable Energy Reviews, 2014. **33**: p. 578-588.
12. Association, F.C.H.E. *Fuel cell Basics*. Available from: https://www.fchea.org/fuelcells.
13. KORKMAZ, S.A. and A.G. CERİT, *Applications of Fuel Cell Technologies in Ships and A System Dynamics Approach.* PROCEEDINGS BOOK, 2016: p. 42.
14. Haile, S.M., *Fuel cell materials and components.* Acta materialia, 2003. **51**(19): p. 5981-6000.
15. Brožová, L., et al., *Sorption of single enantiomers and racemic mixture of (+/−)-α-pinene into Nafion membranes.* Desalination and Water Treatment, 2015. **55**(11): p. 2967-2972.
16. Rajendran, R.G., *Polymer electrolyte membrane technology for fuel cells.* MRS bulletin, 2005. **30**(8): p. 587-590.
17. Denis, M., et al., *High energy ball-milled Pt and Pt–Ru catalysts for polymer electrolyte fuel cells and their tolerance to CO.* Journal of applied electrochemistry, 1999. **29**(8): p. 951-960.
18. Gouerec, P., et al., *High Energy Ballmilled Pt-Mo Catalysts for Polymer Electrolyte Fuel Cells and Their Tolerance to CO.* Journal of the Electrochemical Society, 2000. **147**(11): p. 3989.
19. Larminie, J., *Fuel Cell Technology Handbook.* Proceedings of the Institution of Mechanical Engineers, 2003. **217**(3): p. 339.
20. Barbir, F., *PEM fuel cells: theory and practice*. 2012: Academic press.
21. Zhang, J., J. Wu, and H. Zhang, *PEM fuel cell testing and diagnosis*. 2013: Newnes.
22. Davies, D., et al., *Bipolar plate materials for solid polymer fuel cells.* Journal of Applied Electrochemistry, 2000. **30**(1): p. 101-105.
23. Barbir, F., J. Braun, and J. Neutzler, *Properties of molded graphite bi-polar plates for PEM fuel cell stacks.* Journal of New Materials for Electrochemical Systems, 1999. **2**.
24. Wlodarczyk, R., et al., *A comparison of nickel coated and uncoated sintered stainless steel used as bipolar plates in low-temperature fuel cells.* International Journal of Hydrogen Energy, 2016. **41**(39): p. 17644-17651.
25. Xiong, K., et al., *Modeling, design, materials and fabrication of bipolar plates for proton exchange membrane fuel cell: A review.* Applied Energy, 2021. **301**: p. 117443.

26. Li, X. and I. Sabir, *Review of bipolar plates in PEM fuel cells: Flow-field designs.* International journal of hydrogen energy, 2005. **30**(4): p. 359-371.
27. Wang, C.-Y., *Fundamental models for fuel cell engineering.* Chemical reviews, 2004. **104**(10): p. 4727-4766.
28. Liu, H., et al., *Experimental study and comparison of various designs of gas flow fields to PEM fuel cells and cell stack performance.* Frontiers in Energy Research, 2014. **2**: p. 2.
29. Zhang, G., et al., *Comparison of current distributions in proton exchange membrane fuel cells with interdigitated and serpentine flow fields.* Journal of Power Sources, 2009. **188**(1): p. 213-219.
30. Drive, U., *Fuel cell technical team roadmap.* New York: US Drive Partnership, 2013: p. 1-26.
31. Brett, D.J. and N.P. Brandon, *Review of materials and characterization methods for polymer electrolyte fuel cell flow-field plates.* 2007.
32. Yuan, X.Z., et al., *Bipolar plates for PEM fuel cells-from materials to processing.* Journal of New Materials for Electrochemical Systems, 2005. **8**(4): p. 257.
33. Müller, A., et al., *Injection moulding of graphite composite bipolar plates.* Journal of Power Sources, 2006. **154**(2): p. 467-471.
34. Germany, I., *CFC fuel cell for Stuttgart waste treatment plant.* Fuel Cells Bulletin, 2007: p. 10.
35. Suherman, H., et al., *Improvement of the Electrical-Mechanical Performance of Epoxy/Graphite Composites Based on the Effects of Particle Size and Curing Conditions.* Polymers, 2022. **14**(3): p. 502.
36. Thongruang, W., R.J. Spontak, and C.M. Balik, *Correlated electrical conductivity and mechanical property analysis of high-density polyethylene filled with graphite and carbon fiber.* Polymer, 2002. **43**(8): p. 2279-2286.
37. Scholta, J., et al., *Investigations on novel low-cost graphite composite bipolar plates.* Journal of Power Sources, 1999. **84**(2): p. 231-234.
38. Hu, B., et al., *High performance polyvinylidene fluoride/graphite/multi-walled carbon nanotubes composite bipolar plate for PEMFC with segregated conductive networks.* International Journal of Hydrogen Energy, 2021. **46**(50): p. 25666-25676.
39. Asri, N.F., et al., *Coating of stainless steel and titanium bipolar plates for anticorrosion in PEMFC: A review.* International Journal of Hydrogen Energy, 2017. **42**(14): p. 9135-9148.
40. Inaba, M., et al., *Gas crossover and membrane degradation in polymer electrolyte fuel cells.* Electrochimica Acta, 2006. **51**(26): p. 5746-5753.
41. Yun, Y.-H., *Deposition of gold–titanium and gold–nickel coatings on electropolished 316L stainless steel bipolar plates for proton exchange membrane fuel cells.* International journal of hydrogen energy, 2010. **35**(4): p. 1713-1718.
42. Borup, R.L. and N.E. Vanderborgh, *Design and testing criteria for bipolar plate materials for PEM fuel cell applications.* MRS Online Proceedings Library (OPL), 1995. **393**.
43. Roberge, P.R. and E. Ghali. *A corrosion engineering training model*. in *CORROSION 2000*. 2000. OnePetro.
44. McCafferty, E., *Thermodynamics of corrosion: Pourbaix diagrams*, in *Introduction to corrosion science*. 2010, Springer. p. 95-117.
45. Frankel, G., *Pitting corrosion of metals: a review of the critical factors.* Journal of the Electrochemical society, 1998. **145**(6): p. 2186.
46. Mele, C. and B. Bozzini, *Localised corrosion processes of austenitic stainless steel bipolar plates for polymer electrolyte membrane fuel cells.* Journal of Power Sources, 2010. **195**(11): p. 3590-3596.
47. André, J., L. Antoni, and J.-P. Petit, *Corrosion resistance of stainless steel bipolar plates in a PEFC environment: A comprehensive study.* International Journal of Hydrogen Energy, 2010. **35**(8): p. 3684-3697.

48. Mele, C. and B. Bozzini, *Corrosion performance of austenitic stainless steel bipolar plates for nafion-and room-temperature ionic-liquid-based PEMFCs.* The Open Fuels & Energy Science Journal, 2012. **5**(1).
49. Miyazawa, A., E. Tada, and A. Nishikata, *Influence of corrosion of SS316L bipolar plate on PEFC performance.* Journal of power sources, 2013. **231**: p. 226-233.
50. Davies, D., et al., *Stainless steel as a bipolar plate material for solid polymer fuel cells.* Journal of power sources, 2000. **86**(1-2): p. 237-242.
51. Silva, R., et al., *Surface conductivity and stability of metallic bipolar plate materials for polymer electrolyte fuel cells.* Electrochimica Acta, 2006. **51**(17): p. 3592-3598.
52. Wang, H., M.A. Sweikart, and J.A. Turner, *Stainless steel as bipolar plate material for polymer electrolyte membrane fuel cells.* Journal of Power Sources, 2003. **115**(2): p. 243-251.
53. Wang, H. and J.A. Turner, *Ferritic stainless steels as bipolar plate material for polymer electrolyte membrane fuel cells.* Journal of Power Sources, 2004. **128**(2): p. 193-200.
54. Wang, S.-H., et al., *Performance of the gold-plated titanium bipolar plates for the light weight PEM fuel cells.* Journal of Power Sources, 2006. **162**(1): p. 486-491.
55. Soma, Y., I. Muto, and N. Hara, *Electrochemical properties of titanium in PEFC bipolar plate environments.* Materials transactions, 2010. **51**(5): p. 939-947.
56. Feng, K., et al., *Silver implanted 316L stainless steel as bipolar plates in polymer electrolyte membrane fuel cells.* Materials Chemistry and Physics, 2011. **126**(1-2): p. 6-11.
57. Fu, Y., et al., *Ag–polytetrafluoroethylene composite coating on stainless steel as bipolar plate of proton exchange membrane fuel cell.* Journal of Power Sources, 2008. **182**(2): p. 580-584.
58. Yoon, W., et al., *Evaluation of coated metallic bipolar plates for polymer electrolyte membrane fuel cells.* Journal of Power Sources, 2008. **179**(1): p. 265-273.
59. Ihonen, J., et al., *A novel polymer electrolyte fuel cell for laboratory investigations and in-situ contact resistance measurements.* Electrochimica Acta, 2001. **46**(19): p. 2899-2911.
60. Wind, J., et al., *Metallic bipolar plates for PEM fuel cells.* Journal of Power Sources, 2002. **105**(2): p. 256-260.
61. Hentall, P.L., et al., *New materials for polymer electrolyte membrane fuel cell current collectors.* Journal of Power Sources, 1999. **80**(1-2): p. 235-241.
62. Vite, M., et al., *A study of the abrasive resistance of sputtered CrN coatings deposited on AISI 316 and AISI H13 steel substrates using steel particles.* Wear, 2011. **271**(9-10): p. 1273-1279.
63. Barranco, J., et al., *Influence of CrN-coating thickness on the corrosion resistance behaviour of aluminium-based bipolar plates.* Journal of Power Sources, 2011. **196**(9): p. 4283-4289.
64. Zhang, M., et al., *Composition optimization of arc ion plated CrNx films on 316L stainless steel as bipolar plates for polymer electrolyte membrane fuel cells.* Journal of Power Sources, 2012. **205**: p. 318-323.
65. Pozio, A., et al., *Bipolar plate materials for PEMFCs: a conductivity and stability study.* Journal of Power Sources, 2008. **179**(2): p. 631-639.
66. Antunes, R.A., et al., *Corrosion of metal bipolar plates for PEM fuel cells: A review.* International journal of hydrogen energy, 2010. **35**(8): p. 3632-3647.
67. Nam, D.-G. and H.-C. Lee, *Thermal nitridation of chromium electroplated AISI316L stainless steel for polymer electrolyte membrane fuel cell bipolar plate.* Journal of Power Sources, 2007. **170**(2): p. 268-274.
68. Wang, L., et al., *Corrosion properties and contact resistance of TiN, TiAlN and CrN coatings in simulated proton exchange membrane fuel cell environments.* Journal of Power Sources, 2010. **195**(12): p. 3814-3821.
69. Park, Y.-C., et al., *Effects of CrN/Cr coating layer on durability of metal bipolar plates under a fuel recirculation system of direct methanol fuel cells.* International journal of hydrogen energy, 2013. **38**(25): p. 10567-10576.
70. Choe, C., et al., *Tantalum nitride coated AISI 316L as bipolar plate for polymer electrolyte membrane fuel cell.* international journal of hydrogen energy, 2012. **37**(1): p. 405-411.

71. Larijani, M., et al., *Nitrogen effect on corrosion resistance of ion beam sputtered nanocrystalline zirconium nitride films.* Surface and Coatings Technology, 2009. **203**(17-18): p. 2591-2594.
72. Kumagai, M., et al., *Nanosized TiN–SBR hybrid coating of stainless steel as bipolar plates for polymer electrolyte membrane fuel cells.* Electrochimica Acta, 2008. **54**(2): p. 574-581.
73. Jin, C., M. Jung, and C. Kang, *Fabrication of Aluminum Bipolar Plates by Semi-Solid Forging Process and Performance Test of TiN Coated Aluminum Bipolar Plates.* Fuel Cells, 2014. **14**(4): p. 551-560.
74. Zhang, D., et al., *Corrosion behavior of TiN-coated stainless steel as bipolar plate for proton exchange membrane fuel cell.* International Journal of Hydrogen Energy, 2010. **35**(8): p. 3721-3726.
75. Jin, C.K., K.H. Lee, and C.G. Kang, *Performance and characteristics of titanium nitride, chromium nitride, multi-coated stainless steel 304 bipolar plates fabricated through a rubber forming process.* International journal of hydrogen energy, 2015. **40**(20): p. 6681-6688.
76. Lee, C.-H., et al., *Electrically conductive polymer composite coating on aluminum for PEM fuel cells bipolar plate.* Renewable energy, 2013. **54**: p. 46-50.
77. Du, L. and S.C. Jana, *Highly conductive epoxy/graphite composites for bipolar plates in proton exchange membrane fuel cells.* Journal of Power Sources, 2007. **172**(2): p. 734-741.
78. Huang, J., D.G. Baird, and J.E. McGrath, *Development of fuel cell bipolar plates from graphite filled wet-lay thermoplastic composite materials.* Journal of Power Sources, 2005. **150**: p. 110-119.
79. Liao, S.-H., et al., *Preparation and properties of carbon nanotube-reinforced vinyl ester/nanocomposite bipolar plates for polymer electrolyte membrane fuel cells.* Journal of Power Sources, 2008. **176**(1): p. 175-182.
80. Chung, C.-Y., et al., *Carbon film-coated 304 stainless steel as PEMFC bipolar plate.* Journal of Power Sources, 2008. **176**(1): p. 276-281.
81. Fukutsuka, T., et al., *Carbon-coated stainless steel as PEFC bipolar plate material.* Journal of Power Sources, 2007. **174**(1): p. 199-205.
82. Feng, K., et al., *C/CrN multilayer coating for polymer electrolyte membrane fuel cell metallic bipolar plates.* Journal of power sources, 2013. **222**: p. 351-358.
83. Bi, F., et al., *Multilayered Zr–C/aC film on stainless steel 316L as bipolar plates for proton exchange membrane fuel cells.* Journal of Power Sources, 2016. **314**: p. 58-65.
84. Ding, M.-h., et al., *Characterization of ZrC coatings deposited on biomedical 316L stainless steel by magnetron sputtering method.* Surface and Coatings Technology, 2013. **224**: p. 34-41.
85. Gou, Y., et al., *Nb–Cr–C coated titanium as bipolar plates for proton exchange membrane fuel cells.* Journal of Power Sources, 2022. **520**: p. 230797.
86. Yi, P., et al., *Performance of a proton exchange membrane fuel cell stack using conductive amorphous carbon-coated 304 stainless steel bipolar plates.* Journal of Power Sources, 2010. **195**(20): p. 7061-7066.
87. de Oliveira, M.C.L., G. Ett, and R.A. Antunes, *Materials selection for bipolar plates for polymer electrolyte membrane fuel cells using the Ashby approach.* Journal of power sources, 2012. **206**: p. 3-13.
88. Li, M., et al., *Corrosion behavior of TiN coated type 316 stainless steel in simulated PEMFC environments.* Corrosion science, 2004. **46**(6): p. 1369-1380.
89. Wang, H.-C., et al., *The study of electroplating trivalent CrC alloy coatings with different current densities on stainless steel 304 as bipolar plate of proton exchange membrane fuel cells.* Thin Solid Films, 2014. **570**: p. 209-214.
90. Jiang, L., et al., *In-situ electrodeposition of conductive polypyrrole-graphene oxide composite coating for corrosion protection of 304SS bipolar plates.* Journal of Alloys and Compounds, 2019. **770**: p. 35-47.

91. Zhiani, M., S. Majidi, and M. Taghiabadi, *Comparative Study of on-Line Membrane Electrode Assembly Activation Procedures in Proton Exchange Membrane Fuel Cell.* Fuel cells, 2013. **13**(5): p. 946-955.
92. Khan, A.A. and S. Boddu, *Hybrid membrane process: an emerging and promising technique toward industrial wastewater treatment*, in *Membrane-Based Hybrid Processes for Wastewater Treatment*. 2021, Elsevier. p. 257-277.
93. Susanna, G., et al., *Airbrush spray-coating of polymer bulk-heterojunction solar cells.* Solar Energy Materials and Solar Cells, 2011. **95**(7): p. 1775-1778.
94. Husby, H., *Carbon based coatings for metallic bipolar plates in PEM fuel cells*. 2013, Institutt for materialteknologi.
95. Madadi, F., et al., *Improving performance in PEMFC by applying different coatings to metallic bipolar plates.* Materials Chemistry and Physics, 2019. **238**: p. 121911.
96. Gago, A., et al. *Titanium coatings deposited by thermal spraying for bipolar plates of PEM electrolysers*. 2013. 4th European PEFC and H2 Forum 2-5 July 2013, Lucerne Switzerland.
97. Rendón-Belmonte, M., et al., *Evaluation of a Cr3C2 (NiCr) coating deposited on S4400 by means of an HVOF process and used for flow plates of PEM fuel.* Int. J. Electrochem. Sci, 2012. **7**: p. 1079-1092.
98. Tucker Jr, R., *Introduction to coating design and processing.* Thermal Spray Technology, 2013. **5**: p. 76-88.
99. Zhang, M., et al., *Honeycomb-like nanocomposite Ti-Ag-N films prepared by pulsed bias arc ion plating on titanium as bipolar plates for unitized regenerative fuel cells.* Journal of power sources, 2012. **198**: p. 196-202.
100. Shreir, L.L., *Corrosion: corrosion control*. 2013: Newnes.
101. Antonucci, P., et al., *Electrochemical corrosion behavior of carbon black in phosphoric acid.* Carbon, 1988. **26**(2): p. 197-203.
102. Hamilton, P.J., *The development of PVD coatings for PEM fuel cell bipolar plates*. 2014, University of Birmingham.
103. Shiri, S., et al., *Evaluation of Stoney equation for determining the internal stress of DLC thin films using an optical profiler.* Surface and Coatings Technology, 2016. **308**: p. 98-100.
104. Freller, H., et al., *Influence of intermediate layers and base materials on adhesion of amorphous carbon and metal-carbon coatings.* Diamond and Related Materials, 1992. **1**(5-6): p. 563-569.
105. Wang, Y. and D.O. Northwood, *Effects of O2 and H2 on the corrosion of SS316L metallic bipolar plate materials in simulated anode and cathode environments of PEM fuel cells.* Electrochimica Acta, 2007. **52**(24): p. 6793-6798.
106. Avasarala, B. and P. Haldar, *Effect of surface roughness of composite bipolar plates on the contact resistance of a proton exchange membrane fuel cell.* Journal of Power Sources, 2009. **188**(1): p. 225-229.
107. Ahmad, M., et al., *Validation of a fuel cell compression spring equivalent model using polarisation data.* International Journal of Hydrogen Energy, 2017. **42**(12): p. 8109-8118.
108. Angayarkanni, R., et al., *Self-humidified operation of a PEM fuel cell using a novel silica composite coating method.* International Journal of Hydrogen Energy, 2022. **47**(7): p. 4827-4837.
109. Chaudhry, A., et al., *Corrosion mechanism in PVD deposited nano-scale titanium nitride thin film with intercalated titanium for protecting the surface of silicon.* Electrochimica Acta, 2018. **264**: p. 69-82.
110. Zaheri, S., et al., *Corrosion behavior of Ti/TiN multilayer nanostructured coatings applied on AISI 316L by Arc-PVD method in the simulated body fluid.* Analytical and Bioanalytical Electrochemistry, 2020. **12**(7): p. 904-921.
111. Zhang, D., et al., *TiN-coated titanium as the bipolar plate for PEMFC by multi-arc ion plating.* International journal of hydrogen energy, 2011. **36**(15): p. 9155-9161.

112. Avasarala, B. and P. Haldar, *Electrochemical oxidation behavior of titanium nitride based electrocatalysts under PEM fuel cell conditions.* Electrochimica Acta, 2010. **55**(28): p. 9024-9034.
113. Panjan, P., et al., *Growth defects in PVD hard coatings.* Vacuum, 2009. **84**(1): p. 209-214.
114. Omrani, M., et al., *Improvement of corrosion and electrical conductivity of 316L stainless steel as bipolar plate by TiN nanoparticle implantation using plasma focus.* International journal of hydrogen energy, 2012. **37**(19): p. 14676-14686.
115. Gao, P., et al., *Electrochemical characteristics and interfacial contact resistance of Ni-P/TiN/PTFE coatings on Ti bipolar plates.* Journal of Solid State Electrochemistry, 2018. **22**: p. 1971-1981.
116. Shi, J., et al., *Investigation on electrochemical behavior and surface conductivity of titanium carbide modified Ti bipolar plate of PEMFC.* International Journal of Hydrogen Energy, 2020. **45**(16): p. 10050-10058.
117. Quan, C. and Y. He, *Properties of nanocrystalline Cr coatings prepared by cathode plasma electrolytic deposition from trivalent chromium electrolyte.* Surface and Coatings Technology, 2015. **269**: p. 319-323.
118. Takai, K., et al., *Structure and electronic properties of a nongraphitic disordered carbon system and its heat-treatment effects.* Physical Review B, 2003. **67**(21): p. 214202.
119. Yari, M., et al., *Physical properties of sputtered amorphous carbon coating.* Journal of alloys and compounds, 2012. **513**: p. 135-138.
120. Lian, Y., et al., *Solvent-free synthesis of ultrafine tungsten carbide nanoparticles-decorated carbon nanosheets for microwave absorption.* Nano-micro letters, 2020. **12**(1): p. 1-13.
121. Dash, T., et al., *Preparation and neutronic studies of tungsten carbide composite.* Fusion Science and Technology, 2014. **65**(2): p. 241-247.
122. Voevodin, A., et al., *Nanocrystalline WC and WC/a-C composite coatings produced from intersected plasma fluxes at low deposition temperatures.* Journal of Vacuum Science & Technology A: Vacuum, Surfaces, and Films, 1999. **17**(3): p. 986-992.
123. Konishi, T., K. Yukimura, and K. Takaki, *Fabrication of diamond-like carbon films using short-pulse HiPIMS.* Surface and Coatings Technology, 2016. **286**: p. 239-245.
124. Zhang, S., et al., *A superhard CrAlSiN superlattice coating deposited by multi-arc ion plating: I. Microstructure and mechanical properties.* Surface and Coatings Technology, 2013. **214**: p. 160-167.
125. Song, Y., et al., *Review on current research of materials, fabrication and application for bipolar plate in proton exchange membrane fuel cell.* International Journal of Hydrogen Energy, 2020. **45**(54): p. 29832-29847.
126. Kumar, A., M. Ricketts, and S. Hirano, *Ex situ evaluation of nanometer range gold coating on stainless steel substrate for automotive polymer electrolyte membrane fuel cell bipolar plate.* Journal of Power Sources, 2010. **195**(5): p. 1401-1407.
127. Ferrari, A.C., et al., *Raman spectrum of graphene and graphene layers.* Physical review letters, 2006. **97**(18): p. 187401.
128. Show, Y., *Electrically conductive amorphous carbon coating on metal bipolar plates for PEFC.* Surface and Coatings Technology, 2007. **202**(4-7): p. 1252-1255.
129. Pasaja, N., et al., *Mo-containing tetrahedral amorphous carbon deposited by dual filtered cathodic vacuum arc with selective pulsed bias voltage.* Nuclear Instruments and Methods in Physics Research section B: Beam Interactions with Materials and Atoms, 2007. **259**(2): p. 867-870.
130. Li, X., H. Miao, and H. Zhu, *Deposition and Characterization of Diamond-like Carbon Films by Electron Cyclotron Resonance Microwave Plasma Enhanced Unbalanced Magnetron Sputtering.* Chemical Engineering Transactions, 2018. **66**: p. 19-24.
131. Alba, G., et al., *Comprehensive nanoscopic analysis of tungsten carbide/Oxygenated-diamond contacts for Schottky barrier diodes.* Applied Surface Science, 2021. **537**: p. 147874.

132. Khamnualthong, N., K. Siangchaew, and P. Limsuwan, *Influence of thermal heating on diamond-like carbon film properties prepared by filtered cathodic arc.* Thin solid films, 2013. **544**: p. 477-481.
133. Constantinou, M., et al., *Metal (Ag/Ti)-containing hydrogenated amorphous carbon nanocomposite films with enhanced nanoscratch resistance: Hybrid PECVD/PVD system and microstructural characteristics.* Nanomaterials, 2018. **8**(4): p. 209.
134. Zhang, L.-N., et al., *Ultrafine cable-like WC/W 2 C heterojunction nanowires covered by graphitic carbon towards highly efficient electrocatalytic hydrogen evolution.* Journal of Materials Chemistry A, 2018. **6**(31): p. 15395-15403.
135. Huang, W., et al., *Metallic tungsten carbide nanoparticles as a near-infrared-driven photocatalyst.* Journal of Materials Chemistry A, 2019. **7**(31): p. 18538-18546.
136. Taccani, R. and N. Zuliani, *Effect of flow field design on performances of high temperature PEM fuel cells: Experimental analysis.* International Journal of hydrogen energy, 2011. **36**(16): p. 10282-10287.
137. Baker, M.J., *CFD simulation of flow through packed beds using the finite volume technique.* 2011.
138. Manso, A., et al., *Influence of geometric parameters of the flow fields on the performance of a PEM fuel cell. A review.* International journal of hydrogen energy, 2012. **37**(20): p. 15256-15287.
139. Shimpalee, S., et al., *Understanding the effect of channel tolerances on performance of PEMFCs.* International Journal of Hydrogen Energy, 2011. **36**(19): p. 12512-12523.
140. Jeong, M.-G., et al., *Formability evaluation of stainless steel bipolar plate considering draft angle of die and process parameters by rubber forming.* International journal of precision engineering and manufacturing, 2014. **15**(5): p. 913-919.
141. Turan, C., Ö.N. Cora, and M. Koç, *Effect of manufacturing processes on contact resistance characteristics of metallic bipolar plates in PEM fuel cells.* international journal of hydrogen energy, 2011. **36**(19): p. 12370-12380.
142. de Melo Furtado, J.G., et al., *Performance analysis of a 5 kW PEMFC with a natural gas reformer.* International Journal of Hydrogen Energy, 2010. **35**(18): p. 9990-9995.
143. Park, Y.-c., et al., *Corrosion Resistance, Cell Performance and Long-term Stability of Metal Bipolar Plates for Direct Methanol Fuel Cell.* ECS Transactions, 2009. **25**(1): p. 861.
144. Han, B.B., et al., *Corrosion resistance of dlc film-coated sus316l steel prepared by ion beam enhanced deposition.* Advances in Materials Science and Engineering, 2019. **2019**.